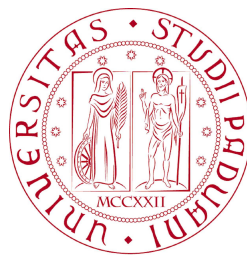


UNIVERSITÀ DEGLI STUDI DI PADOVA
SCUOLA DI DOTTORATO IN INGEGNERIA INDUSTRIALE
INDIRIZZO PROGETTAZIONE E DINAMICA DEI SISTEMI MECCANICI



Completed on January 28, 2014 using L^AT_EX 2_ε



UNIVERSITÀ
DEGLI STUDI
DI PADOVA

SEDE AMMINISTRATIVA: UNIVERSITÀ DEGLI STUDI DI PADOVA
DIPARTIMENTO DI INGEGNERIA INDUSTRIALE

SCUOLA DI DOTTORATO IN INGEGNERIA INDUSTRIALE
INDIRIZZO PROGETTAZIONE E DINAMICA DEI SISTEMI MECCANICI
CICLO XXVI

ANALYSIS OF MUSCLE COORDINATION FOR THE
DESIGN OF IMPROVED INTERACTING ROBOTIC
SYSTEMS

Direttore della Scuola: Ch.mo Prof. Paolo Colombo
Coordinatore d'indirizzo: Ch.mo Prof. Alberto Doria
Supervisore: Ch.mo Prof. Giulio Rosati

Dottorando: Christian Finetto

Contents

Abstract	IX
Sommario	XI
Introduction	XIII
1 Motor modules: a tool to explain muscle coordination	1
1.1 Motor control: a quick overview	2
1.2 Patterns underlying muscle coordination	5
1.2.1 Motor modules may simplify muscle coordination in animals . . .	9
1.2.2 Evidence for a modular organization of motor control in humans	13
1.3 Stroke from the perspective of motor modules	18
1.4 Criticism against a pure modular control strategy	22
2 Electromyography	25
2.1 The electromyographic signal	26
2.2 Acquisition of EMG signals	31
2.2.1 Electrodes	33
2.2.2 Surface electrode setup and placement guidelines	35
2.3 Processing of electromyographic signals	37
2.3.1 Properties of the EMG signal	37
2.3.2 Extraction of linear envelopes	40
3 Algorithms for extracting motor modules	45
3.1 Factorization of EMG signals	46
3.1.1 A linear model	46

3.1.2	Common algorithms	48
3.1.3	Which algorithm is “best”?	50
3.2	Non-negative Matrix Factorization	51
3.2.1	Variants of NMF	55
3.2.2	Convergence and stopping criteria	58
3.3	Other models	59
3.3.1	Time-varying modules	59
3.3.2	Shared modules	61
4	Materials and methods	63
4.1	Design of experiment	64
4.2	Experimental setup	70
4.2.1	EMG data acquisition system	70
4.2.2	Motion capture system	77
4.2.3	Software	81
4.2.4	Preparation procedures	86
4.3	Data processing	87
4.3.1	Interpolation and smoothing of kinematic data	87
4.3.2	Definition of events	88
4.3.3	EMG processing	90
4.3.4	Extraction of motor modules	91
4.3.5	Shared and specific modules for each side	91
4.3.6	Healthy control subjects	92
4.3.7	Stroke patients	95
5	Results	99
5.1	Extracted motor modules	100
5.1.1	Healthy control subjects	100
5.1.2	Stroke patients	106
5.2	Shared and side-specific modules	107
5.3	Healthy control subjects	112
5.3.1	Similar coordination strategies between subjects	112
5.3.2	Biomechanical functions associated with motor modules	114

5.3.3	Most relevant tasks	121
5.4	Stroke patients	126
5.4.1	Comparison between impaired and unimpaired side	126
5.4.2	Comparison with healthy controls	127
5.4.3	Relationship between level of motor impairment and number of modules	128
5.4.4	Changes after stroke	129
	Discussion	133
	References	139

Abstract

Despite the increasing effort put in the development of robotic systems for neurorehabilitation, justified by the big potential of such applications as additional end efficient tools for therapy, their clinical effectiveness is still being discussed. Many of the systems developed to date were designed from an engineering point of view and do not meet therapy demands, which is reflected by unsatisfactory clinical outcomes. In order to improve these systems, new rehabilitation protocols need to be based upon a deeper knowledge of how motor control and muscle coordination are achieved on a neurological level, and of how they are affected by neurologic injury.

In this research project, which is a combined effort between the Mechatronics group of the University of Padua and the Upper Extremity Motor Function Laboratory of the Medical University of South Carolina, we approached the study of muscle coordination by searching for fundamental coordination patterns used to execute various movements and shared by different subjects. We recorded the EMG activity of 16 upper limb muscles of 15 healthy control subjects and 14 stroke patients during the execution of a wide variety of fast reaching movements. We then applied a non-negative factorization algorithm to the processed EMG envelopes and extracted motor modules, which represent the coordination strategies used by each subject.

We found that a very limited set of motor modules can explain the muscle activation patterns of all healthy control subjects, and that these coordination strategies are mostly shared between dominant and non-dominant side. Furthermore, most healthy participants seem to use similar coordination patterns, and we could associate each of the most commonly shared motor modules with a corresponding biomechanical function.

We also found that the effects of stroke can be seen both by looking at the number of modules and by analyzing their composition. In fact, stroke patients use significantly

less modules both on their impaired and on their unimpaired side, and some of these modules can be explained as a combination of several merged modules found in healthy controls.

These results suggest that motor impairment after stroke can be explained by a reduction in the set of motor modules. Together with the apparent inability to control certain modules independently, and which are therefore identified as merged, this could justify the limited movement complexity observed in stroke patients. We propose that new robotic rehabilitation protocols could use the information obtained by the extraction of motor modules to assess the patient's motor impairment and to address his/her specific needs. In fact, the comparison of the patient's modules with those identified in healthy control subjects can give precious information on the nature of the patient's disabilities, and provide guidelines for the choice of motor functions that should be trained during therapy.

Sommario

Nonostante l'impegno sempre maggiore per lo sviluppo di sistemi robotici per la neuroriabilitazione, giustificato dal grande potenziale di queste applicazioni come strumenti aggiuntivi ed efficienti per la terapia, la loro efficacia dal punto di vista clinico è tuttora discussa. Molti dei sistemi sviluppati fino ad oggi sono stati progettati da una prospettiva ingegneristica senza tener conto di alcune fondamentali richieste necessarie per la terapia, il che si riflette nei risultati clinici poco soddisfacenti ottenuti da queste soluzioni. Per migliorare questi sistemi, i nuovi protocolli per la riabilitazione devono basarsi su una conoscenza più approfondita su come il controllo motorio e la coordinazione muscolare sono ottenuti al livello neurologico, e su come sono modificati da danni al sistema nervoso.

In questo progetto di ricerca, che nasce da una collaborazione tra il gruppo *Mechanics* dell'Università degli Studi di Padova e il *Upper Extremity Motor Function Laboratory* della *Medical University of South Carolina*, abbiamo impostato lo studio della coordinazione partendo dalla ricerca di schemi basilari di coordinazione muscolare, usati per eseguire movimenti diversificati e condivisi da vari soggetti. Abbiamo registrato l'attività di 16 muscoli dell'arto superiore di 15 soggetti sani e di 14 pazienti con ictus durante l'esecuzione di un elevato numero di movimenti rapidi. Successivamente abbiamo applicato un algoritmo di fattorizzazione non negativa agli involucri dei segnali elettromiografici e abbiamo estratto i relativi moduli motori, i quali rappresentano le strategie di coordinazione usate da ogni soggetto.

Abbiamo scoperto che un numero molto limitato di moduli motori può spiegare l'attività muscolare di tutti i soggetti sani, e che molte di queste strategie di coordinazione sono condivise tra il lato dominante e quello non dominante. Inoltre ci risulta che la maggior parte dei soggetti sani usi delle strategie simili, e abbiamo potuto associare

ognuno dei moduli motori più comunemente condivisi con delle corrispondenti funzioni biomeccaniche.

Oltre a ciò abbiamo visto che gli effetti dell'ictus possono essere quantificati osservando il numero di moduli motori e analizzando la loro composizione. Infatti i pazienti con ictus hanno un numero di moduli significativamente più basso su entrambi i lati, e alcuni di questi moduli possono essere visti come la fusione di due o più moduli riscontrati nei soggetti sani.

Questi risultati indicano che le disabilità motorie post ictus possono essere spiegate da una riduzione del set di moduli motori. Insieme all'apparente inabilità nel controllare certi moduli in maniera indipendente, i quali quindi risultano come fusi, questo potrebbe giustificare la limitata complessità osservata nei pazienti con ictus. Nuovi protocolli per la riabilitazione robot-assistita potrebbero usare le informazioni ottenute dall'estrazione di moduli motori per valutare le disabilità motorie del paziente e per indirizzare la terapia verso le sue specifiche necessità. Il confronto tra i moduli motori del paziente con quelli identificati nei soggetti sani può dare delle informazioni preziose sulla natura delle disabilità del paziente, e fornire delle linee guida per la scelta delle funzioni motorie su cui indirizzare la terapia.

Introduction

The use of robotic and electromechanical systems for neurorehabilitation purposes is a relatively young concept which was introduced in 1992 at MIT [1], and has seen a rapid growth since then [2]. The goal of this line of research is to use advanced technologies in the field of robotics, virtual reality and haptics, and theories in neuroscience and rehabilitation, to develop new methodologies for treating neurologic injuries. The main field of application is the neurorehabilitation of stroke patients, but many of these technologies can be applied also to patients with traumatic brain injury or spinal cord injury [2].

Stroke is the first cause of permanent disability in the industrialized world [3], and the number of people requiring rehabilitation after stroke is rapidly increasing due to changes in the population demographics [4, 5]. This puts increasing pressure on healthcare budgets [6]. Furthermore, healthcare economies have shortened the length of stay in treatment facilities and reduced the number of therapists, thereby decreasing the amount of individual treatment received by a patient prior to discharge [6, 7]. The rush to discharge the patient from the rehabilitation facility has promoted a tendency to obtain functional improvement by applying compensatory strategies. However, clinical results suggest that this leads to disuse of the impaired limb, thereby reducing the potential for a future reduction of the disability [7]. It follows that there is a strong demand for new technologies allowing to implement more effective and affordable rehabilitation programs [6].

Robotic rehabilitation systems are an efficient approach to this problem, as they are well suited to produce an intensive, task-oriented motor training as part of an integrated set of rehabilitation tools, including also simpler non-robotic solutions [2]. In fact, the labor intensive aspects of therapy can be done by the robotic system, while the therapist

could focus on functional rehabilitation during individual training [6]. Additionally, a single therapist could supervise multiple robotic rehabilitation stations and work on more than one patient at the same time. In other words, robotic systems could help automating the repetitive part of neurorehabilitation in a controlled manner. Besides improving therapy at the rehabilitation facility, affordable robotic devices would allow patients to continue rehabilitation at home [2].

The rehabilitation robots developed in the last years can be classified roughly in passive systems, which act as support and stabilizer of the limb, active systems, relying on actuators to guide the patient through predefined movements, and interactive systems, which include more sophisticated control paradigms that react to the patient's actions [8]. The most commonly used paradigm is to use robotic devices for physically supporting the patient during the execution of certain movements [2, 8–13]. However, robotic systems offer far more possibilities than just the repetition of simple and stereotyped movement patterns. For example, they can generate a more complex, multisensory stimulation, they can provide the patient with extrinsic feedback containing information on his performance during training, or they can create a more engaging environment by using virtual reality concepts [6]. Another advantage is that such devices can promote recovery by distorting reality. One example is the implementation of an error-augmenting strategy, i.e. the application of a force that pushes the patient away from the desired trajectory. Indeed, preliminary results have shown that this approach can have positive effects on the patient's functional recovery [2].

Moreover, robotic systems can measure and record a variety of variables during therapy, such as the patient's position, velocity and acceleration, or the amount of support provided by the system [2, 6, 8]. The recorded data can be used for online and offline processing, allowing to evaluate several indicators related to the patient's performance [8]. Such measured parameters could offer a substantial improvement over current evaluation techniques, as they would provide quantitative and objective data in contrast with today's most used assessments, which rely heavily on subjective judgments made by the clinician [2].

It has been reported by various authors that the use of robotic systems in neurorehabilitation improves the patient's recovery and quality of life, especially when the robot-assisted therapy is administered in the subacute phase and when it is combined

with traditional treatment [8, 14–17]. However, many of these results are contradictory, and not all robotic systems have undergone rigorous clinical testing [6]. Furthermore, there is a lack of data showing improvements on measures related to activities of daily living [16], and some experimental evidence indicates that to date robotic training fails to transfer to improvement on the functional level [8]. As a result, the effectiveness of robotic rehabilitation is still being discussed [6].

Even though to date there is not yet enough evidence to definitely confirm the efficacy of robotic therapy, the development of these systems is still in an early stage and the potential of robotics in rehabilitation is still unexploited [8, 15]. Many of the developed systems have been designed from an engineering perspective rather than based on therapy demands, and most rehabilitation paradigms are based on the repetition of stereotypical movements instead of applying more advanced principles of motor control and motor learning [6]. Robot-assisted therapy would offer an ample set of technologies and tools to implement very complex rehabilitation protocols, but there is a lack of quantitative information on the effects of stroke on motor control. In fact, a better understanding of how motor control and muscle coordination patterns change after stroke could help developing new rehabilitation protocols, and suggest new strategies for personalized treatments targeting the deficits of each individual patient [18–20].

A promising methodology that could give us a better insight in how muscle coordination is achieved, and that could help us quantifying the effects of stroke on a neuromuscular level, is the analysis of muscle activation patterns from the perspective of motor modules. It has been suggested by various authors that the activity of a large number of muscles could be explained by the activation of a very limited set of motor modules [21]. Each module controls the activity of a group of muscles, which it activates synchronously. This strategy would significantly reduce the complexity of motor control, allowing the central nervous system to generate complex movements by controlling just a few motor modules. Motor modules would therefore represent fundamental strategies to achieve muscle coordination. Recent studies have shown that these coordination strategies are very similar across different subjects, and that they are significantly affected by stroke [19, 22].

The focus of this study is to gain a better understanding of how muscle coordination of the upper limb is achieved and how it changes after stroke, and to apply this information to rehabilitation concepts. We recruited 15 healthy control subjects and 14 mildly to moderately impaired stroke patients, and recorded their muscle activity and movement kinematics while they executed a wide variety of fast reaching tasks. The recorded data was used to extract the motor modules of each subject. Coordination patterns found in healthy control subjects were used to generate a reference model to which we could compare the motor modules each stroke patient. The analysis was performed by looking at the number of modules used by each subject, by matching the muscles participating in a module, and by observing the activation pattern of each module. As will be presented in the discussion, the results were used to identify the most significant coordination strategies used by healthy control subjects, and to see how these strategies changed in stroke patients.

Chapter 1 will give a brief overview on motor control and introduce the theory of motor modules. We present this concept from the perspective of different authors and mentioning various studies that either support or criticize the existence of motor modules as a fundamental building block of motor control.

Chapter 2 presents the techniques for recording and analyzing electromyographic data. Electromyography is the most common tool to study the activation and coordination of muscles and was used also in this study. In this chapter we discuss the neurophysiological origin of the electromyographic signal, how it can be properly measured, and how it can be processed and interpreted.

Chapter 3 explains the computational methods used to extract motor modules from the recorded muscle activation patterns, showing how to prepare the inputs to the algorithm and how to interpret the outputs.

Chapter 4 describes the materials and methods used in this study, giving an overview of the experimental protocol, of the used instrumentation and of the techniques used to process and analyze the recorded data.

Chapter 5 presents the main results, starting from the extracted modules and ending at the differences found between the coordination strategies of healthy subjects and stroke patients. These results will be further examined in the discussion section.

Chapter 1

Motor modules: a tool to explain muscle coordination

This chapter aims at giving a general overview on motor control, explaining fundamental concepts of how the CNS might achieve such a complex task. In the second part we introduce the concept of motor modules as a strategy to explain motor control in a simplified way and we show how the underlying theory developed throughout the years. The end of the chapter is dedicated to stroke, on its effects on motor control and on how recent studies try to explain the resulting motor impairments by alterations in motor modules.

1.1 Motor control: a quick overview

Motor control is a multidisciplinary field, which combines aspects of biomechanics, neuroscience, cognitive science and other scientific areas, to study how movements of the human body can be generated [23]. From a mechanical point of view, movement is initiated by the presence of a force, generated by the activity of one or more skeletal muscles. By contracting these muscles, forces and torques are generated in the joints of the skeletal system and, when properly coordinated, they allow humans to perform a wide variety of motor tasks. Each muscle consists of many muscle fibers, their number depending on the type of muscle, which act in parallel. Muscle fibers are the main force generators, each of them adding a fraction of the total muscle force. Normally not all fibers are active at the same time but follow a cyclic recruitment pattern that alternates active periods with resting periods in order to reduce fatigue. The higher the force generated by the muscle, the more fibers will be active at the same time, and the shorter the force can be maintained before fatigue occurs [24].

The activity of muscle fibers is controlled by motoneurons. A single motoneuron may innervate multiple muscle fibers, the union of the motoneuron and all its muscle fibers is called motor unit. All muscle fibers within a motor unit activate together and almost at the same time (there is a small time delay due to a difference in length of the axons). The axon of the motoneuron connects to the muscle fibers through specialized synapses, called neuromuscular junctions, which transmit the activation signal (action potential) to the fiber. The motoneuron is in turn connected to the descending neural pathways in the spinal cord, thereby forming a bridge between the central nervous system (CNS) and the muscles (see figure 1.1).

The way the signals coming from the spinal cord and transmitted to the motoneurons are generated is still not fully known. The current idea is that motor control is structured on three levels: a low level control on the segmental level, an intermediate control on the projection level and a high level control on the precommand level.

The segmental level is the lowest level of the motor hierarchy and consists mainly of spinal cord circuits. Segmental circuits stimulate specific groups of muscles and some of them, called central pattern generators (CPGs), control locomotion and other oft-repeated motor activities. CPGs consist on networks of oscillating inhibitory and

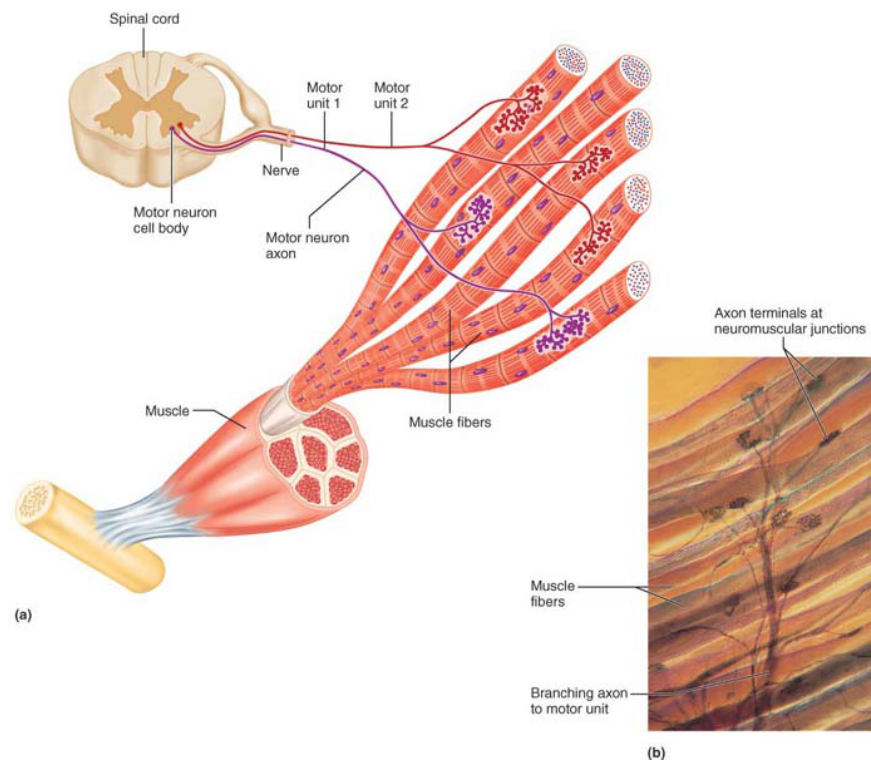


Figure 1.1: (a) Schematic view of two motor units: the cell body of the motor neurons reside in the spinal cord and their axons extend to the muscles, each axon divides into axon terminals which innervate muscle fibers. (b) Photomicrograph of a portion of a motor unit ($80\times$) [24].

excitatory neurons, which set crude rhythms and alternating patterns of movements [24].

The projection level has direct control over the spinal cord. It consists of two systems, a direct (pyramidal) system and an indirect (multineuronal) system. The direct system is initiated by neurons of the motor cortex and is in charge of producing discrete voluntary movements of the skeletal muscles. Each skeletal muscle has a specific representation in the primary motor cortex: muscles of the left side in the right hemisphere and muscles of the right side in the left hemisphere. The size of the area that projects to a certain part of the body is proportional to how finely its movements can be controlled. The map of the projected body parts in the motor cortex is called the cortical homunculus (figure 1.2).

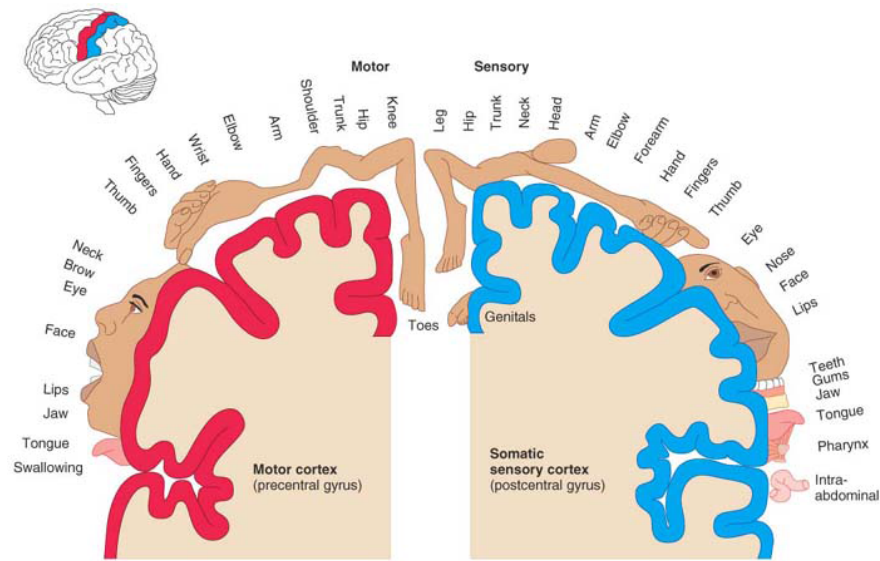


Figure 1.2: Motor and sensory areas of the cerebral cortex. The relative size of each body area in the drawing represents the relative amount of the cerebral cortex dedicated to that body area. The amount of the gyrus occupied by the body diagrams indicate the amount of cortical tissue assigned to that function. [24]

The indirect system on the other side is controlled by some areas of the brain stem and supervises the activity of the segmental apparatus, thereby influencing reflex and CPG-controlled motor actions. Information coming from the projection motor pathways is both transmitted to lower motoneurons and to higher command levels as an internal feedback. Even though direct and indirect systems provide separate and parallel pathways to control the spinal cord, they are interrelated at all levels.

The precommand level consists of two additional systems, located in the so called precommand areas, which control the outputs of the motor cortex and the brain stem. The cerebellum is responsible for an online sensorimotor integration and control. It receives ascending proprioceptor, tactile, equilibrium and visual inputs, and information coming from the motor cortex and the brain stem. All this information is used to rapidly correct errors in motor activity and fine-tune movements. Even though it lacks a direct connection to the spinal cord, the cerebellum can act on motor pathways through the projection areas of the brain stem and the motor cortex via the thalamus.

The second system of the precommand level is located in the basal nuclei. Compared to the cerebellum, the basal nuclei seem to be involved in more complex aspects in motor control. They act primarily as a control system for the activity in the premotor cortical area, to which they are connected through the thalamus. The basal nuclei have two main functions, which happen unconsciously. The first is the inhibition of various motor centers of the brain under resting conditions. The second is the planning of complex motor tasks in advance of willed movements [24].

Even though the layout of the signal pathways allowing motor control is fairly clear, it is not yet fully understood how movements are actually planned and generated. Many theories have been developed in the past years, but there is not enough evidence for any of them. The next paragraphs will introduce a theory used throughout the rest of this thesis work and claiming that motor control is achieved through a modular organization.

1.2 Patterns underlying muscle coordination

A central problem in motor physiology is how the activity of many muscles is coordinated to produce movement. In this context, motor coordination is the process by which the degrees of freedom of the nervous system interact to produce a purposeful movement [25, 26]. To generate a purposeful behavior, the central nervous system has to coordinate the many degrees of freedom of the musculoskeletal system [27]. Besides controlling the activity of a large amount of motor units, a challenging task by itself, the CNS has to take into account biomechanical constraints of the musculoskeletal system, dynamic properties of the body, task-specific parameters such as movement kinematics, and many other factors which make the problem even more complex. In many circumstances, the CNS cannot rely on sensory feedback, but must use an open-loop control law to generate appropriate muscle patterns. Implementing such a controller, however, presents a great computational challenge because it requires mapping a potentially infinite number of different goals onto an infinite set of muscle patterns [21]. These remarks have led many authors to believe that the CNS adopts simplifying strategies to overcome the complexity of motor control [26, 28–31].

In 1906 Sir Charles Sherrington published *The Integrative Action of the Nervous System*, where he introduced the concept of synapse and postulated that the reflex is

the simplest unit of nervous integration and co-ordination. According to Sherrington, complex and unified behavior is enabled by the interaction of elementary reflexes [32], and temporal sequences of reflexes can generate the complex motor behavior seen in mammals [33, 34].

Brown took Sherrington's work one step further, bringing it closer to the current idea of modular motor control. While Sherrington hypothesized that the rhythmic muscle activation might be generated through sensory feedback (reflexes), Brown showed that locomotion is possible even when the afferent nerves responsible for feedback were put out of action [35]. He hypothesized the existence of two antagonistic units of motor output located at the spinal level, which could be responsible for the rhythmic excitation of limb flexion and extension. He also proposed that the alternation between the two units was determined by a fatiguing inhibiting action of one unit over the other.

In 1981 Grillner hypothesized the *unit burst generator model*. Unit burst generators are control elements that can produce rhythmic bursts of output at a single joint. Burst generators at adjacent joints are interconnected and can generate synergistic activation patterns: the unit burst generator at one joint can either excite or inhibit an adjacent generator, thereby producing complex biomechanical output [29, 36].

Jordan postulated the existence of neural networks at the spinal level that he called modules and that could represent various units of motor output [37]. These modules could work together and produce motor output by activating a set of motor neurons and by inhibiting some motor neurons of antagonistic muscles.

Evidence supporting the aforementioned claims was collected mainly through experiments on animals, over which Tresch et al. provided a good overview [26]. Stein and collaborators examined the possibility of a modular organization of motor control in the turtle [38–42]. They found that in the spinalized turtle (i.e. with complete transection of the spine) one could evoke rhythmic motor behavior by continuous cutaneous stimulation of certain areas. Three different forms of scratch reflex could be evoked by changing the location of the cutaneous stimulus, and were characterized by a temporal reconfiguration of three fundamental units of motor behavior which could be reconfigured in a flexible way. Furthermore, they found that these units of motor output were distributed throughout different spinal segments, but they could not locate the systems producing each distinct type of scratching [43].

Another set of experiments was performed on the mudpuppy (*Necturus maculatus*) [44,45], giving similar results. Application of NMDA to some locations of the severed spinal cord (even just of a single cervical segment) generated a rhythmic walking motor pattern in the forelimb muscles. Cheng et al. [44] discovered that different components of this motor rhythm were generated by specific segments of the spinal cord. This suggested that the motor activity during locomotion of the mudpuppy was achieved through the activity of distinct neuronal networks localized in different sections of the spinal cord. Interestingly, the authors found that stimulation of a single caudal spinal segment would produce extension of the forelimb, while the rostral segment would produce flexion.

Similar experiments were performed also on frog preparations, and led to the formulation of a similar hypothesis as for turtle and mudpuppy [46–48]. Bizzi, Mussa-Ivaldi and Giszter stimulated specific areas of the spinal cord in spinalized frog, finding evidence suggesting that the spinal neural circuits are organized in a modular way [49]. The force responses of microstimulation of the gray matter were summarized as force fields that converge to an equilibrium point, and the simultaneous excitation of two different areas would result in a linear summation of the two respective force fields. The combination of these equilibrium paths could explain a large variety of motor behavior. They concluded that fixed-pattern force fields elicited in the spinal cord may be considered movement primitives [46, 48]. More evidence was provided by Kargo and Giszter [50], whose experiments studied the execution of wipe reflexes in the spinalized frog. They stimulated the wiping reflex by cutaneous stimulation, and found that the electromyographic patterns during wipe could be explained by the superposition of at least three components, i.e. units of motor output. Furthermore, they found that these units of motor output could be flexibly reconfigured by the spinal cord to produce correcting movements in order to avoid obstacles. Saltiel et al. [51] applied NMDA iontophoresis to different areas of the transected spinal cord, discovering that different stimulation sites would evoke different motor behaviors. This suggested that production of motor output could be achieved through the coordinated action of simple units located in particular regions of the spinal cord.

Although locomotion of mammals can be more complex than that of the previously mentioned animals, evidence collected in some studies supports the hypothesis that their locomotor systems might rely on a modular structure. However, due to the difficulty

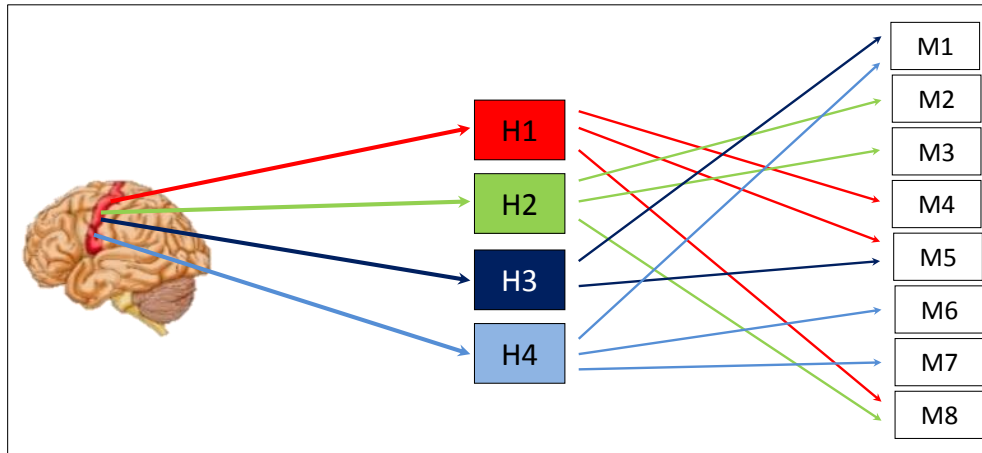


Figure 1.3: Motor modules could simplify motor control. In this example, the activity of four modules (H_1 to H_4) is controlled by descending signals. Each module is associated with a certain number of muscles, modulating their activation profiles. This shows how a limited number of signals can control a larger number of muscles (in this case eight, M_1 to M_8), thereby simplifying the control problem.

in evoking locomotion in spinalized mammals, there is still no clear consensus as to whether this modular organization is actually present in the spinal cord [26]. Even though the motor pattern produced by spinalized animals is simpler than during normal locomotion, Grillner and Zangger [52] studied the spinalized cat, stimulating the isolated spinal cord, and reported a strong coupling of flexor muscles at one joint with a looser coupling with muscles acting on other joints. Furthermore, they provided evidence that even the spinalized animal could generate muscle activity patterns similar as in normal locomotion. It has also been shown that, given sufficient rehabilitation training, the spinalized animal could recover a motor behavior very similar to locomotion [26]. Thus, the neural networks in the spinal cord are capable of reproducing this behavior even after transection. As in the mudpuppy, researchers found evidence for the localization of different units of motor output in the spinal cord. Some studies on cats and rats even confirmed the rostrocaudal localization of flexor and extensor units [53–55].

In the past decade a new and promising way to explain motor control has gained ground, claiming that the number of variables controlled by the CNS can be greatly reduced by a modular organization of muscles. Motor modules, also called synergies by

some authors, are groups of muscles that activate synchronously to produce a specific biomechanical output. Each module is characterized by a set of muscles that is part of the module and by its activation profile. Since the activation profile acts on all muscles that participate in the module, it could potentially represent the descending neuronal signal controlling the module (see figure 1.3). Various studies have shown that a very limited number of such modules would be sufficient to describe the activity of many muscles, thereby effectively reducing the complexity of motor control. In fact, the CNS could only be in charge of coordinating the activation of a small set of modules, which in turn would be responsible of organizing the activity of all motor units involved in a specific task. It has been shown in literature that motor modules can effectively describe muscle activation patterns in both animals and humans, and for both isometric force generation and dynamic tasks. However, it is not yet completely clear if modules represent actual neural structures, and at which level of the CNS they are positioned.

1.2.1 Motor modules may simplify muscle coordination in animals

Building upon the evidence supporting the hypothesis of a modular organization of motor control, many authors tried to further analyze these motor modules and to understand their role in muscle coordination. The method adopted by most authors is to record electromyographic data during natural behavior or while certain stimuli are provided to the nervous system, and then to look for repeating patterns in the EMG activity. In fact, if motor control relies on a modular strategy, then this should be visible by inspecting the muscle activation patterns.

Tresch et al. studied the muscle responses during isometric contraction of hindlimb muscles in 7 spinalized adult frogs [56]. They fixed the frog's limb on the horizontal plane and at a predefined angle, and applied cutaneous stimulation to certain areas of the leg. At the same time electromyographic data of 9 muscles was recorded through fine wire electrodes. By using a computational analysis (see chapter 3 for details) they looked for common activation patterns in different muscles, assuming that muscles activating synchronously would be controlled by the same module. They found that the combined activity of 4 distinct modules could account for more than 90% of the variance in the EMG signals. Furthermore, even though stimulation of certain areas could evoke similar modules as found in other areas, many skin areas evoked very different modules. This

led the authors to the conclusion that motor control might use a modular strategy, but that different responses might be obtained through the activity of different modules.

Another study on isometric contractions was done by Saltiel et al. [27]. They positioned the hindlimb of 10 spinalized frogs on a force sensor at a fixed angle and stimulated intraneuronal sites of the ipsilateral spinal cord through NMDA iontophoresis. EMG activity of 12 leg muscles was recorded and analyzed. They used a computational method to extract motor modules from the EMG data of each frog, and then from the pooled data of all frogs. They found that 4 to 8 modules were sufficient to explain the muscle activity of each frog, and that the extracted modules were quite similar between frogs. Furthermore, 7 modules would explain more than 91% of the variance in the pooled data, and these 7 modules were very similar to those obtained by clustering the individual modules of each specimen. Another interesting result is that these 7 modules obtained from the pooled data could generate most modules extracted from a single frog through a linear combination. This suggested that all frogs had a similar modular organization of motor control, even though some specimens would combine some modules in a preferred way.

D'Avella, Saltiel and Bizzi changed the approach slightly and looked at muscle activation patterns during unrestrained motion of intact frogs [21]. The authors analyzed the activation patterns of 13 hindlimb muscles during defensive kicking movements in different directions. The kicking action was initiated by cutaneous stimulation. They showed that three time-varying modules could explain most of the EMG signals, and they were able to give each of them a biomechanical meaning. Additionally, these three modules proved to be very consistent across animals, and that a subset of these modules could be found also in other behaviors such as swimming or jumping.

In 2005 Cheung et al. attempted to combine the concepts exposed in the aforementioned studies [57] by analyzing the modular composition of muscle activation patterns in frogs before and after spinal deafferentiation. They recorded EMG activity of 13 hindlimb muscles of bullfrogs before and after deafferentiation during swimming and jumping. The deafferentiation procedure was performed by severing some descending pathways at the seventh vertebra. They found that, to a large degree, the extracted modules were shared between the intact and deafferented preparations. This result suggested that most motor modules describing frog locomotor behaviors could be centrally organized structures

activated by spinal and/or supraspinal commands. However, since both amplitude and temporal activation of the modules were significantly altered by the deafferentation, the authors concluded that these parameters were regulated by feedback given by sensory inflow.

D'Avella and Bizzi confirmed these results with a similar study, where they looked at characteristic muscle activation patterns of the frog's hindlimb during a variety of jumping, swimming and walking tasks [58]. Their results support the hypothesis that motor control might adopt a modular organization, and show that a small set of 5 motor modules could explain most of the EMG activity in each task. They also discovered that many of these modules were shared across tasks, while some seemed to be task-specific.

Ting and Macpherson performed an experiment aimed at understanding if motor modules could underlie postural tasks in cats [59]. They positioned three cats on a moving platform and recorded the EMG activity from some hindlimb muscles. The platform was inclined in 16 different directions, and the EMG recordings were used to analyze how the animals would adapt to the different perturbations. Motor modules were extracted through computational techniques from the pooled EMG data of all perturbation directions. Furthermore, the recorded ground reaction forces during all trials. Results show that four modules are sufficient to explain more than 95% of the EMG variability, and that each module could be associated with a unique force vector. This suggested that postural modules might be organized to control endpoint force during balance task. Building on these results, Torres-Oviedo, Macpherson and Ting designed a second set of experiments where they assessed whether these modules were able to describe postural adaptations at various stances characterized by a different fore-and-hind paw distance [60,61]. These experiments showed that 5 modules could describe the muscle activation patterns during all different stances and for all perturbations, and that 4 of these modules were similar to those found in the previous experiment (see [59]). Each of these functional modules was characterized by a unique force vector, as calculated from the ground reaction forces. Interestingly, the ground reaction forces could be reconstructed well by using the activity of each motor module and by summing up the respective force vectors. All results were very similar across animals.

Overduin et al. investigated the possibility of a modular organization of motor control in primates [62], observing the EMG activity of two rhesus macaques during pick

and place movements. The two primates were trained to grasp objects of different shape and mass and to transport them to a predefined position. Intramuscular electrodes were implanted in 15 to 19 forelimb muscles acting on hand, wrist, elbow and shoulder. The authors found that three time-varying modules could describe all grasping movements quite well, and that these modules were consistent across animals. They also found that these modules were scaled in amplitude and shifted in time depending on the properties of the grasped object.

An analogous study was performed on frogs by Cheung, d'Avella and Bizzi [63]. The authors observed different motor behaviors of four bullfrogs with and without inertial perturbations, and compared the motor modules resulting from the analysis of each study condition. EMG activity of 13 hindlimb muscles was recorded during natural behaviors before, during and after the application of an additional weight to the calf. The results showed that most modules were shared across all loaded and unloaded motor behaviors, although their amplitude and onset times were significantly affected by the loading and depended on the motor task. This led the authors to the conclusion that motor modules are robust across different dynamic conditions and that the CNS can quickly compensate for perturbations by modulating their activations.

Roh, Cheung and Bizzi designed an experiment to determine the localization of the neuronal structures responsible for the modular composition of motor control. [64]. 9 adult bullfrogs were implanted with 13 intramuscular EMG electrodes in the hindlimb and were observed during activities such as jumping, swimming, kicking and stepping. The descending motor pathways of all frogs were subsequently transected at the height of either brain stem, medulla or spine. Motor output was evoked through cutaneous stimulation certain skin areas. One interesting fact showed by the results was that the motor modules activated by animals transected at the brain stem or medulla were very similar to those found prior to transection, and that medulla and spinal cord might be sufficient for the expression of motor modules in most behaviors. This supported the hypothesis that motor modules might rely on neuronal structures located within the brain stem and the spinal cord and activated by descending commands from supraspinal areas.

In a very recent study, Overduin et al. evoked involuntary hand movements in two rhesus macaques through intracortical microstimulation (ICMS) [65]. They wanted to see

whether ICMS could evoke hand movements towards specific final postures and whether the muscle activation patterns could be described with motor modules. Indeed ICMS could systematically drive the hand and digits towards particular postures. Furthermore, the muscle activation patterns evoked by ICMS were very similar to those found in a previous study on voluntary grasping movements [62]. The fact that stimulation of the motor cortex would activate the same modules found in voluntary movements led the authors to the conclusion that ICMS acted on areas projecting to neuromuscular structures in the spinal cord, similar to those hypothesized by Roh [64].

All these studies provided evidence supporting the hypothesis that motor control could be built upon a modular structure. Many different animals seem to adopt similar control strategies, in both intact and spinalized preparations. This suggests that motor modules might be implemented as neuronal structures localized at a spinal level, and that they might be able to generate motor output by either following commands coming from a supraspinal level or by relying on sensory feedback. The variety of animal species showing evidence of a modular motor control strongly supports the hypothesis that humans might implement a similar control strategy.

1.2.2 Evidence for a modular organization of motor control in humans

Similar methods of analysis as already mentioned in the previous section, although only in their less invasive form, were applied also to humans. These experiments reflect the effort of various authors to understand how the human nervous system manages to control all its degrees of freedom, and whether our motor control system could rely on a similar modular organization as observed in other species. The vast majority of these studies are based on the observation of muscle activation patterns during voluntary movements or isometric contractions, and can be subdivided into experiments on the lower extremity (mainly gait analysis and pedaling) and on the upper extremity (e.g. reach and grasp, hand postures or isometric force generation).

Lower extremity

One of the first studies addressing the possibility of a modular neural control strategy for human gait was done by Ivanenko et al. in 2003 [66]. The authors studied a group of 11 patients with spinal cord injury (SCI) and a group of control subjects walking on a

treadmill with body weight support. EMGs of leg, trunk and arm muscles were recorded during most trials, and motor modules were extracted from the average muscle activation patterns over one gait cycle. The authors reported that patients were able to recover shape of the foot motion after sufficient training, even though the muscle activation patterns differed substantially from the healthy controls. However, they also showed that in both control subjects and patients 5 modules could account for most of the EMG variability, and that after training the time-varying activation profiles of these modules were strikingly similar between the two groups. On the other side, the muscle weights of each motor module were significantly different between controls and SCI patients, suggesting that the neuroplastic recovery after the injury might have rewired the neural networks related to each module. Ivanenko, Capellini and collaborators repeated similar experiments only on healthy subjects, which were asked to walk or run on a treadmill at different speeds [67, 68] and to perform other tasks such as kicking a ball, walking over obstacles or reach down to grasp an object [69]. The results confirmed what was seen in the previous study, i.e. that 5 basic units of motor output could explain more than 90% of the total EMG variance. Furthermore, even though muscle activation patterns were significantly affected by the study condition, the basic components hidden in the EMG signals were very stable from condition to condition.

Morin extracted motor modules from the EMG recordings of 6 lower limb muscles during normal gait [70]. The author found that four or five modules could describe most of the variance in the muscle activation patterns, and that at least two of these modules were very consistent across all 7 subjects. Additionally, all modules could be associated with biomechanical functions corresponding to specific phases of gait.

Torres-Oviedo and Ting expanded their set of experiments on the postural control of cats to humans [71]. In this study of 2007, they observed the muscle activity of 16 muscles of the lower back and leg during the adjustment to postural perturbations. Nine healthy subjects were asked to stand on a moving platform that could translate in 12 different directions on the horizontal plane, and had to adopt different stances. For each subject, a few motor modules (six or less) were found to reproduce the muscle activation patterns well, and most of the trial to trial variation could be accounted for by adaptations of the time-varying activity of each module. Furthermore, all subjects exhibited motor modules that had both a similar distribution of muscle weights and

similar activation patterns.

An interesting analysis was presented by Neptune, Clark and Kautz, which showed experimentally that motor modules could represent actual biomechanical functions [72]. The authors extracted four modules from experimental data of 14 healthy subjects and used them to drive a computational forward dynamics simulation of a complete gait cycle. Results showed that the simulation could be driven with the experimental muscle weights of each module and with activation patterns that were very similar to the ones collected experimentally. Since each module was active during a specific phase of gait, and could therefore be associated with a biomechanical subtask, the fact that walking could be generated by just using these modules suggested that motor modules could represent specific biomechanical functions.

Clark et al. hypothesized that walking in healthy subjects is achieved through the variable activation of a small set of motor modules [22]. They tested this hypothesis by recording EMG signals of 8 leg muscles and of 20 healthy subjects, which had to walk on a treadmill at various speeds. They saw that four modules were typically enough to reconstruct the muscle activation patterns at self-selected speed, each of which was phased to a particular region of the gait cycle. The same muscle weightings could describe the muscle activity of a wide range of walking speeds, needing only an adjustment of the respective activation profiles. Similar results were obtained also by McGowan et al. [73], who performed another simulation study and showed that modules could consistently describe muscle activation patterns even when the mechanical demands were altered, i.e. when the subject's weight was increased or decreased by up to 25%.

Another approach was presented by Hug et al., who analyzed the activation of 11 leg muscles during cycling [74]. Eleven well trained cyclists were asked to pedal with varying velocity-torque conditions and with different body postures. Speed was varied between submaximal and all-out sprint while changing the resisting torque, and body postures varied between seated and standing. Interestingly, whatever the mechanical constraints, three motor modules were enough to explain most of the EMG variability. Moreover, the three modules were very stable across conditions and between subjects. This study provided additional evidence to confirm the hypothesis that the nervous system can select, activate and flexibly combine motor modules to produce motor output.

Chvatal and Ting investigated the effect of perturbations to walking and the stability

of motor modules throughout different conditions [75]. They recorded the electromyographic activity of 16 muscles in the right leg of nine healthy subjects while these were walking along a straight path low or self-selected speed. When stepping on a force plate, this plate would shift in one of four possible directions, thereby applying the perturbation. For all subjects, six to eight motor modules found in unperturbed walking were able to describe the muscle activation patterns of all studied conditions, ranging from different walking speeds to different directions of perturbation. However, consistent with previously published results, they found a significant variation in module activation patterns during perturbed walking. In another study [76], the same authors hypothesized that similar motor modules could coordinate muscle activity in reactive balance, as tested in [71], and walking at various speeds, as seen in [75]. They found that the muscles activated in response to different perturbations were very similar between standing and walking, even though there were important changes in the amplitude of activation. Motor modules were extracted from each study condition individually, showing great consistency between conditions, and then separately for all walking and all standing recordings. Modules extracted from walking and standing had a significant similarity, suggesting that different motor tasks could rely on the same modular control strategies.

Upper extremity

An experiment very similar to the one presented in this thesis was done by d'Avella et al. [77]. The authors investigated the possibility that the muscle activity patterns during fast-reaching movements could be explained through a modular organization of motor control. Nine subjects were trained to perform point-to-point movements directed to targets positioned circularly on two vertical planes (parallel to sagittal and coronal plane). In a second phase, they had to execute more complex movements, including via-points and direction reversals. Additionally, the movements were repeated with different loads applied to the subject's hand. Motor modules were extracted from the EMG activity of 19 shoulder and arm muscles, relative only to the point-to-point movements. Four or five modules could explain a great percentage of the EMG activity, and could also effectively explain reversal and via-point movements. Even though modules were consistent throughout all movements, their activation amplitude was tuned to each

specific movement. These results led the authors to the conclusion that the CNS might implicitly implement an efficient model of the dynamics of the musculoskeletal by relying on motor modules. Thereby motor modules could be used as a feedforward mechanism, where each module represents a specific goal in the task space. This feedforward system could then be fine-tuned by a feedback controller to achieve higher performance.

D'Avella et al. repeated the previous experiment with slight modifications, identifying the effect of movement speed on the phasic and tonic component of muscle activation patterns and on the postural response [78]. Five subjects were trained to reach towards eight targets in the frontal plane, while varying movement speed from repetition to repetition. They found that a few motor modules could describe the EMG activity during the movements very well, and all these modules could be associated either with a tonic (gravity compensation and postural control) or a phasic (dynamic control) component of muscle activation patterns. Although modules were consistent across all conditions, the activation coefficients of phasic modules were significantly affected by movement direction and speed, while those of tonic modules were influenced only by the direction. Another set of modules was extracted from data relative to the end of each movement in order to capture postural responses. These modules showed similar properties to tonic modules, confirming that these are mainly responsible for postural control.

While the previous two studies focused on muscle coordination during gross motion, Ajiboye and Weir changed the approach and analyzed the fine-tuning of muscle activation patterns during the generation of hand postures [79]. Seven right-dominant healthy subjects executed the 33 static hand postures of the American Sign Language while EMG of eleven muscles (three intrinsic and eight extrinsic) of the hand were recorded. Motor modules were extracted from the pooled data of a few postures, and were used to predict the muscle activity during all remaining postures. The authors found that on average eleven postures and eight modules were sufficient to represent all 33 postures. Many modules were similar between subjects, although these modules were usually dominated by a single muscle. This showed that motor modules could form a predictive framework for muscle activation patterns.

Muceli et al. investigated the possibility of describing a multijoint reaching task by using just a few motor modules [80]. Eight healthy subjects performed various reaching

tasks on the plane while their arm was supported by a 2-dof manipulandum, and electromyographic activity of 12 upper limb muscles was recorded during each reach. Modules were extracted separately from single-joint movements of shoulder and elbow and from multijoint movements directed to twelve targets placed on a circumference. Results showed that modules extracted from single-joint movements were not well suited to reconstruct the multijoint reaches, as more many modules were needed to get a good reconstruction of the muscle activity. However, modules extracted from only a few multijoint reaches could give a good overall reconstruction. The authors noticed that modules relative to reaches to only three targets were sufficient to describe all movements, provided that the directions of these three targets were sufficiently diverse (the angles between directions should be equally spaced). This showed that a representative set of movements could describe the coordination patterns used for all reaches.

A very recent study of 2012 by Roh, Rymer and Beer was aimed at the analysis of motor modules during isometric force generation at the hand [81]. Eight healthy subjects had to follow a three-dimensional force matching protocol by applying a given force vector to the end-effector of a cable-driven robot. Force magnitude and direction were changed from repetition to repetition, while the application point was held constant. The same procedure was then repeated with different end-point positions. Motor modules were extracted from the EMG signals of eight muscles of the proximal upper limb. Interestingly, four modules were sufficient to explain, on average, 95% of the EMG variance. Furthermore, the extracted modules were very consistent across the different loadings and biomechanical constraints, showing also a great similarity between subjects. The activation magnitude of each module changed with the applied load, but all muscle weights stayed constant across all conditions.

1.3 Stroke from the perspective of motor modules

Stroke is one of the leading causes of death or permanent disability: every year approximately 15 million people worldwide have a stroke. Of these, about six million die and another five million are left with permanent disabilities. Furthermore, the age range of the affected population is extremely widespread. Globally, stroke is the second leading

cause of death above the age of 60 years, and the fifth leading cause of death in people aged 15 to 59 years old [82]. It follows that an effective prevention strategy, together with up-to-date treatment and rehabilitation techniques are of fundamental importance to reduce the risk of disease, increase the quality of life of patients and of their relatives and reduce the burden on the health care system [83].

Stroke is a clinical syndrome characterized by rapidly developing symptoms and/or signs of more or less focalized loss of cerebral function, with no apparent cause other than that of vascular origin [84]. It is initiated by a disruption of blood flow to an area of the brain, that can be caused either by a clot obstructing a blood vessel (*ischemic stroke* - 87% of all cases), or by a vessel that ruptures and bleeds into the surrounding brain (*hemorrhagic stroke* - 13% of all cases).

If the stroke occurs in the motor cortex, it could affect motor control and cause movement dysfunctions like spasticity, muscular weakness and, above all, abnormal movement coordination [85]. Even though the mechanisms underlying stroke are well studied and understood, it is not completely clear how it affects motor control and muscle coordination. Various researchers have studied the consequences of stroke on motor control, and recent work has attempted to explain the alterations in motor control through abnormal muscle coordination patterns, i.e. through changes in motor modules or their activation. In fact, a better understanding of the effects of stroke on motor modules could help developing new rehabilitation protocols, and suggest new strategies for personalized treatments targeting the deficits of each individual patient [18–20].

Quantitative measurements of post-stroke motor impairment have been proposed by various authors as a tool to guide rehabilitation and training. For example, Dewald, Beer and colleagues developed a method to measure abnormal joint torques in the impaired arm [85, 86]. A similar strategy was adopted by Ellis et al., who looked at abnormal joint torque couplings in individuals with severe stroke [20]. Li et al. applied an analysis similar to the extraction to motor modules in a study involving stroke patients [87]. They recorded electromyographic data of thirteen stroke subjects and nine healthy controls and from seven upper limb muscles. Muscle synergies were modeled through a Bayesian network, which was shown to be consistent across subjects and was able to reflect the changes in muscle recruitment patterns after stroke.

Cheung et al. used the theory of motor modules for the first time to explain changes

in muscle activation patterns post stroke [19]. They recorded EMGs from 12 to 16 arm and shoulder muscles from both sides of eight stroke patients having moderate-to-severe unilateral ischemic lesion in the frontal motor cortical areas, and of six healthy control subjects. The analysis of the muscle activity recorded during seven different tasks showed that in seven of eight patients modules for both the affected and unaffected arms were strikingly similar to each other, even though EMGs and arm trajectories were very different. Motor modules were also very similar across subjects, all of which had cerebral lesions in different areas of the motor cortex. They concluded that modules might be located on a lower level, possibly in the brain stem or the spinal cord, and were therefore preserved after stroke. The EMG differences may be described as differences in the spatiotemporal recruitment pattern of these fixed modules.

A similar conclusion was drawn by Clark et al. in a study already mentioned in a previous paragraph. They compared motor modules of 20 healthy control subjects and used during walking with modules of 55 stroke patients [22]. In a first analysis, they found that the impaired walking performance of stroke subjects could be explained by a reduced number of modules, which would result in a limited set of options available to controlling the biomechanical output. Interestingly, they also found that modules of stroke patients were not a completely new set of primitives, but that they could rather be described as a combination of the four modules found in healthy subjects. This suggested that stroke does not affect the structure of motor modules, but rather the subject's ability to control their activation patterns independently.

Gizzi et al. reached a very different conclusion. They measured the activity of muscles of the lower and upper limb and of the trunk during locomotion, and compared the data of 10 patients affected by stroke with that of healthy controls [88]. They confirmed the possibility of a modular control both before and after stroke, finding that four motor modules could describe a high percentage of the EMG signals in all subjects. However, modules of the impaired side of stroke patients were very different from those of the unimpaired side and of healthy controls. In contrast with the two previous studies, they discovered that the activation patterns of all modules were preserved after stroke, and that these were similar across all subjects and tested sides. This suggested the presence of a neural network of central pattern generators that control the activation timings of muscle groups.

A work by Cheung et al. analyzed the changes in coordination of the upper limb after stroke [89]. Thirty-one stroke patients were asked to perform multiple upper limb tasks with both impaired and unimpaired arm, consisting either of virtual reality tasks or point-to-point reaches. EMGs of 10-12 muscles of each arm were recorded and used to extract motor modules. Results showed that the difference in the number of modules between impaired and unimpaired arm depended on the level of motor impairment, as measured by the Fugl-Meyer score. Subjects with a high score had approximately the same number of modules on both side, which had also a high degree of similarity. On the other side, subjects with a low Fugl-Meyer score had less modules on their impaired side than on the unimpaired side. Further data analysis suggested that, for strongly impaired subjects, some of the modules of the impaired side could be explained as a merging of modules of the affected side, while others could be seen as fractioned modules of the unimpaired side. The same data was used in a subsequent study by Allen, Kautz and Neptune [18], who used it to drive a computational forward dynamics simulation. These simulations helped in analyzing the effects of merged modules, showing that different combinations of merged modules have different effects on the biomechanical output and on the walking performance. In most subjects the module controlling plantarflexors was merged with other modules, which was consistent with the reduced control of plantarflexors in all subjects and suggested that therapy should focus on improving forward propulsion and the activation of this muscle group. The remaining motor deficits depended on the combination of merged modules and could be located in different phases of gait. These results led the authors to the conclusion that future rehabilitation techniques should be based on a more detailed knowledge of the motor deficits of a specific patient, which could be evaluated through an analysis of motor modules.

Another experiment focusing on the upper extremity was performed by Roh et al. [81]. Using an isometric three dimensional force matching protocol, they analyzed the activation patterns of several arm and shoulder muscles of severely impaired stroke survivors and of healthy controls. The experimental protocol has already been described in the previous paragraph. They found that the modular organization of motor control was preserved in stroke patients, and that four motor modules could account for most of the EMG variability. The modules controlling predominantly the elbow joint seemed to be preserved after stroke, while those activating the shoulder muscles were significantly

altered. The recruitment of the altered synergies reflected the abnormal task performance of stroke survivors. The authors concluded that the impairments in motor control post stroke might be caused by alterations in the structure of motor modules. They also suggested that new rehabilitation protocols might obtain an increased efficacy by focusing therapy on the impaired motor modules, and that assistive technologies could potentially be useful to restore the original structure of motor modules.

1.4 Criticism against a pure modular control strategy

The aforementioned authors have provided us with evidence supporting the theory of motor modules. However, there is still no conclusive proof for their existence. On the other side, some authors have argued against this theory, showing some cases and examples where it seems to fail.

For example, Kutch et al. found that the force generation at the finger tip seems to rely on a flexible cooperation of muscles rather than on fixed motor modules [90]. The authors asked healthy subjects to perform an isometric force matching protocol at the finger tip and observed how muscle activations changed with force direction. If the CNS used motor modules to generate endpoint force, then there would be many active muscles for every direction. Furthermore, due to signal dependent noise (SDN), the force contribution of each muscle has a certain variability, represented as fluctuations of the endpoint force along the direction of action of that muscle. Therefore, the use of motor modules would imply a significant variance in the generated force regardless of the direction, visible as random force fluctuations outside the main direction. However, the authors found that the force variance outside the main direction is dependent on the direction itself. They also identified three directions where most of the variance was along the main force direction. This means that force was generated mainly by the one muscle whose action was along the given direction, with negligible contribution of other muscles. This implied that muscles can be activated independently, thereby undermining the hypothesis of a modular activation. It has to be noted that the performed tasks were very simple, and as shown by Muceli et al. [80] tasks must be more complex to reliably find motor modules. Furthermore, these results are in contrast with the study by Ajiboye and Weir [79], which supports the use of motor modules in the hand. A possible

conclusion might be that motor control does not rely solely on motor modules, but that it can alternate between a modular control and a flexible combination of muscles depending on the complexity of the task.

In a review on the state of the art in the field of motor modules, Tresch and Jarc compare arguments for and against motor modules [91]. Even though many authors have found evidence supporting the theory of motor modules, others have argued that one could reach the same conclusions by using optimal control theory to obtain a task-relevant subspace of low dimensionality. Additionally, one of the main critiques to the experiments supporting motor modules is that most of them analyze muscle activation patterns during well defined and usually simple tasks. The low dimensionality of the set of modules might therefore be the result of the task constraints might not reflect the real structure of the CNS. In fact, the key to obtaining meaningful modules seems to be the use of EMG signals recorded under a rich enough range of behavioral conditions. Another theory in contrast with a modular control is the uncontrolled manifold hypothesis, which is supported by some authors and states that the CNS might allow for a certain variability in muscle activations, as long as this variability does not prevent the accomplishment of the planned task.

This last hypothesis, also called minimal intervention principle, was supported by Valero-Cuevas et al. [92]. The authors measured intramuscular EMG of all index finger muscles during isometric force generation, and showed that the EMG variability is much more evident in the task-irrelevant subspace and less important in the task-relevant space. This could in fact mean that the CNS might give much more importance to the control of task-relevant parameters, controlling the task-irrelevant parameters with less accuracy. They also found that motor modules could not represent the measured task very well. The authors argued that motor modules might be used by the CNS as a feed forward strategy in an open loop control, while the measured task might have used a closed loop control to accurately match the endpoint force. Furthermore, the task might have been too simple to provide evidence for modules.

While the previous papers focused mainly on alternative theories, Hug made some methodological considerations regarding how surface EMG (sEMG) can actually be used to study muscle coordination [74]. In fact, sEMG has various drawbacks which could affect the extracted motor modules, such as a non-linear representation of muscle force

due to amplitude cancellation, crosstalk and a spatial variability of muscle activity depending on how electrodes are placed. Other problems can be found in how EMG signals are processed. For example, EMGs are usually low-pass filtered in order to obtain the so-called linear envelopes. However, it has been shown that the low-pass frequency significantly affects the number of extracted modules [93]. Furthermore, different techniques for the normalization of the time-scale and of the EMG amplitude can yield very different motor modules. All this means that the results of all studies regarding motor modules should be interpreted carefully, as the methods of data recording and processing have a significant effect on the conclusions that can be drawn.

Another critique is aimed at the actual capability of motor modules to produce biomechanical output. De Ruyg, Loeb and Carroll investigated how well modules could reconstruct the biomechanical behavior in task-space, finding that they can't always provide an accurate representation [94]. Even though some studies have shown that forward dynamics simulations based on motor modules can reconstruct the recorded task kinematics [18, 72], the authors argue that these reconstructions required substantial tuning to obtain the required accuracy. On the other side, they extracted motor modules from EMG recorded during a force aiming task and showed that while these modules could give a good reconstruction of the EMG signals, they performed poorly when used to reconstruct the generated force. This suggested that modules are not well suited to represent parameters in task-space, and thereby reopened the question if they actually represent structures in neural control.

It should however be noted that the debate for and against modules is mainly concerned with their existence within the CNS, i.e. if the CNS uses a modular organization as a control strategy. This doesn't undermine the usefulness of explaining muscle coordination with the theory of motor modules and their potential application in driving future rehabilitation protocols.

Chapter 2

Electromyography

Electromyography, often abbreviated as EMG, is an instrument to measure the electrical activity of muscle fibers. Among other things, it is a powerful tool to measure muscle coordination, which is why it is important to understand how it works before going into the details of how motor modules can be extracted.

The electromyographic signal is acquired by applying electrodes in the proximity of the muscle of interest and by feeding it into a data acquisition system. Depending on the type of analysis, various signal processing techniques can then be applied to extract the desired information. After a short introduction to the physiological nature of the EMG signal, this chapter will describe how muscle activity can be recorded and how electrodes can be chosen and properly placed. In the following paragraphs some of the most important properties of the EMG signal will be reviewed, and the last part of the chapter will provide an overview of the processing techniques used in this research project.

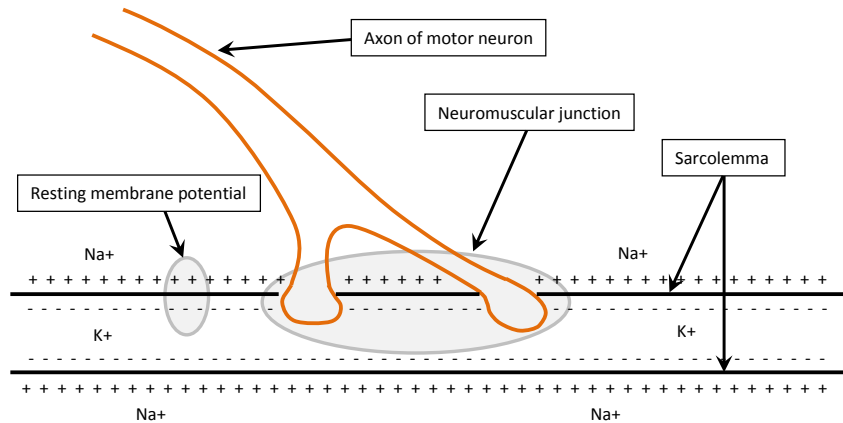


Figure 2.1: Schematic representation of the neuromuscular junction. The axon of the motor neuron connects to the muscle fiber at the motor end plate. At rest the muscle fiber is slightly polarized with a voltage difference of about 90 mV between the two sides of the sarcolemma. Inside the muscle fiber there is a high concentration of potassium (K^+), while outside the prevailing ion is sodium (Na^+). The concentration gradient is kept constant thanks to the impermeability of the sarcolemma to both ions.

2.1 The electromyographic signal

In order to contract and generate force, a muscle fiber must be stimulated by a nerve ending. This stimulus then propagates through the muscle fiber in the form of an action potential and thereby initiates a chemical reaction that causes the fiber to contract. The action potential itself is an electric signal that originates from a ionic flow through the sarcoplasm, the membrane of the muscle fiber. Due to it's cause-effect relationship with fiber contraction, and since it is relatively easy to measure an electric signal, it is common practice to use the action potential as an indirect measure of muscle fiber activity.

In fact, the electromyographic signal is the manifestation of the action potential of one or more muscle fibers as seen by an electrode [95]. As will be explained in the next section, these electrodes can either be placed on the skin over the muscle of interest, or intramuscularly. However, it is useful to explain a few more details of the origin and propagation of the action potential in order to better understand the nature of the

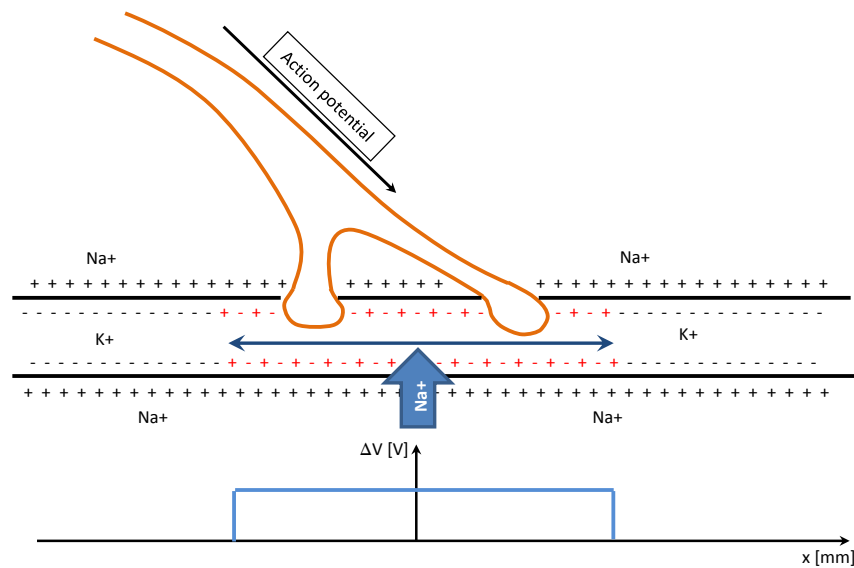


Figure 2.2: Depolarization of the muscle fiber. Once the action potential reaches the axon terminal, the neurotransmitter acetylcholine (ACh) is released. ACh binds to the sarcolemma, opening gates that allow sodium to enter the muscle fiber and potassium to exit. Since the sodium flow is much stronger, the membrane potential decreases and the muscle fiber gets depolarized. The change in potential triggers more adjacent membrane gates, which causes the depolarizing wave to travel along the fiber at a speed of about 4 m/s.

electromyographic signal.

As shown in figures 1.1 and 2.1, every muscle fiber is innervated by the axon of a motor neuron. This connection happens at the neuromuscular junction, also called motor end plate, which is approximately located midway along the fiber's length. Axon terminal and muscle fiber are separated by the synaptic cleft, a 1-2 nm wide space filled with a gel-like extracellular substance that helps transmitting the signal from the axon to the fiber. The sarcolemma separates the inside of the muscle from the extracellular space. Both these regions are characterized by the prevailing presence of certain ions: inside the muscle fiber the prevailing ion is potassium (K^+), while outside there is a high concentration of sodium (Na^+). Furthermore, at rest the muscle fiber is slightly polarized with a voltage difference between the two sides of the membrane of 90 mV (the inside of the fiber is at a lower potential than the outside). This difference in potential

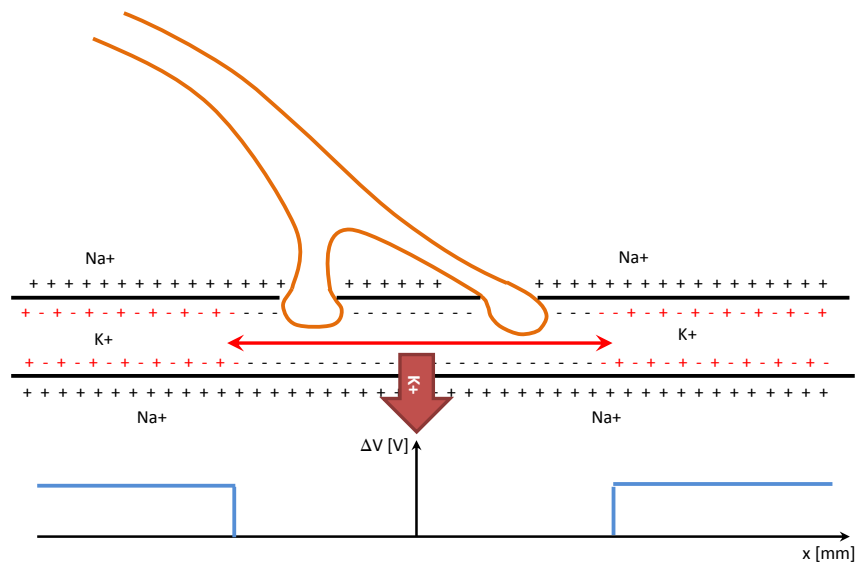


Figure 2.3: Repolarization of the muscle fiber. Shortly after the depolarizing wave, the Na^+ gates close while the potassium increases. Thereby the resting membrane potential is re-established, which is necessary before the fiber can contract again.

and the concentration gradient of Na^+ and K^+ is kept constant by the impermeability of the sarcolemma to both ions.

Once the motor command travels down the neuron and the action potential reaches the termination of the axon, the signal has to be transmitted to the muscle fiber. This happens through the release of acetylcholine (ACh), a neurotransmitter stored in the synaptic vesicles of the axon terminal, which travels through the synaptic cleft and attaches to ACh receptors at the motor end plate. This opens the ion channels in the sarcolemma, allowing sodium to enter the muscle fiber and potassium to exit. Since the flow of sodium ions is stronger, the muscle fiber gets depolarized. The process close to the neuromuscular junction changes the permeability of the sarcolemma, opening new adjacent ion gates. Thus the depolarizing wave travels rapidly (about 4 m/s) to both ends of the muscle fiber in the form of an action potential (figure 2.2).

Shortly after the depolarization, the flow of sodium ions is reduced and new potassium gates are opened, causing the resting membrane potential to be restored. Due to the short time interval between depolarization and repolarization, only a short section of the muscle fiber is depolarized at one time (figure 2.3). The action potential generates

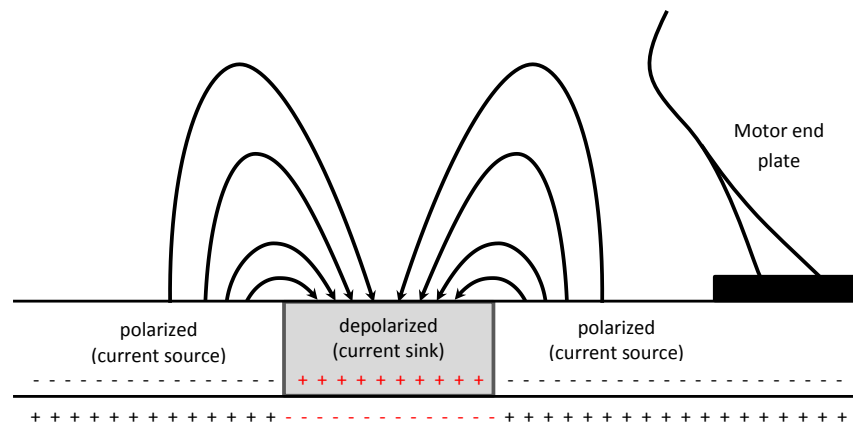


Figure 2.4: Representation of the current field generated by the propagation of the action potential. The localized depolarization of the muscle fiber generates a tripole, where the depolarized zone is referred to as current sink, while the two neighboring polarized sections are current sources. Because the tissue surrounding the fiber is conductive, currents also travel in radial direction.

an increase in the concentration of calcium inside the fiber cell, which in turn initiates the contraction. However, the duration of the action potential is so short (1-2 ms) that by the time the fiber contracts the original electric potential is already re-established (the action potential anticipates the mechanical output by about 10-100 ms).

Because of the short time interval between depolarization and polarization, three distinct zones are created along the muscle fiber: the depolarized zone and two adjacent polarized sections. This generates a tripole, where the depolarized zone is referred to as current sink, while the two neighboring polarized sections are current sources. The main current flow happens parallel to the muscle fiber, but because the tissue surrounding the fiber is conductive, currents also travel in radial direction (figure 2.4). This current field propagates through the neighboring tissue, as does the voltage difference at the leading edge and the trailing edge. However, the amplitude of the signal decreases with the radial distance from the muscle fiber.

The EMG signal results from the spatial and temporal summation of the electric fields generated by all muscle fibers in the proximity of the electrode. It is therefore hard to imagine the shape of the resulting signal. Let's assume for one moment that only one

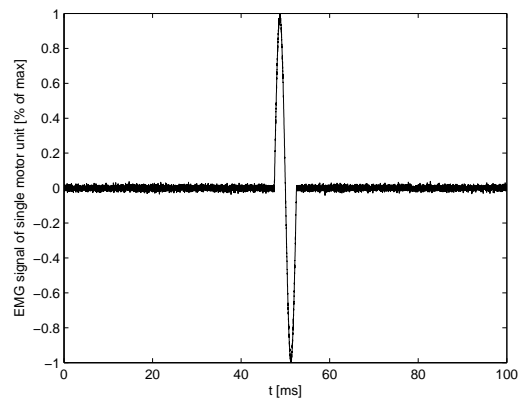


Figure 2.5: Simulated EMG signal generated by a single motor unit and as seen by a bipolar electrode.

muscle fiber is active, and that a bipolar electrode is applied along the direction of the fiber. In this case, we can identify five distinct phases (see figure 2.5):

1. The leading edge has not yet reached either pole of the electrode, both of which are above the polarized zone. The difference in potential measured between the two poles is equal to zero.
2. The leading edge reaches the first pole, and we start detecting a voltage difference. Depending on the adopted sign convention, the difference in potential will be either positive or negative; let's assume it's positive. The signal will increase in amplitude until the whole contact area of the first pole is above the polarized zone.
3. The leading edge reaches also the second pole, gradually evening out the voltage difference between the two poles. The signal decreases back to zero.
4. The trailing edge crosses the first pole, with the opposite effect of phase 2. The measured signal gradually becomes negative.
5. The trailing edge reaches the second pole, and the voltage difference tends again to zero.

The actual electromyographic signal is the superposition of multiple such waves. Since every muscle fiber may activate at a different time, and since the signal coming from each fiber could be more or less attenuated due to different distances from the electrode, the resulting signal has a significant random component that makes it hard

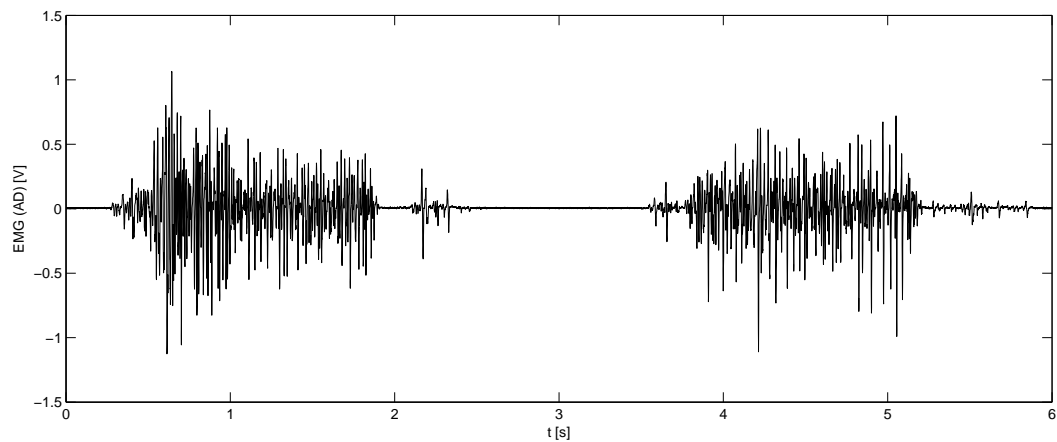


Figure 2.6: Example of an electromyographic signal. It shows the activity of the anterior deltoid muscle during a reaching task, and was recorded with a bipolar electrode with 20 mm spacing. The signal went through two amplification stages, so the showed amplitude is not as seen my the electrode but as recorded by the data acquisition system.

to describe analytically. A typical EMG signal is shown in figure 2.6.

2.2 Acquisition of EMG signals

Electromyographic signals are recorded by placing an electrode close to the muscle of interest. Depending on the type of analysis, the electrode can either be placed on the skin above the muscle or intramuscularly. Furthermore, electrodes can have a single pole or can be bipolar. Bipolar electrodes are by far more common, because they allow to perform a differential measurement which cancels out all noise components common to both poles. In order to acquire a reference potential around which the recorded signals can be centered, another electrode is placed on a neutral body part (usually a bony landmark such as the elbow or the ankle). As shown in figure 2.7, the measurement chain consists of various stages:

- Electrodes applied near the muscle of interest
- A first amplification stage located very close to the electrodes. This preamplifier includes a differential amplifier that measures and amplifies the voltage difference

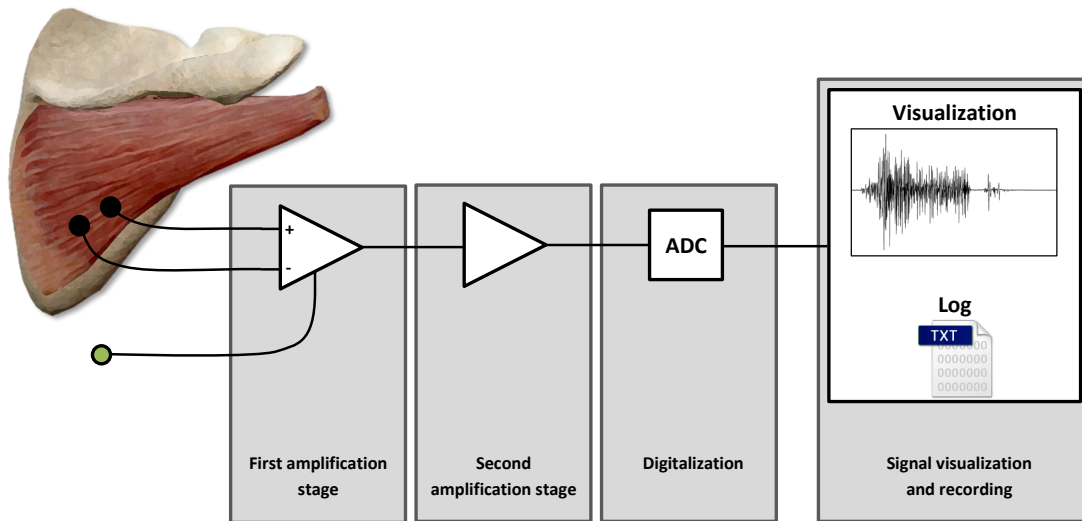


Figure 2.7: Acquisition of an EMG signal. A bipolar electrode is placed along the muscle fiber and a reference probe is positioned above a neutral body part. A differential amplifier is positioned very close to the electrode, and a second amplification stage precedes the analog to digital converter. The digital signal is acquired by a processing unit that can both visualize and record the received data.

between the two poles of the electrode. The gain is usually in the order of $\times 10$ to $\times 20$. Additionally, in most cases it also includes a notch filter that eliminates the frequency of the power supply and a band-pass filter that reduces noise outside the EMG frequency spectrum. It is important to position this stage as close as possible to the electrode, as this helps reducing the effects of the electromagnetic noise picked up by the wires.

- A second amplification stage, needed to bring the signal amplitude from a few millivolts to a few volts. This stage is important as it allows to use the full voltage range of the data acquisition system, which is usually of $\pm 5 V$ or $\pm 10 V$. It is crucial to set the gains of this stage appropriately, as a too low value will use only a part of the available voltage range and will result in a reduced resolution, while a too high value will result in a signal amplitude exceeding the maximum allowable voltage, which causes signal clipping and therefore loss of information.
- An analog to digital converter, which samples the incoming analog signal at a given

frequency and transforms it into digital data that can be processed by a computer. This component is characterized by the admissible voltage range, usually either $\pm 5 V$ or $\pm 10 V$, and by its resolution. The resolution is given by the number of bits that are used to describe the analog signal, and this value usually varies between 8 and 16 bits.

- A processing unit, usually a computer, that receives the incoming digital data and can be used to visualize it in real time and to write it to a file. Data is normally stored in a ASCII text file so that it can be used later on to perform further processing steps and to extract the desired information.

2.2.1 Electrodes

There are two main types of electrodes used to detect EMG signals, surface (or skin) electrodes and inserted (wire or needle) electrodes.

Surface electrodes are the most commonly used type, and can be either passive or active. Passive electrodes consist of one or two conductive detection surfaces that, when applied to the skin, measure the voltage difference between the application point and an electric reference or between the two contact surfaces. The simplest form is made out of two silver disks that adhere to the skin. However, the electrical contact is greatly improved by adding a conductive gel or paste between the electrode and the skin.

Active electrodes add a high input impedance amplifier in the proximity of the detection surface (some types of electrodes have a single housing containing both). They can be resistively or capacitively coupled to the skin. The advantage over passive electrodes is that the the signal to noise ratio is greatly improved.

Since surface electrodes depend on the conductance of the skin layers on which they are placed to acquire the EMG signal, particular attention has to be given to skin preparation. Signal quality can be significantly increased by shaving the application zone, scraping off the layers of dead skin cells and by cleaning the surface with alcohol.

This type of electrodes is particularly popular because they are relatively easy to use and to apply, and because surface EMG is not invasive and can be performed without specialized clinical personnel. However, even though many studies can be conducted by just recording the activity of surface muscles, the main limitation of surface EMG

(sEMG) is that it can't accurately measure the activity of deeper muscles. Furthermore, due to signal dispersion caused by the conductance of the tissue above the muscle fibers, in some cases an electrode placed above one muscle could pick up a signal coming from an adjacent muscle. This phenomenon, called cross-talk, is particularly significant when measuring the activity of small muscles or when multiple muscles are layered on top of each other.

Intramuscular electrodes are either needles or fine wires that are implanted into a muscle. In needle electrodes, one or two stiff cannulas are inserted in the desired location. An insulated wire is contained in the cannula, and only its tip is exposed and acts as a detection surface. Wire electrodes consist of insulated fine wires that are inserted through a hypodermic needle. Since they are more flexible and thinner than needle electrodes, they are easily implanted and withdrawn and are generally less painful.

The advantage of intramuscular electrodes is that they can be used to measure the activity of deep muscles. Furthermore, their detection surface is much smaller than that of surface electrodes and is positioned much closer to the muscle fibers. This means that even EMG of smaller muscles can be measured, and that the problem of cross-talk is significantly reduced. These electrodes give a very localized measurement and can detect the activity of individual motor units even during low force contractions. On the other side, this measurement might not be representative of the activity of the whole muscle. The main disadvantage is that they represent an invasive method. For this reason specialized personnel is required to insert them, and test subjects must be willing to have them inserted.

Due to the limitations of intramuscular electrodes, the lack of appropriate instruments and facilities, and since for the analysis of muscle coordination surface electrodes are generally deemed to be sufficient, in this study we used only surface electromyography. For this reason, the following paragraphs focus on this technique and on the properties of the sEMG signal.

2.2.2 Surface electrode setup and placement guidelines

The setup of the EMG acquisition system greatly influences the properties and the quality of the recorded signal. For this reason, the European Union and its Biomedical Health and Research Program (BIOMED II) have attempted to create guidelines and to initiate a standardization process. The SENIAM project (surface EMG for non-invasive assessment of muscles) provides recommendations for surface electromyography (sEMG) regarding both sensor design and placement [96,97].

sEMG sensors are characterized by various properties, each of which can influence the quality of the resulting EMG signal. One important property is the size and shape of the conductive area of the electrode. Upon an increase of the size in the direction of the muscle fibers, it can be shown that it has an integrative effect on the signal, thereby increasing its amplitude and adding a low-pass filtering effect. SENIAM recommends not to increase the size in the direction of muscle fibers beyond 10 mm. An increase in the size perpendicular to the muscle fibers allows the detection of more muscle fibers. SENIAM does not give clear indications on which shape is best, but recommends to use surfaces with the same geometry when adopting a bipolar configuration. Furthermore, the type of electrode may add some constraints on the possible shapes. For example, for production limitations gel electrodes can only have a circular shape, while dry electrodes are usually circular or bar shaped (elongated perpendicularly to the fiber direction). For bipolar configurations the size of the detection surfaces should be large enough to record a reasonable pool of motor units, but at the same time small enough to reduce the risk of cross-talk. When using circular electrodes, SENIAM recommends a diameter of 10 mm.

Another important property, relative only to bipolar configurations, is the inter-electrode distance. This is the distance between the centers of the two detection surfaces, and SENIAM recommends to keep its value at 20 mm. Furthermore, when measuring particularly small muscles, the inter-electrode distance should not exceed 1/4 of the muscle fiber length. This helps avoiding unstable recordings that would result due to tendon end motor end plate effects.

From the point of view of their design, sEMG electrodes should have contact surfaces made out of a material that creates a good interface with the skin. The electrode-skin

impedance should be as low as possible and the behavior in time should be stable, meaning that the electric properties of the interface should be constant in time. For these reasons SENIAM recommends the use of pre-gelled Ag/AgCl electrodes. The construction of the electrode, i.e. the assembly of electrodes, cables and (if applicable) the preamplifier, should not directly affect the characteristics of the recorded signal. The inter-electrode distance should be fixed, and the material should be lightweight so as to avoid slipping due to inertial effects. Cables should be held in place with tape or an elastic band in such manner that artifacts coming from pulling or electrode slipping can be avoided.

Sensor placement is another important aspect to keep in mind. As already mentioned, a good electrode-skin contact is critical to obtain good EMG readings in terms of amplitude, reduction of artifacts and noise, and of a lower risk of electrical imbalance between electrodes. SENIAM recommends to shave the area of interest if it is covered with hair, to clean the skin with alcohol and to allow the alcohol to vaporize. The skin should be dry before electrodes are placed.

The location where bipolar electrodes should be placed is specific for each individual muscle, but can be based on some general guidelines. First, with respect to the longitudinal location, the sensor should be placed on the muscle belly halfway between the most distal motor end plate and the distal tendon. Regarding the transverse location, the best position is as far away as possible from other subdivisions or muscles. The orientation of bipolar electrodes should be parallel to the direction of muscle fibers so that both detection surfaces pick up the same action potential as it travels along the fibers. It is recommended to use elastic band or tape for the fixation of the electrodes, and to tape part of the cables to the skin so they don't pull on the electrodes. Furthermore, cables should be fixed so that they don't hinder the subject's movements. The reference electrode needs to be placed on an electrical inactive surface such as wrist, elbow or ankle.

Prior to the actual data collection it is recommended to test the signal of each individual muscles. These tests are generally accepted muscle tests which, under normal circumstances, guarantee that the tested muscle is active. However, they don't need to be selective contractions in which only the tested muscle is active.

2.3 Processing of electromyographic signals

After recording EMG signals from a variety of muscles and through the measuring chain shown in figure 2.7, the data can be further processed offline. The processing techniques applied to study muscle activation patterns depend on the type of analysis performed by the researcher and can extract different information from the raw signal. In a study like this, where muscle coordination is the main concern, most authors extract so-called linear envelopes from the EMG signals. Before describing the steps that need to be applied to get these linear envelopes, it is however essential to give an overview of some important properties of the analyzed signal.

2.3.1 Properties of the EMG signal

In the field of biomechanics surface EMG is mainly used for three applications, which are its use as an indicator of the timing of muscle activation, its relationship to the force produced by a muscle and its use as an index of fatigue processes occurring within the muscle [98]. All these applications rely on different properties of the EMG signal: muscle activation timing is related to the time scale of the signal, muscle force to its amplitude, while fatigue can be measured by looking at the frequency spectrum. Here we'll give a short overview of these three properties.

Muscle activation timing is strongly related to the representation of the EMG signal on the time scale. In fact, since the EMG signal is a measurement of the action potential in the muscle fibers, it anticipates the mechanical output of the muscle by a time interval called electromechanical delay. The delay between the EMG signal and the muscle force is variable and depends on a series of factors, such as the type of fibers inside the muscle, and electric and mechanical properties of the muscle. For example, more aerobic and slower fatiguing muscle fibers have relatively slow force rise-times. In general, the electromechanical delay is between 10 and 100 ms. Of course the time delay depends also on the placement of the EMG electrode. Since the action potential travels along the muscle fibers at about 4 m/s, depending on the distance of the electrode to the innervation zone it might be picked up various milliseconds after it starts from the neuromuscular junction [98]. Furthermore, with increasing muscle fatigue the conduction

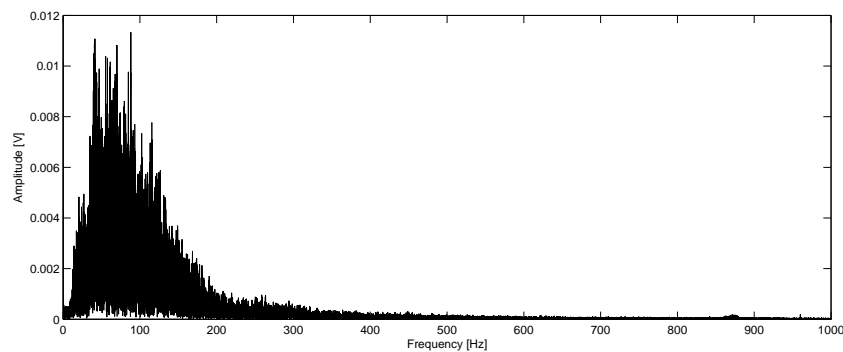


Figure 2.8: Typical frequency spectrum of an EMG signal. This spectrum was calculated on the signal shown in figure 2.6. Most of the signal power lies between 10 and 500 Hz.

velocity decreases [99] and therefore the arrival time of the EMG signal increases.

Another very important factor influencing the timing of the EMG signal is cross-talk, a phenomenon where the EMG electrode placed above one muscle picks up a signal coming from an adjacent muscle. This can be particularly evident if the measured muscle is very small, very close to another muscle or even overlapping other muscles. Cross-talk can make the interpretation of EMG signals quite challenging, as in some cases signals the tested muscle can appear to active when it is not. A similar problem arises when measuring the activity of muscles on the left side of the thorax, where EMG electrodes might pick up ECG noise. However, since during a data collection session the subject's heart beat frequency stays in a known range, it is much easier to remove ECG noise from the EMG signal.

Muscle fatigue has been found to affect the average EMG amplitude, the amplitude of the action potential of motor units and the EMG frequency spectrum [99]. The average frequency has been used by various authors as a measure of fatigue, as it was shown that there is a clear and reliable relationship between the two variables [99, 100].

A typical EMG power spectrum is shown in figure 2.8. In general, the frequency spectrum is limited to the 0 to 500 Hz range, although the dominant energy is within the 50-150 Hz range. However, with increasing fatigue, the whole power density curve is shifted towards lower frequencies with a high frequency decay. This can be measured by using the value of the mean frequency, which decreases linearly as a function of fatigue

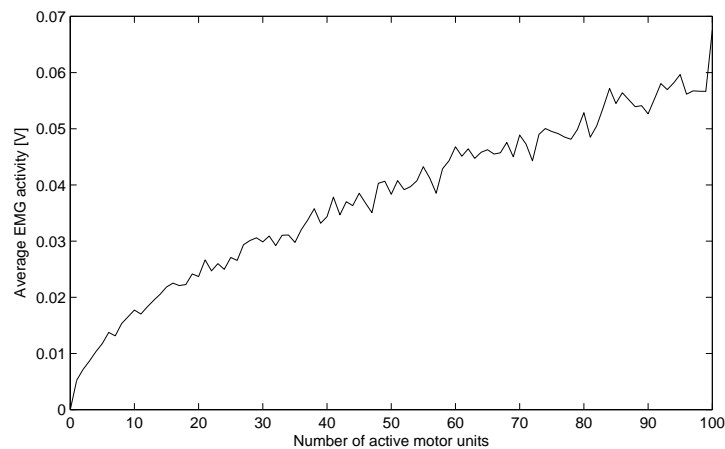


Figure 2.9: Average EMG signal over a 0.5 second interval and with a given number of active motor units. Because the probability of destructive interference increases with the number of active motor units, the resulting EMG amplitude does not increase linearly.

time [99].

Force generated by a muscle is generally believed to be somehow proportional to the amplitude of the EMG signal. However, even though it can be observed that the EMG amplitude increases with muscle force or with contraction velocity, a simple equation describing this relationship has not yet been found.

One first factor influencing the relationship between EMG amplitude and force is the quality of the signal picked up by the electrodes. Depending on where these electrodes are placed with respect to the measured muscle, on the properties of the muscle, on the conductivity of the tissue in between muscle and electrode and on the quality of the electrode-skin interface, the amplitude of the EMG signal may change even if the muscle force is the same. This problem can be greatly reduced by properly normalizing the EMG signal, i.e. by referring it to a reference value instead of looking at the exact voltage reading. This reference value is usually a measurement collected with the same setup and with the same electrode placement. The choice of the correct normalization procedure is a very wide and debated topic, and allows not only to get a better interpretation of the applied force, but also to compare the results between subjects and between

different studies. Most authors agree that the best normalization value is the EMG signal recorded during an isometric maximum voluntary contraction [101, 102], also called MVC, which represents the maximum force that the subject can apply in a given direction and in a certain position/configuration. Sometimes it is not possible to acquire an MVC (for example many stroke patients cannot express a maximum contraction of a single muscle), and therefore some authors use alternative methods, such as the maximum recorded value during all recordings of a certain subject in a single data collection session.

Another important aspect to consider is amplitude cancellation, i.e. the cancellation of EMG data by superposition of positive and negative phases of motor unit action potentials (destructive interference). This phenomenon is more evident at high muscle forces when many motor units are active, as this increases the probability of two action potentials being in phase opposition. It has been shown that amplitude cancellation in surface EMG can reach 62% at maximal activation [103], while it is less significant at lower contractions. This makes the relationship between the number of active motor units and the resulting EMG amplitude non linear (see figure 2.9) and may confound the interpretation of changes in the absolute EMG activity level [102]. This problem can be partially solved by normalizing the EMG readings with respect to a MVC, but this also results in an overestimation of the EMG activity at low and intermediate levels of muscle activity.

2.3.2 Extraction of linear envelopes

In a study analyzing muscle coordination it is common practice to extract the linear envelopes of the recorded EMG signals. This processing technique allows to simplify the data by eliminating some unnecessary information (such as the activation of each single motor unit, which is visible in the high frequency content), while still maintaining enough information to study muscle activation timing and amplitude.

One first important step to get a good reading of the activation timing is to remove signal components that were not generated by the tested muscle. As explained in the previous paragraph, cross-talk and ECG noise can make the interpretation of EMG signals quite challenging and should therefore be removed. While cross-talk can be quite difficult to remove in the post-processing phase, and should therefore be eliminated

during the system setup, ECG noise is quite easy to filter out. A common technique is to apply a high pass filter with a cutoff frequency of about 20 to 60 Hz. This guarantees that those amplitudes in the ECG frequency range are significantly reduced, while most of the EMG power, which lies in the 50-150 Hz range, is still preserved. Drake and Callaghan gave a guideline for the choice of the high-pass frequency, suggesting the use of a 30 Hz fourth-order Butterworth filter [104]. This is also the technique adopted in this study. Figure 2.10a shows the activity of the right pectoralis major muscle during a very unlucky recording. Due to the low activation during the analyzed task, the ECG noise has the same amplitude as the measured muscle activity. However, by applying the high-pass filter this effect is significantly reduced, maintaining the original shape of the muscle activation pattern while making it more evident (figure 2.10b).

The next step is to demean the EMG signal, so as to center it around zero. This takes care of eliminating any DC bias, which would not have a physiological meaning. This step is followed by a full wave rectification, i.e. by taking the absolute value of the recorded signal (figure 2.10c - black line). In fact, negative values do not represent any physiological process and are only the result of the bipolar electrode configuration. Furthermore, rectifying the signal makes it easier to apply the next processing step, which aims at obtaining a signal representing muscle contraction (which cannot change its sign as muscles can't expand).

The last step is the actual calculation of the linear envelope. As already mentioned, their purpose is to represent the timing and amplitude of muscle contraction in a simplified way. Since muscle force and muscle contraction are strongly related to the dynamic behavior of the musculoskeletal system, their frequency content cannot be as high as the highest EMG frequency. This is why linear envelopes represent only the low frequency part of the EMG signal. Various techniques have been proposed to calculate linear envelopes, some suggesting to integrate or average the rectified signal over a biomechanically significant time frame, others relying on low-pass filters. The use of low-pass filters has become very popular in studies on muscle coordination and on motor modules, and was adopted also in this project. The suggested cutoff frequencies vary significantly, ranging from 3 to 30 Hz. It has however been suggested that the cutoff frequency should be adjusted to the kinematics of the studied movement [102]. Figure 2.10c shows the linear envelope obtained with a 4 Hz fourth-order Butterworth

low-pass filter (red line), superimposed over the rectified EMG signal (black line).

In order to obtain a signal whose amplitude can be interpreted, it is necessary to normalize the calculated linear envelopes. As previously mentioned, the best method would be to normalize it by the muscle activation during maximum voluntary contraction. However, since part of the participants in this study were stroke patients who could not express an MVC, we took used the maximum average activation over a time of 90 ms instead. This value was calculated by reading the EMG activity of a specific muscle relative to all recorded trials (hoping that the muscle was maximally active during at least one trial), by calculating a moving average over 90 ms windows and by taking the maximum value. The 90 ms window was chosen as it represents a biomechanically significant value.

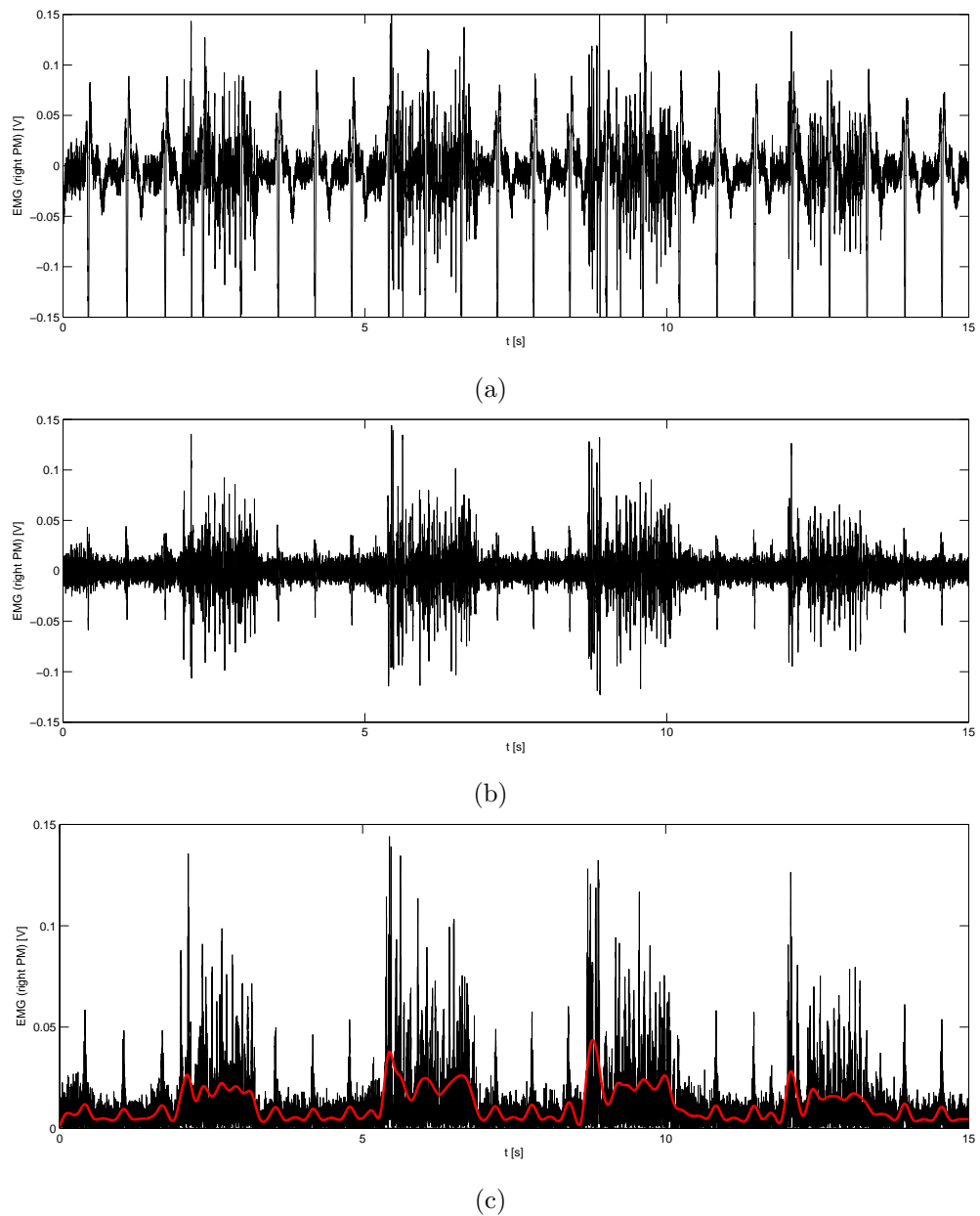


Figure 2.10: EMG processing steps. (a) Raw EMG signal of the right pectoralis major muscle during a reaching task. The ECG noise is very evident. (b) Application of a 30 Hz high-pass filter. The ECG noise is greatly reduced (but still visible) and the activation profile of the tested muscle is more clear. (c) Demeaned and rectified signal (black), and subsequent application of a 4 Hz fourth-order Butterworth low-pass filter to obtain the linear envelope (red).

Chapter 3

Algorithms for extracting motor modules

From a very general point of view, motor modules represent hidden structures underlying muscle activation patterns. Due to technological limitations and a yet incomplete understanding of their nature, these structures cannot be observed through a direct measurement. However, we can infer some of their properties by observing the activity of a relatively large number of muscles (usually between 8 and 16), which can be measured through well-known techniques such as sEMG. The general procedure is to analyze the muscle activations by applying specific statistical and/or computational methods, which look for underlying correlations and patterns. This chapter will provide an overview of the most commonly used methods to extract motor modules from EMG data, with a particular focus on the non-negative factorization algorithm that was used in this research study.

3.1 Factorization of EMG signals

EMG signals provide us with a huge quantity of information. For example, one could analyze the signal amplitude to get an estimate of muscle force, the frequency content of the signal to infer muscle fatigue [105], or the muscle activation timing during movement to identify biomechanical functions. Another possibility is to use EMG signals to study muscle coordination [102]. The methods applied to each type of analysis vary substantially, as well as the processing techniques used on the raw EMG signals.

In a study of muscle coordination, a category that encompasses the analysis of motor modules, one is mainly concerned with the the muscle activation timings and how these are interrelated. Before diving into the details of how this information can be extracted from the muscle activation patterns, it is important to note that the analysis can be significantly simplified by discarding all the irrelevant information contained in the EMG signals. Muscle coordination is strongly related to the timing of muscle force [106], and muscle force lies at the basis of movement dynamics. This means that in the study of muscle coordination we are looking for changes in muscle activity that happen approximately at the same frequency as movement kinematics. It has been shown that movement kinematics have a frequency content that is generally below 10-15 Hz [107], and therefore we can neglect a big portion of the EMG frequency spectrum. In fact, as noted by Winter [108], EMG should be filtered at a frequency related to the biomechanics of the observed task. For this reason, the statistical and computational techniques used in the analysis of muscle coordination are usually applied not to the raw EMG signals but to strongly filtered EMG envelopes.

3.1.1 A linear model

The first choice one has to make when looking for latent variables in the observed EMG signals is the type of model to apply. Even though some authors have developed more complex models (some of which will be briefly described at the end of this chapter), it is far more common to use of a linear model.

Such model requires the definition of a matrix containing all the EMG signals, which we'll call V . Each column of the matrix V contains the data relative to one EMG channel, while each row represents an observation, i.e. a sample. Figure 3.1 provides a

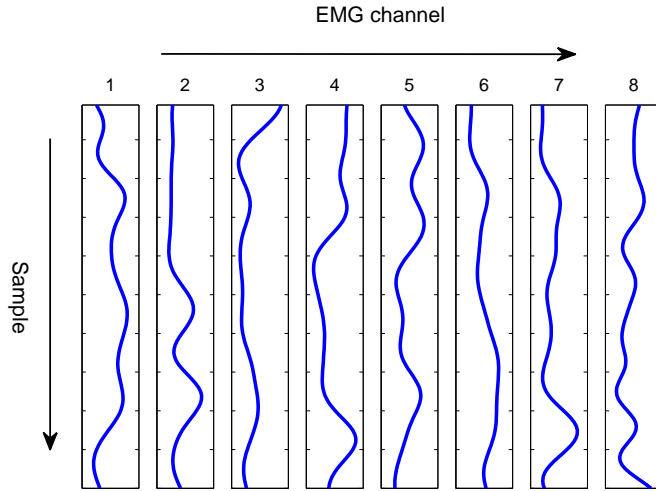


Figure 3.1: Graphical representation of the EMG matrix V

graphical representation of the EMG matrix.

We can now factorize V into two matrices, usually called W and H . Even though the product between W and H can yield exactly V , which happens either if V can be fully described by the latent variables or in the trivial case where H is unitary and W equals V , this isn't always the case. In general we need to formulate the linear model by taking the inexactness of the factorization into account:

$$V = WH + \varepsilon \quad (3.1)$$

Here ε is a matrix of residuals, and it will be the task of the factorization algorithm to find a solution that minimizes the elements of ε .

This model can be applied to many different problems, and the interpretation of the information contained in the two matrices W and H varies from case to case. However, in the analysis of motor modules, most authors agree that H describes the modules and W the timing of each module. If n_m is the number of modules extracted from the EMG matrix, then the matrix H has n_m rows and one column for each EMG channel. Each row can be seen as a vector representing one module, in which each element is an index of how much a muscle participates to this module. On the other hand, the matrix W has as many rows as V , one for each sample, and n_m columns. Each column multiplies a corresponding row of H , i.e. a module, and thereby scales it in time. In other words,

each column of W represents how much a module is active at different time steps.

3.1.2 Common algorithms

Various algorithms have been developed to solve the factorization of equation 3.1. These algorithms can differ significantly from one another, and these differences can be found mainly in the constraints put on the matrices W and H and on the type of approach, which can be either statistical or computational (i.e. optimization of an objective function).

Non-negative matrix factorization, including its variants, is probably the algorithm most commonly found in the literature on motor modules, although some authors prefer different approaches. However, an interesting study by Tresch, Cheung and d'Avella [109], which we'll discuss later, showed that the results obtained with different algorithms can be comparable. Since there isn't yet a complete agreement on one specific algorithm to apply to the extraction of motor modules, the next paragraphs will give a quick overview on the various available options.

Vector quantization (VQ) is probably the simplest method to extract features shared by different observed variables. To the best of my knowledge it has not been used for the analysis of motor modules, although Tresch et al. used a very similar approach to extract modules [56]. This method is mainly mentioned here because it was used by Lee and Seung in one of the most important papers on non-negative matrix factorization [110] as a standard to which they compared principal component analysis and non-negative matrix factorization. VQ works in a very similar way as a k-means cluster analysis. It treats each sample (in the case of EMG signals this means each row of V) as a data point, and attempts to group all data points into n_m clusters. The centroid of each cluster is the resulting motor module. The number of extracted motor modules (n_m) must be specified by the user. In its most basic form, VQ works in the following way:

1. generate n_m random cluster centroids
2. pick one random sample and find the closest centroid
3. move the selected centroid closer to the sample by a fraction of their euclidean distance

4. go back to step 2 and repeat until a certain criterion is met (number of repetitions, average distance between samples and closest centroid, ...)

Each row of V is therefore represented by one single motor module. If we place each module in a row of H , this means that the rows of matrix W will be unitary vectors with the element that multiplies the module representing the current sample equal to 1, and all other elements equal to 0. It follows that VQ would be an adequate analysis if motor modules were governed by an on-off mechanism, without any kind of amplitude modulation and superposition.

Factor analysis (FA) is a statistical method to discover latent variables in a set of observed variables. In this case W becomes a matrix of factors, and H a loading matrix. If we call EMG_i the i -th observed EMG channel, μ_i the average EMG activity over all samples, W_j the j -th column of W (the j -th factor) and ε_i the i -th column of ε , then we can write the statistical model in the following way:

$$EMG_i = \mu_i + \sum_{j=1}^{n_m} W_j H_{j,i} + \varepsilon_i \quad (3.2)$$

Equation 3.1 still holds, but must be applied to the demeaned EMG signals. In addition, FA introduces a few constraints: The factors must be uncorrelated ($COV(W) = I$), each column of W must have zero mean and W and the error matrix must be independent. As a consequence of the type of factorization, both modules and activation coefficients can have negative values. Negative weights in a motor module could be interpreted as an inhibitory effect on a muscle. However, most authors prefer to work with factorizations that yield only positive values.

Principal component analysis (PCA) has much in common with FA. The goal of this method is to find linearly uncorrelated variables, the so-called principal components, that describe the set of possibly correlated observed variables. In addition to the constraints introduced by FA, PCA adds an orthonormality constraint on the columns of W and an orthogonality constraint on the rows of H (in some cases these constraints are switched, so that W is orthogonal and H orthonormal). The PCA algorithm works by solving an eigenvector problem in an iterative way. Eigenvectors (columns of W) are extracted one at a time following these steps:

1. find the eigenvector of V that lies on the direction of highest variance
2. subtract the variance explained by this eigenvector from V
3. go back to step 1 and repeat until all of the variance of V is explained (step 2 causes all eigenvectors to be orthogonal)

As with FA, PCA yields both positive and negative activation coefficients and modules. However, this method has the advantage that each factor can be associated to a percentage of explained variance. If one decides that a certain percentage of the EMG variance can be attributed to noise, then the factors need only to explain a portion of the variance in order to capture the underlying latent variables. One option is to pick the first n factors that together explain most of the variance (e.g. 95%), and to neglect the remaining ones. In fact, some authors even use PCA only to determine the number of latent variables, and then perform the actual factorization with another algorithm [56].

Non-negative matrix factorization (NMF) differs from the previous algorithms inasmuch it relies more on computational techniques than on a statistical approach. It still solves the problem of equation 3.1, but it does it by finding two matrices W and H that minimize some metric of the difference between the EMG matrix V and its approximation WH . The flexibility of this numerical approach allows to introduce one important additional constraint, which gives the method its name: the non-negativity of the matrices W and H . However, this requires also the matrix V to be positive. For this reason NMF is particularly well suited for problems where negative values in W and H would be difficult to interpret or wouldn't be compatible with the model applied to the measured variables. More details on this algorithm and its implementation are given in section 3.2.

3.1.3 Which algorithm is “best”?

Two interesting studies have analyzed the effectiveness of different algorithms applied to problem 3.1. In one of their first papers on NMF, Lee and Seung [110] compared VQ, PCA and NMF applied to the analysis of a database of over 2000 facial images. They found that VQ discovered a basis of prototypes representing the average of similar faces, and PCA gave a more abstract result of “eigenfaces” which were distorted versions of

whole faces. On the other side, NMF was capable of discovering features common to different individuals. The main difference was that VQ and PCA looked at each face as a whole, while NMF described them as a summation of different features that had an actual anatomical meaning, such as noses, eyes, beards etc. This study had a radical impact on many following research projects, as it provided evidence that NMF was a useful tool to extract significant parts of objects.

In another more recent paper of 2006, Tresch, Cheung and d'Avella provided a comparison between various algorithms for the extraction of motor modules [109]. The compared algorithms were FA, PCA, NMF, independent component analysis (ICA) and some of their variants. These algorithms were applied to a simulated data set, constructed by the product of predefined W and H matrices and by adding noise. Interestingly, they found that FA, ICA and NMF identified very similar motor modules. Two variants of ICA, i.e. ICA applied to a subspace defined by PCA and a probabilistic version of ICA with nonnegativity constraints performed best in identifying modules in the simulated data set, NMF and FA followed closely, while PCA was not able to identify the correct modules. On one side, this result gives more freedom in the choice of the algorithm to the researcher, as there is no optimal choice. On the other side, it also shows that motor modules are not numerical artifacts introduced by a specific algorithm, but are truly features present in the EMG signals.

3.2 Non-negative Matrix Factorization

NMF was first introduced by Paatero and Tapper in 1994 [111] and then by Lee and Seung in their paper of 1999 *Learning the parts of objects by non-negative matrix factorization* [110], where they explained how NMF could recognize features of objects. Seung and Lee further explained their method in 2001, when they showed how one could easily implement the algorithm through multiplicative update rules [112]. These multiplicative update rules were rapidly adopted by numerous researchers making Lees and Seungs algorithm one of the most popular NMF variants. However, since the first introduction of NMF various authors have come up with alternative algorithms, some of which will be described in the next section. All these algorithms solve equation 3.1 by describing the EMG signals as a superposition of the activity of a certain number

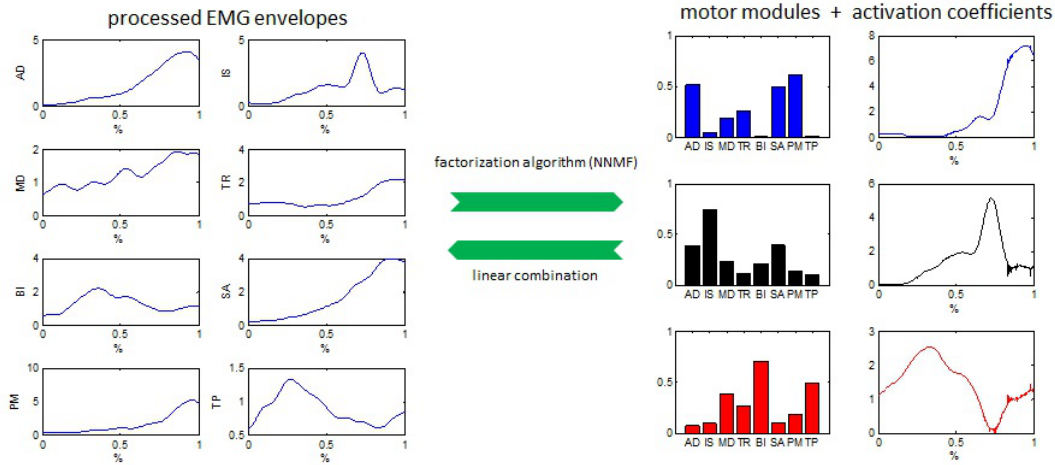


Figure 3.2: Factorization of muscle activity recordings into motor modules and activation coefficients

of motor modules. Each module consists only of positive weights, and each activation coefficient must also be positive. By multiplying the activation coefficients with their respective modules, one can obtain an approximation of the original EMG signals. An example of the factorization and reconstruction process is shown in figure 3.2.

All NMF algorithms attempt to minimize a certain objective function which represents a metric of the difference between the original EMG matrix V and its approximation WH . The most widely used objective function is the square of the Frobenius norm of ε :

$$f(W, H) = \|V - WH\|_F^2 = \sum_{i,j} (V_{i,j} - (WH)_{i,j})^2 \quad (3.3)$$

However, it can be shown that equation 3.3 is convex only in W or only in H , but not in both variables at the same time. This means that minimizing this objective function does not guarantee the convergence to a global minimum, but rather to a local minimum. All other objective functions for NMF have the same problem, and therefore there is no algorithm yet that can find the globally best positive factorization of V . One possible solution is to repeat the factorization multiple times, starting from different initial guesses of W and H . If each repetition converges to a local minimum, one could pick the best solution and use that as an approximation of the global minimum.

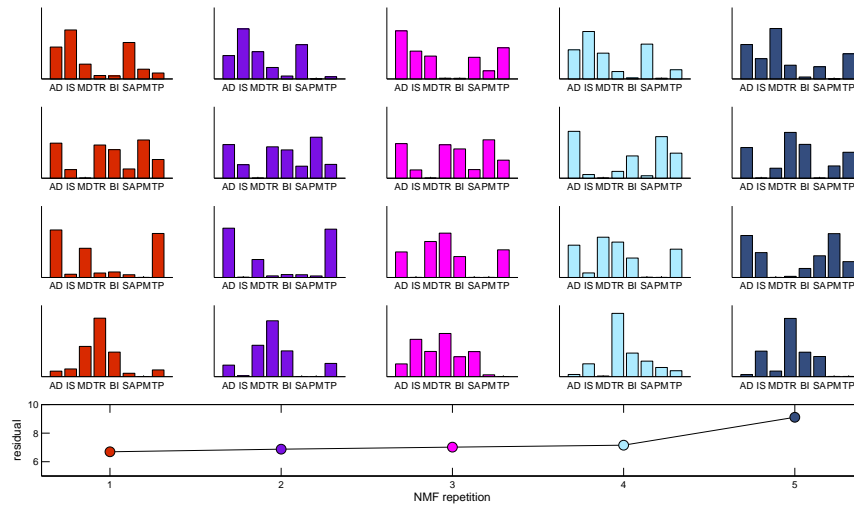


Figure 3.3: Choice of the repetition with the smallest residual: each color represents a different local minimum, and each bar plot represents a row of matrix H . The factorization was repeated 100 times with different random starting points, but only 5 solutions are shown. The solution to the left has the lowest residual and could be a good approximation of the global optimum, while the solution to the right has the highest residual.

An example of this method is shown in figure 3.3. Here the factorization was repeated 100 times with 100 different random initial guesses. Only five solutions are shown, and each bar graph represents a row of matrix H , i.e. a module. The solution to the left of the figure has the lowest residual, and could therefore be used as an approximation of the globally best solution.

Another common property of all NMF algorithms is their inability to choose the correct number of modules (or factors) automatically. As a matter of fact, the user has to specify the number of modules *before* performing the factorization. This is not a trivial choice, as the user is applying the algorithm to discover hidden properties in the signal and might not know the correct number of latent variables. In order to solve this issue, one could start from the opposite site and think about the EMG signals as the result of the activity of different discrete motor modules. When looking at the problem

from this perspective, most of the variance in the EMG signals will be caused by the activity of modules and a small amount of variance by random noise [57]. This thought process can lead to two possible solutions.

The first solution is fairly simple, and consists in attributing a certain fixed percentage of variance to noise. One could then perform the factorization with an increasing number of modules, starting from one. The higher the number of modules, the more of the signal variance will be explained, and one could stop when only the variance attributed to noise is left unexplained.

The second solution is quite popular in literature [19, 21, 57, 78, 80, 88] and is based on the hypothesis that the random portion of the EMG signal is structureless, and is therefore hard to describe with motor modules. As with the previous solution, one could apply the factorization with an increasing number of modules. However, once we hit the correct number of modules, most of the hidden structures in the EMG data will be explained fairly well and only the structureless part remains. Even by adding more modules to the factorization, the algorithm won't be able to explain a significantly higher amount of variance. This means that if we imagine a plot with explained variance vs. number of modules, this graph will have a change in slope where the number of modules coincides with the actual number of latent variables. Many authors exploit this property and search for this change in slope to find the correct number of modules. However, this method is not always applicable as sometimes the change in slope is not so clear. For this reason we chose to use the first solution with a fixed threshold, which gave us more consistent results.

In this context it is quite important to note that the variance of the original EMG envelopes is significantly influenced by the degree of smoothing that was applied to the raw EMG signals. As a consequence, it has been shown that the frequency of the low-pass filter affects the number of modules detected by either one of the aforementioned criteria [93].

One way to quantify the amount of explained variance is to use a dimensionless index called variability accounted for (VAF) [22, 72]:

$$VAF = 1 - \frac{\|V - WH\|_F^2}{\|V\|_F^2} \quad (3.4)$$

This index is usually smaller than one, and is equal to one only when the factorization

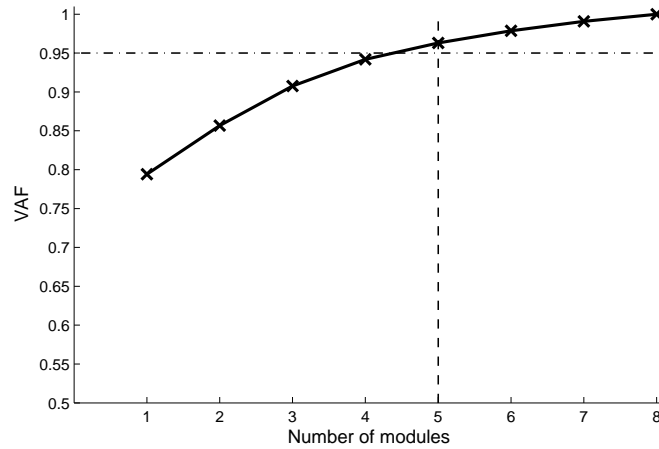


Figure 3.4: Example for the changes in variability accounted for as a function of the number of modules. When attributing 5% of the EMG variability to noise, 5 modules are sufficient to explain all the remaining variability.

yields a perfect reconstruction of V . Figure 3.4 shows a typical example of how the VAF index changes as the number of modules increases. If one decides that noise is responsible for 5% of the total variability, then the number of modules could be picked as the smallest value that yields a VAF of at least 95%.

3.2.1 Variants of NMF

As mentioned above, non-negative matrix factorization can be performed with various algorithms. The most popular is definitely Lees and Seungs multiplicative update rule, but, as pointed out by Lin [113], other authors have found alternative methods that some claim are more computationally efficient or have a more rapid convergence. The next paragraphs will present some of the best known NMF algorithms.

Multiplicative update rules

In their paper of 2001 *Algorithms for non-negative matrix factorization* Lee and Seung presented two simple algorithms to perform NMF. Both of them rely on an iterative update of the factorization by multiplying the solution of the previous iteration by a certain coefficient. The two rules are aimed at minimizing two different objective function. The first is the Frobenius norm of the difference between V and WH (equation 3.3),

while the second is the generalized Kullback-Leibler divergence of WH from V , i.e. a measure of the information lost through the approximation:

$$f(W, H) = D(V \| WH) = \sum_{i,j} \left(V_{i,j} \log \frac{V_{i,j}}{(WH)_{i,j}} - V_{i,j} + (WH)_{i,j} \right) \quad (3.5)$$

Lee and Seung introduced the following update rules, providing proof that when applying them the respective objective function is non-increasing:

Objective	Updated H	Updated W
$\ V - WH\ _F^2$	$H_{\alpha,\mu}^{i+1} = H_{\alpha,\mu}^i \frac{((W^i)^T V)_{\alpha,\mu}}{((W^i)^T W^i H^i)_{\alpha,\mu}}$	$W_{\delta,\alpha}^{i+1} = W_{\delta,\alpha}^i \frac{(V(H^{i+1})^T)_{\delta,\alpha}}{(W^i H^{i+1} (H^{i+1})^T)_{\delta,\alpha}}$
$D(V \ WH)$	$H_{\alpha,\mu}^{i+1} = H_{\alpha,\mu}^i \frac{\sum_j \frac{W_{j,\alpha}^i V_{j,\mu}}{(W^i H^i)_{j,\mu}}}{\sum_k W_{k,\alpha}^i}$	$W_{\delta,\alpha}^{i+1} = W_{\delta,\alpha}^i \frac{\sum_j \frac{H_{\alpha,j}^{i+1} V_{\delta,j}}{(W^i H^{i+1})_{\delta,j}}}{\sum_k H_{\alpha,k}^i}$

For reasons of numerical stability, some authors such as Piper et al [114, 115] suggested to add a small non zero number to the denominator of these update rules, so as to avoid dividing by zero.

Lee and Seung showed that their multiplicative update rules are a special case of a gradient descend approach with an appropriate acceleration coefficient.

These rules are simple to implement and guarantee the convergence to a stationary point. However, the performance of the algorithm depends heavily on the initialization of W and H , the convergence can be slow and require many iterations, and due to the multiplicative nature of the algorithm all zero-elements in W and H are locked for all following iterations.

Alternating least squares

This algorithm is a more general form of one of the previous update rules, and applies to the objective function 3.3. It was first introduced by Paatero [111, 116] and was described also by Chu [117]. As with the multiplicative update rules, this is an iterative algorithm that works on W and H independently. Instead of updating the two matrices through a fixed rule, this algorithm determines their value by minimizing the objective function. It has been mentioned in the previous paragraphs that equation 3.3 is convex in either W or H , so it can be minimized when either one of the two matrices is held constant. This minimization process does not guarantee that the non-negativity constraint is

maintained, and therefore it has to be enforced in a separate step. At each iteration, the algorithm performs the following operations:

1. holding W^i constant, find H^{i+1} so that it solves $\min_{H^{i+1}} \|V - W^i H^{i+1}\|_F^2$
2. set all negative elements of H^{i+1} equal to zero
3. holding H^{i+1} constant, find W^{i+1} so that it solves $\min_{W^{i+1}} \|V - W^{i+1} H^{i+1}\|_F^2$
4. set all negative elements of W^{i+1} equal to zero

The two minimizations in steps 1 and 3 can be performed through a standard least squares algorithm.

This algorithm has nice optimization properties and a much more solid convergence theory than the multiplicative update rules [113]. Furthermore it works well in practice and shows a fast convergence. Other advantages are that only W has to be initialized and that the least squares approach does not lock the zero elements. On the other side, the nonnegativity is obtained only through the ad hoc addition of steps 2 and 4. The multiplicative update rules are also easier to implement and to customize, which is why we adopted them and not the alternating least squares algorithm in this study.

Gradient descend methods

A third option is to apply a standard numerical method such as a gradient descend algorithm to minimize equation 3.3. The gradient of the objective function has two parts, one relative to W and one to H :

$$\begin{aligned}\nabla_W f(W, H) &= (WH - V)H^T \\ \nabla_H f(W, H) &= W^T(WH - V)\end{aligned}$$

One can then apply a projected gradient method to iteratively minimize the objective function [113]:

$$\begin{aligned}W^{i+1} &= P[W^i - \alpha_i \nabla_W f(W^i, H^i)] \\ H^{i+1} &= P[H^i - \alpha_i \nabla_H f(W^i, H^i)]\end{aligned}$$

Where α_i is a coefficient determining the step size along the descending direction of the gradient and P is a projection operator that maps W and H into their bounded feasible region:

$$P[x] = \begin{cases} x & \text{if } x \geq 0 \\ 0 & \text{if } x < 0 \end{cases} \quad (3.6)$$

A big part of Lin's work [113] presents different strategies to choose α_i . The discussion of such strategies is beyond the scope of this thesis, although it is important to note that the right choice of α_i can yield a very fast converging algorithm, potentially performing better than the multiplicative update rule and the standard alternating least squares approach.

3.2.2 Convergence and stopping criteria

All the aforementioned NMF algorithms are backed some sort of convergence theory. Lee and Seung prove that their multiplicative update rule guarantees convergence to a stationary point. However, even though stationarity is a prerequisite for a local minimum, it does not guarantee that the algorithm actually converges to an optimal point. In practical applications this isn't usually an issue, and in the grand majority of cases the algorithm converges to a local minimum. On the other side, the alternating least squares algorithm and all projected gradient descend methods have a stronger convergence theory, which is not solely based on stationarity but on the actual convergence to an optimum [113, 115].

Figure 3.5 shows an example of the convergence of the multiplicative update rule applied to the Frobenius norm objective function. Even though this is just a single case relative to a specific EMG matrix, it represents the general case quite well. It can be seen that the objective function decreases rapidly after about 10 iterations, and then becomes stationary after approximately 100 iterations. All following iterations don't bring any significant improvement to the residual.

There are several stopping criteria that could apply to this problem:

- stop after a given number of iterations
- stop when the objective function doesn't change much from one iteration to the next: $f(W^i, H^i) - f(W^{i+1}, H^{i+1}) \leq tol$
- stop if the gradient of f with respect to W and H falls below a certain threshold: $\|\nabla f(W^i, H^i)\| \leq \epsilon \|\nabla f(W^1, H^1)\|$

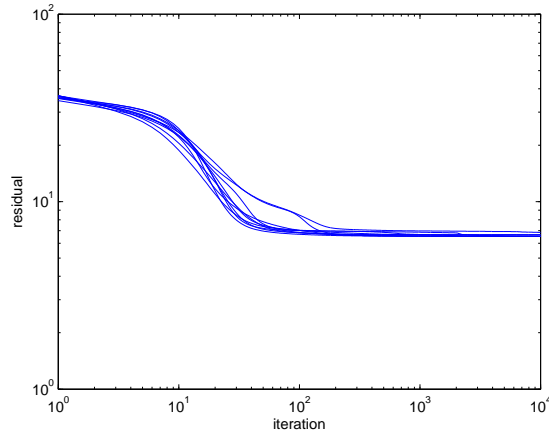


Figure 3.5: Convergence example of the NMF algorithm with the multiplicative update rule. The factorization was repeated 100 times on the same EMG matrix. Each blue line represents one repetition.

In this study we used the first criterion, and stopped the factorization after 100 iterations.

3.3 Other models

Even though the standard linear model of equation 3.1 is the one most often found in literature [27, 57, 109, 118], some authors have modified it or developed an alternative model. This section discusses two different options which have been used in various studies.

3.3.1 Time-varying modules

As stated above, the factorization of equation 3.1 creates a matrix V of time-varying activation coefficients and a matrix W of modules. These modules are fixed structures that don't change over time, and represent a synchronous coactivation of different muscles. Such structures are also called synchronous motor modules.

However, some authors such as d'Avella [119] claim that “muscles within a putative synergy [motor module] were often activated asynchronously”, which suggested that not only the amplitudes but also the activation timings might be part of the coordination pattern. For this reason these authors developed an algorithm able to extract combina-

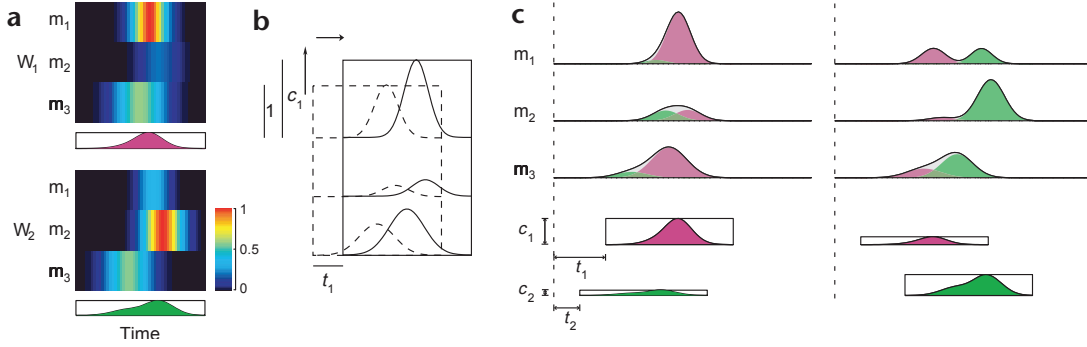


Figure 3.6: Example of the time-varying motor modules model. a) two time-varying modules, \mathbf{w}_1 and \mathbf{w}_2 with the representation of their three elements (muscles) in time. b) Module 1 is scaled by c_1 and shifted in time by t_1 . c) The summation of the two modules reconstructs the original EMG signals relative to two different episodes. From d’Avella et al. [21].

tions of so-called time-varying motor modules. This method was adopted by multiple authors in their research [21, 62, 119].

The first step is to isolate episodes of a given behavior in the EMG data, which the authors describe as for example a set of jumps in different directions, or a set of walking or swimming cycles. Each episode is identified with an index s . The muscle activity \mathbf{m}_s of each episode can then be described as a linear combination of N time-varying modules:

$$\mathbf{m}_s(t) = \sum_{i=1}^N c_{si} \mathbf{w}_i(t - t_{si}) \quad (3.7)$$

Here \mathbf{m}_s is a vector containing the activity of all muscles in a given time instant (analogous to a single row of V), c_{si} is a scaling coefficient specific for each episode s and each time-varying module, \mathbf{w}_i is the i -th module (a vector of the same size as \mathbf{m}_s) and t_{si} is a parameter shifting the onset of the module in time. Differently than in the case of synchronous modules, which are active over the whole episode, each time-varying module is active only for a limited time T . Usually T is the same for all N modules. An example for the results of this algorithm is provided in figure 3.6.

D’Avella, Cheung and Bizzi [58, 63, 77] point out that while synchronous modules capture solely time-invariant features across the recorded muscles, “time-varying modules capture fixed relationships in both spatial and temporal domains”. Furthermore, the

EMG data is represented with less parameters than in the case of synchronous modules. In fact, each time-varying module has only two parameters, c_{si} and t_{si} , while synchronous modules have a different activation coefficient for each sample.

3.3.2 Shared modules

In some cases it is interesting to analyze if some motor modules are similar between study conditions, like before and after a treatment [57], or between different motor tasks [63].

A simple solution could be to extract modules independently from each different study condition and then to compare them pairwise, for example through a scalar product. However, this approach might not always give the best results for two reasons, as pointed out by Cheung et al. [57]:

- even if the subspaces defined by modules extracted from different study conditions share a common subspace, the modules might actually not be similar.
- if in one study condition two modules vary together, then the extraction algorithm might identify them as one single module. Now if in a second study condition they activate independently, the algorithm will see them as such and find two modules that can be very different than the combined one.

For these reasons in 2005 Cheung et al. developed an algorithm capable of extracting shared and specific synchronous modules from two different study conditions. The model can be formulated in the following way [57]:

$$\begin{aligned} V^{sc1} &= W^{sc1,sh} H^{sh} + W^{sc1} H^{sc1} \\ V^{sc2} &= W^{sc2,sh} H^{sh} + W^{sc2} H^{sc2} \end{aligned}$$

The apex $sc1$ identifies the first study condition, while $sc2$ the second study condition. Furthermore W^{sc1} and H^{sc1} are activation coefficients and modules specific for study condition one, and W^{sc2} and H^{sc2} for study condition 2. H^{sh} represents the shared modules, and $W^{sc1,sh}$ and $W^{sc2,sh}$ are their activation coefficients in the two study conditions. If one uses the NMF algorithm with multiplicative update rules, in which zero elements are locked, than the previous formulation can be converted to equation 3.1

by modifying the definition of V , W and H :

$$\begin{aligned}
 V &= \begin{bmatrix} V^{sc1} \\ V^{sc2} \end{bmatrix} \\
 W &= \begin{bmatrix} W^{sc1,sh} & W^{sc1} & 0 \\ W^{sc2,sh} & 0 & W^{sc2} \end{bmatrix} \\
 H &= \begin{bmatrix} H^{sh} \\ H^{sc1} \\ H^{sc2} \end{bmatrix}
 \end{aligned}$$

Cheung, d'Avella and Bizzi expanded this method in 2009 to find shared modules between an arbitrary number of study conditions [63]. The reader is referred to this paper for details on the implementation of the algorithm.

Chapter 4

Materials and methods

As explained in the previous chapters, a better understanding of human motor control and of how it is affected by stroke could help in the development of new and more efficient rehabilitation techniques. We designed a set of experiments aimed at the development of a neuromusculoskeletal model of the proximal upper limb based on the theory of motor modules. The goal was to capture common muscle coordination patterns in healthy subjects, and to observe how these patterns change after stroke. This chapter presents the methods used to obtain this model, starting from the experimental protocol and setup up to the adopted data processing techniques.



Figure 4.1: Experiments were performed at the Upper Extremity Motor Function Laboratory at the Medical University of South Carolina, College of Health Professions, Charleston, SC, USA.

4.1 Design of experiment

In order to obtain a neuromusculoskeletal model that could capture the many different muscle coordination patterns used to control the proximal upper limb, the first step in the design of this experiment was to find a representative set of movements for our EMG recordings. In fact, as suggested by many authors studying motor modules in both animals and humans, one can obtain motor modules representing actual coordination patterns only by using a rich enough set of testing conditions (see chapter 2). However, the human arm can perform an almost infinite number of different movements, and due to constraints of time and physical endurance of our test subjects we had to limit the number of tested movements. Furthermore, the selected tasks had to be complex enough to evoke meaningful coordination strategies [80], but still simple enough to allow subjects to repeat them multiple times with little variation.

Additionally, we wanted the results of our analysis to be easy to interpret and readily applicable to the contexts of assessment of motor functions and of rehabilitation. For this reason we selected movements commonly used in activities of daily living (ADLs), which we hypothesized would be familiar to most subjects and would be useful both to assess motor impairment post stroke and to guide a rehabilitation protocol. We picked movements using most of the available degrees of freedom of shoulder and elbow, and that would cover a big portion of the arm's work space. Since we were interested mainly in the proximal upper limb and in gross motion, we settled for movements involving wide reaches to the edge of the work space and for pick and place movements requiring

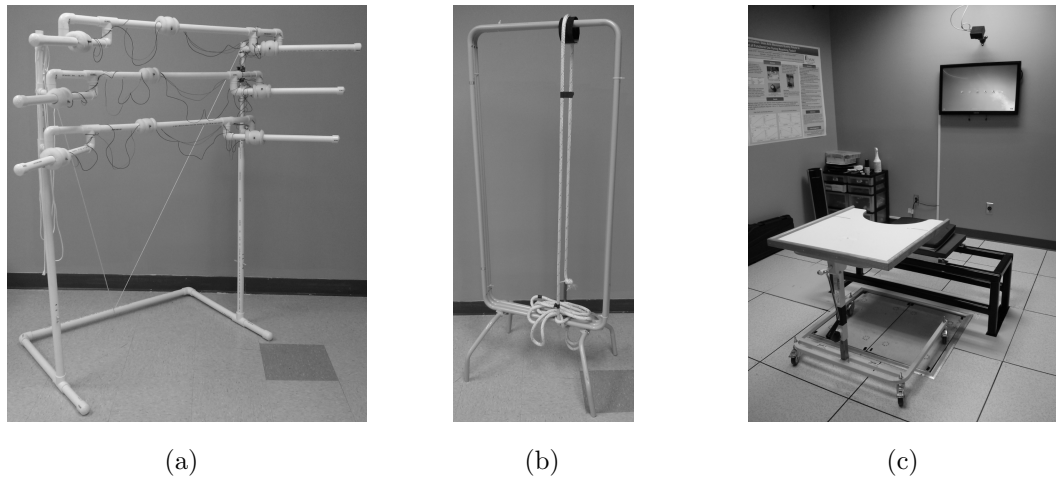


Figure 4.2: Aids used during the execution of tasks. (a) Frame holding the targets for the multidirectional reaching task. Each target is marked by an LED that can be turned on or off by a custom software application. (b) Rope grasped during the reach to side task. A colored tape on the rope marks the grasping location. (c) Table used for moving objects on the transverse and sagittal plane.

large hand displacements. Each movement was part of a particular task, and each task involved reaching towards a predefined position or interacting with a certain object:

Multidirectional reaching: 9 targets were placed in the subject's workspace in a 3 by 3 matrix. The distance of each target to the subject's acromion was equal to 90% of its arm length. The three rows of the target matrix were positioned at 90° , 100° and 110° of humeral flexion respectively, while the three columns were positioned at 45° , 90° and 120° of horizontal adduction (figure 4.2a). Each target was marked with a green LED that could be independently turned on or off by a custom software application. Participants were instructed to bring the tested arm to the start position, with the hand resting on the frontal edge of the seating plane, and to wait for one of the LEDs to turn on. They then had to reach towards the target until touching it with their fingertips, to hold this position for 1 second and to return to the start position only after the LED went off. This was repeated in a random sequence for all 9 targets. Reaching to each target was considered as a separate task.

Reaching to forehead: Participants were asked to bring the tested arm to the start position with their hand resting on the frontal edge of the seating plane, and then to reach towards their forehead until touching it with their fingertips. After holding this position for just enough time to stop the motion completely, they could return to the start position.

Reaching to the side: This task consisted in reaching towards a target positioned on the frontal plane at 120° of humeral abduction, 90° of external rotation and 45° of elbow flexion. The target position was marked on a vertical rope with both ends attached to a frame (figure 4.2b). We instructed the participants to bring their tested arm to the same start position as in the two previous tasks and then to grasp the rope at the marked location. After holding the position for just enough time to stop the movement they could return to the start position. Furthermore, subjects were asked to limit trunk movement as much as possible.

Moving objects on the transverse plane: For this and the next task a table was placed in front of the participant (figure 4.2c). The height of the table was adjusted so that, when placing its hands on it, the subject's elbow was flexed at 90° while its humerus was vertical and rotated by 0° . This was also the position to which we instructed the subject to go initially. Subjects were asked to reach towards a bean bag that was placed in front of their untested hand, to pick it up and to bring it to the start position without sliding it on the table.

Moving objects parallel to sagittal plane: The setup was similar to the previous task, but the pick and place locations were re-defined. The pick location was positioned on the intersection between the table and the sagittal plane and at a distance of 90% of the arm length from the sternoclavicular joint. Additionally, a basket was placed behind the subject as close as possible to the edge of the seating plane, so that the participant could position its hand above it with extended elbow and 0° humeral abduction. The position above the basket was the start location. Participants were asked to reach towards a bean bag positioned at the pick location, to bring it over the basket without sliding it on the table and to release it. They were also instructed to limit trunk movement as much as possible.

All tasks were repeated 6 times in a row with both dominant and non-dominant arm in order to capture most of the intra-subject variability of kinematic and electromyographical data [120].

Each task was divided into two movements: a reaching movement where the subject brought his/her hand towards the target (hand transport phase), and a return movement where the subject went back to the start position (return phase). In our analysis we considered only those movements that involved bringing the hand to pre-defined position to interact with an object (hand transport phase), which included all the reaching movements plus the return movements of the two tasks using bean bags. Therefore the total number of analyzed movements is 15. Of these movements, we were interested only in the coordination during gross motion rather than in the fine motor components of object grasp. In fact, we wanted to study movement phases that could be performed also by stroke patients, many of which don't have the fine motor skills needed for grasping objects.

During the execution of these tasks we recorded the 3D position of the subject's upper body, head, arms and hands, and the electromyographic activity of 16 muscles of the proximal upper limb. EMGs were collected of eight muscles per side, which were the anterior deltoid (AD), infraspinatus (IS), middle deltoid (MD), lateral head of the triceps (TR), biceps (BI), serratus anterior (SA), pectoralis major (PM) and the upper trapezius (TP).

The recorded kinematic data was used to select the five most similar trajectories out of the six repetitions of each task, and to define movement onset and end times. The EMG data relative to each tested movement was then filtered and processed in order to obtain the motor modules that best described the subject's muscle activation patterns.

For healthy control subjects, the extracted motor modules were compared between dominant and non-dominant side, and subsequently also between subjects. The goal was to find out if subjects used similar coordination strategies for both sides, and if there were similarities between different subjects. In fact, if there were similarities, then we could generate a model to which one could compare the results obtained with stroke patients. Additionally, we associated the modules most commonly used by subjects with a biomechanical function.

Motor modules of stroke patients were compared between affected and non-affected

side, but not between subjects. We then attempted to find a relationship between the number of modules of each subject and his/her motor impairment as assessed with a standard scoring system. The last step was to see if motor modules post stroke were completely new coordination strategies, or if they could result from a simplified use of the modules found in healthy controls.

The study included a total of 29 participants, 15 healthy control subjects and 14 stroke patients. In the healthy control group, six participants were female and nine male, three were left-handed and 12 right-handed, and the average age was of 47.8 years (range 20.1 - 77.1 years). Subjects were chosen so as to have matching demographics with the stroke population in South Carolina [121]. Table 4.1 shows the demographics of the control group.

Subject	Age (years)	Gender	Dominant side
1	22.8	F	R
2	30.9	F	R
3	77.1	M	R
4	56.8	M	R
5	56.2	M	R
6	68.1	M	R
7	52.7	F	L
8	59.3	F	L
9	52	M	R
10	44.9	F	R
11	20.1	M	R
12	44.4	M	R
13	56.9	F	R
14	48	M	L
15	26.9	M	R

Table 4.1: Demographic data of healthy participants

Of the 14 stroke patients, six were female and eight male, one left-handed and thirteen right-handed, and the average age was of 59.3 years (range 19.7 - 83.3 years). All patients were in the chronic phase of stroke and the average time elapsed since the incident was of 3.47 years (range 0.9 - 9.0 years). The location of the stroke was almost

Subject	Age (years)	Gender	Dominant side	Impaired side	Time since incident (years)	Impairment	FM	SIS last item
1	69.8	F	R	R	3.7	mild	60	95
2	61.1	F	R	L	0.9	mild	59	90
3	54.5	M	R	R	0.9	mild	57	50
4	67.4	M	R	R	1.1	moderate	47	45
5	77.8	M	R	R	6.1	mild	55	90
6	54.4	F	R	L	1.6	mild	52	35
7	19.7	M	R	R	2.6	moderate	34	75
8	71.5	M	R	R	9	mild	56	70
9	63.1	M	L	L	4	moderate	37	40
10	60.7	F	R	R	2.8	mild	55	90
11	48.1	M	R	L	5.1	moderate	40	50
12	29.9	F	R	L	5	moderate	26	40
13	69.5	M	R	R	4.6	moderate	43	70
14	83.3	F	R	L	1.3	mild	58	90

Table 4.2: Demographic data of stroke patients. Fugl-Meyer scores are relative to the modified assessment (max. 60 points), while SIS scores are in percentage and represent self-perceived recovery.

evenly distributed between left and right brain hemisphere, with six patients having their left arm impaired and eight patients their right arm. Due to the relatively high dexterity required to perform all tasks, we looked for patients with mild to moderate impairment. According to Woodbury et al., this classification can be based on the score obtained through a modified Fugl-Meyer (FM) assessment [122]. This modified assessment eliminates the three reflex items and assigns a maximum score of 60 points. Based on a Rasch analysis, the authors found that the boundary between severely impaired and moderately impaired subjects lies at 19 points, while subjects with a FM score above 47 can be classified as moderately impaired. Following this classification, eight subjects were mildly impaired, while six were moderately impaired. In addition to the modified Fugl-Meyer assessment we also administered the last item of the Stroke Impact Scale (SIS), which describes the subject's self-perceived recovery. Demographic data of the stroke group is shown in table 4.2.

Study procedures were approved by the Institutional Review Boards of the Medical University of South Carolina. All participants provided informed consent in accordance with the Declaration of Helsinki.

4.2 Experimental setup

All experiments were performed at the Upper Extremity Motor Function Laboratory at the Medical University of South Carolina, College of Health Professions, Charleston, SC, USA. The laboratory is equipped with a complex data acquisition system, consisting of a 16 channel EMG acquisition system, a motion capture system, three force plates and an integration software. The following sections describe the single subsystems, besides the force plates which were not used in this study.

4.2.1 EMG data acquisition system

For this study we used a 16 channel electromyography system, coupled with pre-jelled single-use sEMG electrodes, 16 probes with snap connectors and preamplifiers, and a PCI data acquisition card.

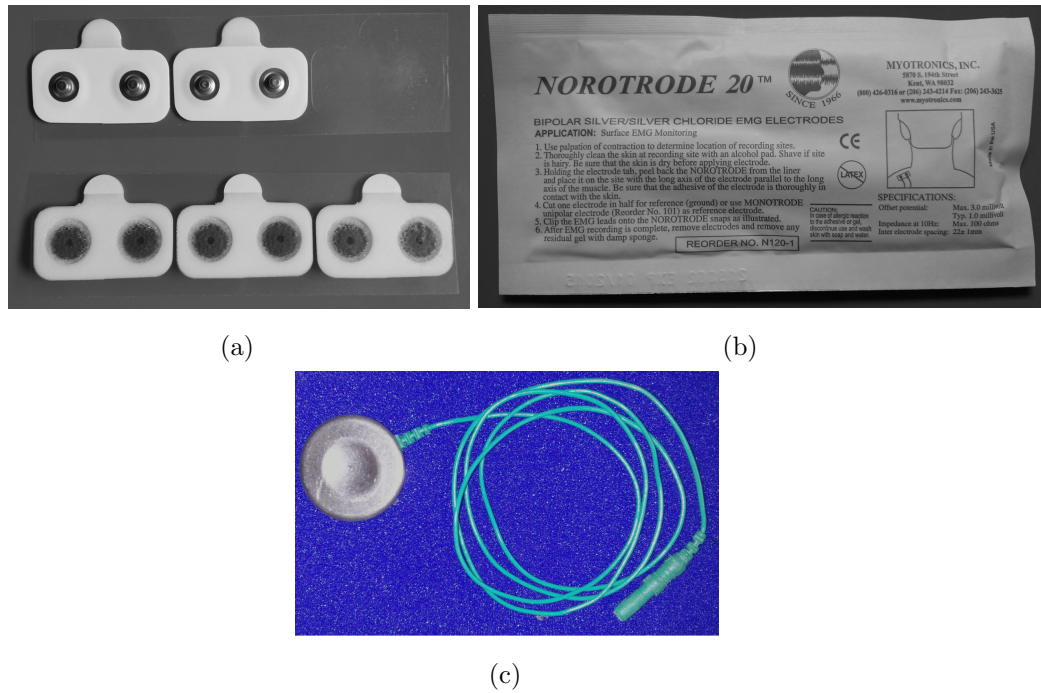


Figure 4.3: Electrodes used for EMG recordings. (a and b) Pre-jelled Ag/AgCl disposable sEMG electrodes. (c) Ground electrode.

Electrodes

We used disposable pre-jelled bipolar Norotrode 20 sEMG electrodes (Miotronics, Inc., Kent, WA, USA) with a 22 mm inter electrode spacing (figure 4.3a) and Ag/AgCl contact surfaces.

Manufacturer	Myotronics, Inc.
Model	Norotrode 20
Type	Bipolar Ag/AgCl, pre-jelled
Inter electrode spacing	22 ± 1 mm
Impedance at 10 Hz	max. 100 Ω
Offset potential	max. 3 mV / typ. 1 mV

Table 4.3: Properties of the pre-jelled bipolar Ag/AgCl electrodes

In a preliminary stage we considered the use of dry electrodes, which included contact surfaces and preamplifier in the same housing (figure 4.4a). However, the housing of



Figure 4.4: (a) Dry electrode considered in a preliminary stage. Due to the high rigidity of the housing they were not suited to collect data of shoulder muscles. (b) MA-420 differential input probe, with snap contacts and preamplifier. This probe can be used with the Norotrode 20 disposable electrodes.

dry electrodes is very rigid and does not guarantee a good contact with high curvature surfaces such as those of shoulder muscles. This resulted in unwanted motion artifacts in the recorded EMG signals. On the other side, the Norotrode 20 electrodes still offer a fixed inter electrode spacing and have equivalent electric properties, but are much more flexible and adapt easily to curved surfaces. With this solution we obtained higher quality readings and, since the electrodes are self-adhesive, reduced the setup time drastically. The properties of the chosen electrodes are listed in table 4.3.

Electrodes were placed on the 16 tested muscles using SENIAM recommendations (see chapter 2). The ground electrode, shown in figure 4.3c, was placed on the medial epicondyle of the humerus of one of the two arms: for healthy control subjects we used the dominant side, while for stroke patients we used the unimpaired side.

Probes

Each electrode was connected to a MA-420 differential input probe (Motion Lab Systems, Inc., Baton Rouge, LA, USA) with snap contacts and preamplifier (figure 4.4b). The preamplifier is contained in a small and lightweight box positioned close to the signal source, which provides a high quality myoelectric signal and reduces motion artifacts. Furthermore, it is equipped with an internal RFI and ESD protection to prevent radio

frequency interference and static damage, and has a high common mode rejection ratio. Additional technical specifications can be found in table 4.4.

Manufacturer	Motion Lab Systems, Inc.
Model	MA-420
Type	Differential input, with snap connectors for disposable electrodes and preamplifier
Preamplifier size	25 mm x 16 mm x 10 mm
Preamplifier weight	12 g
Cable length	1.25 m
Gain at 1 kHz	$\times 20 \pm 1\%$
Input impedance	$> 100 M\Omega$
Noise	$< 1.2 \mu V$ RMS
Common mode rejection ratio	> 100 dB at 65 Hz
Signal bandwidth	100 Hz to 2000 Hz (-3dB)

Table 4.4: Properties of the differential input probes with preamplifier

Electromyography system

EMG signals were acquired through a MA300-XVI electromyography system produced by Motion Lab Systems, Inc., Baton Rouge, LA, USA. This 16 channel system consists of three main components:

- Electrodes and probes attached to each muscle, as described in the previous paragraphs.
- A backpack unit worn by the test subject and with connection ports for each EMG channel (figure 4.5a).
- A desktop unit connected to the backpack and responsible for providing power and for reading the incoming signals (figure 4.5b).

The specifications of the EMG acquisition system are listed in table 4.5.

The backpack unit is usually worn by the subject. In this study we accomplished this by applying it to a Velcro belt that was positioned around the subject's waist. The backpack has 16 slots to which one can connect the individual probes, two connectors



(a)



(b)

Figure 4.5: (a) The backpack unit. Each of the 16 input channels has an individual gain setting, and an anti-alias filter determines the highest frequency of the output signal. (b) The desktop unit (blue/white box at the left) receives the recorded signals from the backpack unit and transmits them to the workstation (right)

Manufacturer	Motion Lab Systems, Inc.
Model	MA300-XVI
Dedicated EMG channels	16
Low pass filter (anti-alias)	350, 500, 750, 1000, 1250, 1500, 1750 and 2000 Hz
EMG signal output mode	Raw Signal (± 5 Volts low impedance source)
EMG Bandwidth	(-3 dB) DC to 1,000 Hz
EMG channel sample rate	5000 samples per second per channel.
Calibrated signal gains	10 settings - 500uV pk-pk (x10,000) to 25 mV pk-pk (x200)
Signal to Noise ratio	50 dB typical
Cross talk (adjacent channels)	50 dB typical
Indicator Lights	Power OK, CRC error, No Signal, Individual event switch
Group delay (input to output)	Less than 2 ms at 1000 Hz.
Output Connector	25-pin male D-Sub
Interconnecting cable	18 meters of 2.66 mm RG174 coaxial cable

Table 4.5: Properties of the MA300-XVI electromyography system

for event switches (eg. foot switches), one port for the ground electrode and one port for the connection to the desktop unit.

After the preamplification stage, each channel is further amplified, filtered and digitally sampled at 5000 Hz by the backpack unit. The data transmission between

backpack and desktop unit therefore uses a digital communication, which significantly reduces the effects of electromagnetic noise.

The backpack's AD converters have an input range of ± 5 V. It is therefore of crucial importance to set the gain of each channel appropriately, so as to use most of the available voltage range but still avoid signal clipping. The gains can be set through red switches that have allow 10 different settings, as shown in table 4.6. For additional control over signal clipping, a blue LED indicator next to each gain switch lights up when the amplified signal exceeds the 5 V mark.

Gain switch	System gain	Maximum input level
0	350	± 14.0 mV
1	2000	± 2.50 mV
2	4000	± 1.25 mV
3	5700	± 875 μ V
4	8000	± 625 μ V
5	9500	± 525 μ V
6	11500	± 435 μ V
7	13200	± 375 μ V
8	16600	± 300 μ V
9	18000	± 275 μ V

Table 4.6: Gain settings of the backpack unit that allow to adjust the EMG signal to the ± 5 V range of the built-in ADC.

The backpack contains an adjustable anti-alias filter that allows to set the maximum EMG frequency that will be processed to avoid the possibility of recording signal aliasing errors. It passes all frequencies lower than the value selected and attenuate all analog signal components higher than the chosen value. The variable anti-alias filter provides seven different settings and is controlled by a rotary switch on the bottom right of the backpack unit. The choice of the filter frequency depends on the sampling rate of the customer-provided data collection system (see next paragraph) as, according to the Nyquist theorem, the sampling rate must be at least twice as high as the highest frequency content of the signal. Possible settings of the anti-alias filter are listed in table 4.7. Since our PCI data acquisition card was set to a sampling rate of 2000 Hz, we positioned the switch on setting number 4.

Filter switch	EMG bandwidth	Minimum sample rate
0	2000 Hz	4000 S/s
1	1750 Hz	3500 S/s
2	1500 Hz	3000 S/s
3	1250 Hz	2500 S/s
4	1000 Hz	2000 S/s
5	750 Hz	1500 S/s
6	500 Hz	1000 S/s
7	350 Hz	700 S/s

Table 4.7: Settings of the anti-alias filter of the backpack unit. A proper setting is necessary to adjust the signal to the sampling rate.

The 16 EMG probes are connected to the two lateral sides of the backpack unit. Even-numbered channels are on the right, odd-numbered channels on the left. Table 4.8 summarizes the used EMG channels and the associated muscles.

Channel	Side	Muscle
1	Right	Anterior deltoid
2	Left	Anterior deltoid
3	Right	Infraspinatus
4	Left	Infraspinatus
5	Right	Middle deltoid
6	Left	Middle deltoid
7	Right	Triceps
8	Left	Triceps
9	Right	Biceps
10	Left	Biceps
11	Right	Serratus anterior
12	Left	Serratus anterior
13	Right	Pectoralis major
14	Left	Pectoralis major
15	Right	Trapezius
16	Left	Trapezius

Table 4.8: EMG channels and associated muscles. We used even-numbered ports for muscles on the subject's left-hand side and odd-numbered ports for the right-hand side.



Figure 4.6: The NI PCI-6225 multifunction DAQ card

The desktop unit powers the backpack unit and receives the digitized EMG readings. It then converts the digital signals to analog signals and makes them available to any custom-provided data acquisition system through a 25-pin D-sub connector. Status lights on the front panel show the DC power status and provide fault detection plus an indication of signal quality. Eight activity indicators are dedicated to the event switch channels and light up when a switch is active.

Besides the bandwidth reduction by the anti-alias filter, the raw EMG signal produced by the desktop unit has not undergone any additional filtering.

PCI multifunction DAQ card

In order to record the EMG signals and to further process them, the analog signals provided by the MA300 desktop unit are fed into a NI PCI-6225 multifunction data acquisition card (National Instruments Corporation, Austin, TX, USA). The card can read up to 40 analog channels in differential mode, and samples them through 16 bit AD converters with a ± 10 V voltage range. The incoming data was sampled at 2000 Hz through drivers and software provided by National Instruments (mxDAQ, LabVIEW). Technical specifications of the DAQ card can be seen in table 4.9.

4.2.2 Motion capture system

The subject's position was tracked through a PhaseSpace Impulse motion capture system (PhaseSpace Inc., San Leandro, CA, USA). Eight cameras positioned on the walls of the laboratory were used to track the 3D position of 54 active markers. The coordinates

Manufacturer	National Instruments Corporation
Model	NI PCI-6225
Form factor	PCI
Measurement type	Quadrature encoder, Digital, Voltage, Frequency
Analog input channels	80 single-ended, 40 differential
ADC resolution	16 bits
Analog sample rate	250 kS/s
Max. voltage range	± 10 V
Analog output channels	two 16 bit channels updated at 833 kS/s
Digital I/O	24 bidirectional channels
Counters/Timers	two 32 bit counters, max frequency of 80 MHz

Table 4.9: Properties of the PCI multifunction DAQ card

of all markers were then processed by a custom software (see next section) to map the position of a multibody model of the subject's upper body.

Motion capture is accomplished by placing several PhaseSpace cameras around the capture volume, and moving objects with active LED markers attached to them. The information coming from all cameras is transmitted to a central computer that processes the data and calculates the position of each marker. The calculated positions are then available for further processing by client systems in a client-server environment.

The motion capture system available at the Upper Extremity Motor Function Laboratory consists of:

- Eight PhaseSpace cameras positioned around the perimeter of the laboratory
- Active LED markers to be placed on the subject
- Two LED driver units controlling the individual markers
- An LED base station communicating with the driver units
- A HUB to which the cameras and the LED base station are connected
- A server computer running a Linux OS and which communicates with the HUB
- A calibration wand used to calibrate the position of the cameras
- Server and client software

The PhaseSpace Impulse system has four primary components. LEDs are affixed to the target at predetermined positions. These LEDs are detected by the cameras, which

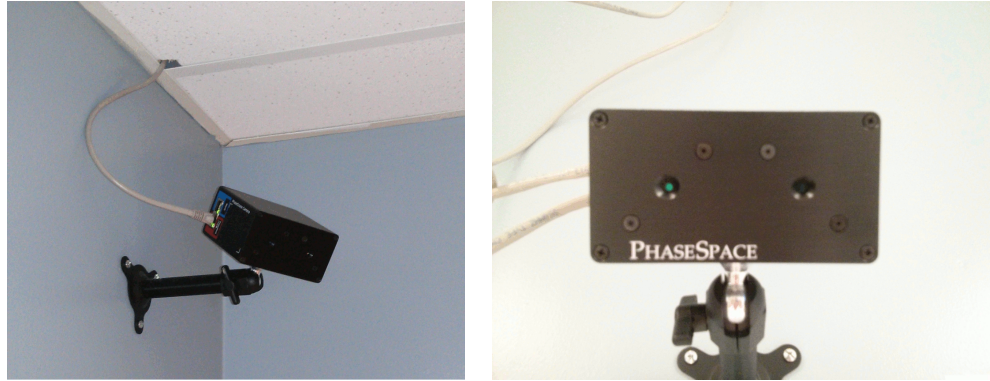


Figure 4.7: Eight PhaseSpace cameras are attached to the walls of the Upper Extremity Motor Function Laboratory. Each camera is connected to the central HUB.

then transmit data to the HUB. The HUB combines the information from multiple cameras and sends it to the server computer. The server can perform some further processing, like calculating position and orientation of certain pre-programmed objects, and makes the information available to all connected clients in the form of a TCP data stream. In addition, there is a calibration object that is required for camera calibration (mainly the extrinsic parameters).

Cameras: the system uses high-speed, high-resolution linear CCD cameras to triangulate the position of LED markers in real time. Each PhaseSpace camera has two detectors (figure 4.7). Each detector consists of a semi-cylindrical lens and a linear CCD at the focal distance of the lens and perpendicular to the axis of the lens. Cameras can be connected to each other and the HUB in a chain.

On the front of each camera are two apertures, behind each of which are the lens assembly and the CCD detector. On the side of each camera are two ethernet ports that are used to connect the camera to the HUB. Each camera achieves an optical resolution of 3600×3600 (12Megapixel) using two linear detectors with 16-bit dynamic range.

Active LED markers: The LED markers contain the actual light sources that are tracked by the cameras. Along with the light source each marker contains a microprocessor that controls the modulation of the LED's pulse duration and amplitude. Each LED has one of 12 LED designations (labeled A through L, figure 4.8a). This designation

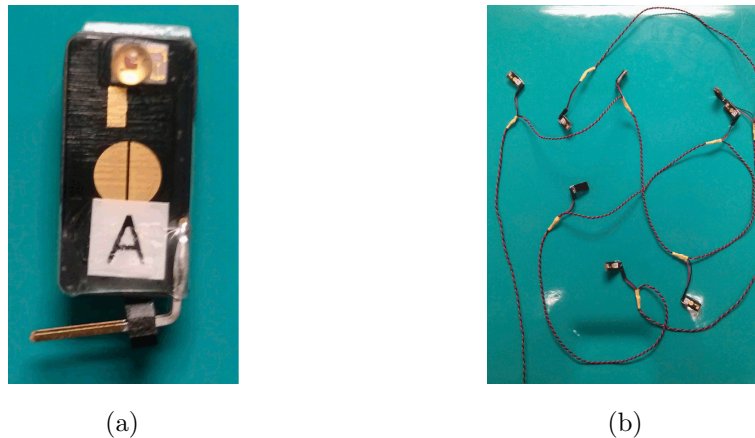


Figure 4.8: (a) Active LED marker. Each marker contains a light source (top), a microprocessor controlling the LED's pulse duration and amplitude, and is identified by a label (bottom). (b) Marker strings are connected to the ports of the driver unit and may contain up to 12 differently labeled markers.

along with the identifier of the LED driver gives each LED a unique identifier. Each LED is modulated at a unique frequency. This unique identification of each marker is one of the big advantages that the PhaseSpace system has with respect to other motion capture systems. In fact, other systems (such as the widespread Vicon system) rely on passive markers. This requires the operator to label each marker during the post-processing phase, which is a very time-consuming process, and can lead to problems when marker drop-out occurs (e.g. when a marker is covered during part of the data collection).

LED marker string: Markers are organized into strings, which consist of an LED cable and the LED cable connectors (figure 4.8b). The LED cable consists of two wires, one of which is colored. The connector has two sockets, one for each wire of the LED cable. A total of six LED strings can be attached to a driver unit. Each LED string is capable of having up to 12 LED modules attached to it using the proper LED connectors. Each LED module on a particular LED string must have a unique label.

LED driver unit: This unit is the driver of the LED modules (figure 4.9). The unit consists of a battery pack as well as an RF receiver, which receives a timing signal from



Figure 4.9: The LED driver unit communicates with the base station and can drive up to 72 active markers.

the LED base station. A total of six LED strings can be connected to a single driver unit. In our setup we used two driver units, seven strings and 54 markers; the positions of each LED marker are listed in table 4.10.

LED Base Station: The LED base station functions as the primary link between the PhaseSpace HUB and the LED system. The LED base station has the function of transmitting a timing signal to the LED driver units, and can also be used for programming the LED drivers. The transmission of the timing signal occurs once per frame and happens wirelessly through RF antennae, or directly through a 6-pin connection. The base station also has the capability to drive LED strings independently.

The position of all LED markers can be recorded at various frequencies, ranging from 120 Hz to 480 Hz. During this study kinematic data was captured at 240 Hz.

4.2.3 Software

We used two distinct software applications to collect and process the data of each trial. OBSIS (Orbis Biomechanical System Integration Suite) was adopted to collect and record the information coming from the various data sources, while a custom MATLAB code performed all the post-processing operations.

ID	LED string	Position	ID	LED string	Position	
0 A	left arm	arm	27 D	right arm	medial epicondyle	
1 B			28 E		lateral epicondyle	
2 C			forearm		29 F	
3 D		30 G				
4 E		31 H				
5 F		head	forearm	32 E	left hand	index knuckle
6 G				33 F		index nail
7 H				34 G		middle nail
8 A	top of the head		35 H	thumb nail		
9 B	back of the head		36 I	radial styloid		
10 C	forehead		37 J	ulnar styloid		
11 D	forehead		38 K	middle knuckle		
12 E	back of the head		39 L	back of the hand		
13 F	not used	40 E	right hand	index knuckle		
14 G	sternum	41 F		index nail		
15 H	not used	42 G		middle nail		
16 A	cervical v. (C7)	43 H		thumb nail		
17 B	thorax v. (T10)	44 I		radial styloid		
18 C	pelvis	back of the pelvis		45 J	ulnar styloid	
19 D				46 K	middle knuckle	
20 E		front of the pelvis		47 L	back of the hand	
21 F			48 E	scapula	left scapula	
22 G	49 F					
23 H	50 G	right scapula				
24 A	51 H					
25 B	52 I					
26 C	right arm	arm	53 J			

Table 4.10: Marker set used during the data acquisition. Seven LED strings were used to track the body segments. Each LED has a specific ID that consists of a number and a label (a letter) for each LED string.

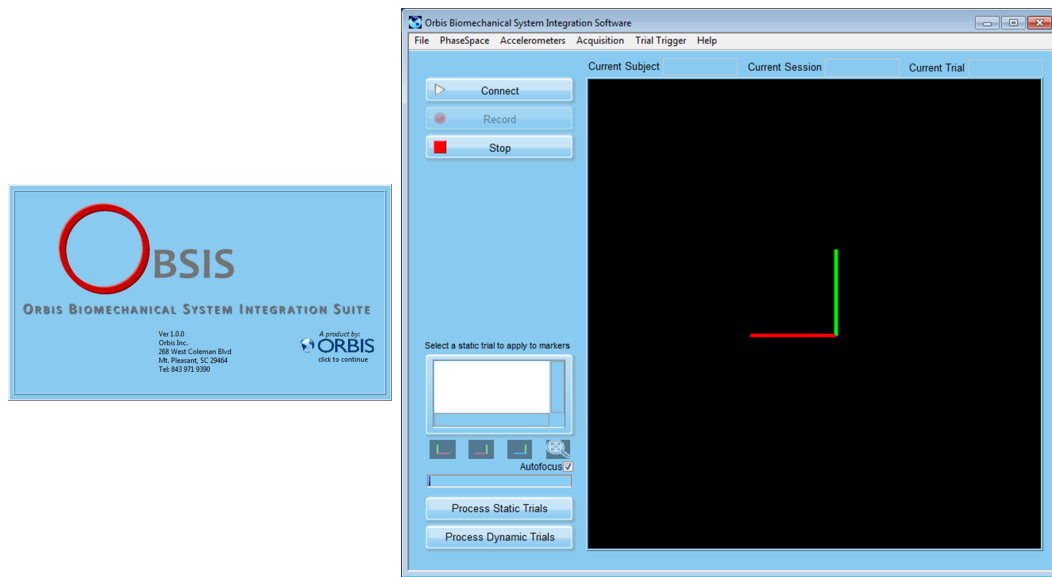


Figure 4.10: The OBSIS biomechanical integration suite was used to collect, record and synchronize data coming from the EMG and the motion capture systems.

OBSIS is a software tool based on LabVIEW (National Instruments Corporation, Austin, TX, USA) and was developed by Orbis, Mt. Pleasant, SC, USA. It was designed to integrate the PhaseSpace motion capture system with other data sources, such as EMG systems, force plates or goniometers. The software communicates with the PhaseSpace server through a TCP socket and interfaces to other analog or digital data sources with a National Instruments data acquisition card. The default option is a USB data acquisition system, but the version used for our experiments was customized to use the PCI-6225 DAQ card. Two parallel threads manage the data coming from PhaseSpace and from the DAQ card and synchronize all sources with a common time stamp. During the data collections the software provides a live preview of the incoming data, and writes all recorded parameters to text files.

Kinematic data coming from PhaseSpace can be previewed and logged in various ways. The simplest option is to use the raw data, i.e. the unprocessed 3D coordinates of each marker. In this case the preview window shows the position of each marker as red dots in a 3D virtual environment, and only the x, y and z coordinates of each marker are logged. A more advanced mode allows the user to use a model file that specifies how each marker is mapped to a multibody model of the upper body. The model is

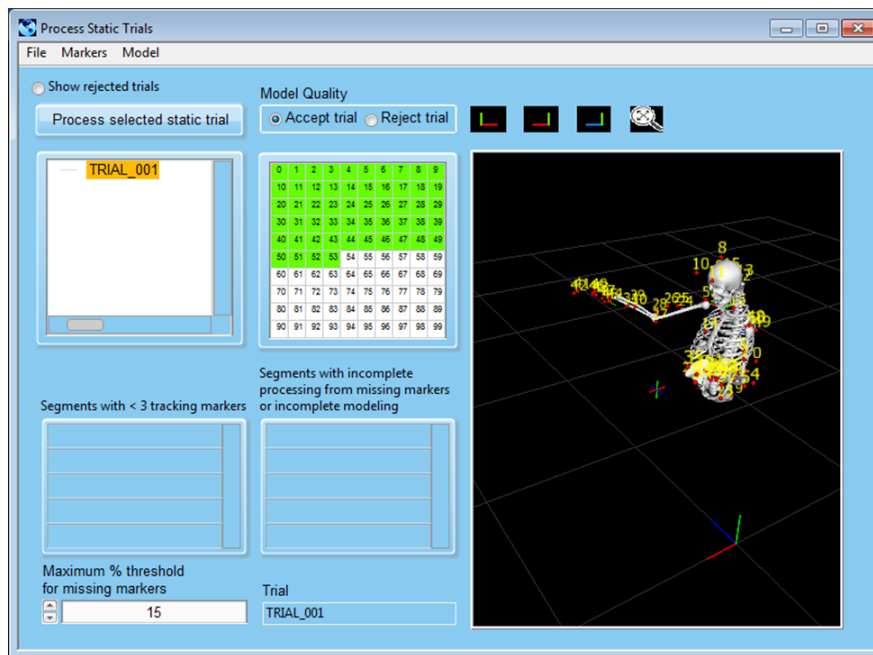


Figure 4.11: A static trial is necessary to calibrate the kinematic model and adapt it to the current test subject. After successful calibration the model can be previewed as a 3D skeleton following the subject's movements.

structured into segments such as pelvis, trunk, head, arm, forearm and hand. The user can associate groups of markers to a certain segment, specify the position of each marker on the segment and define a local reference frame describing the 3D position and orientation of that segment. Prior to the data collection it is necessary to run a static trial which is used to calibrate the model to the current test subject (figure 4.11). After successful calibration the model can be previewed as a 3D skeleton following the subject's movements. Furthermore, by knowing the position and orientation of each segment OBSIS can calculate additional parameters like joint angles and angular velocities.

EMG and other analog signals can be recorded by selecting the desired channels of the DAQ board. Each channel can be labeled with a custom text string, simplifying their identification during the following processing steps. No further settings are required and all channels are readily available for preview and logging. The preview of the EMG data is particularly useful, as it allows to test the connections during the placement of

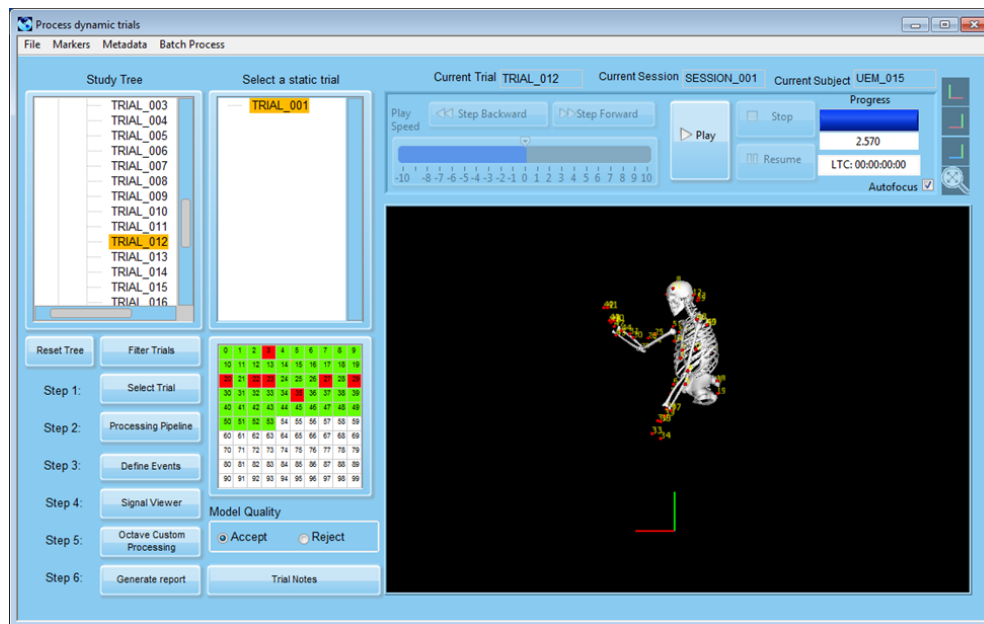


Figure 4.13: In the post-processing step the user can replay the selected trial and apply various processing techniques and filters.

4.2.4 Preparation procedures

Prior to the data collection session each subject was given a detailed description of the experimental protocol and was then asked to sign a consent form. Additionally, stroke patients had to undergo three clinical assessments, namely the Fugl-Meyer assessment, Activity Card Sort and the Stroke Impact Scale.

After giving informed consent, all subjects were asked to sit on a bench located at the center of the laboratory, which was adjusted in height so that their knees were bent at a 90° . We then proceeded with the preparation of the skin around the areas where the EMG electrodes would be placed by wiping it with alcohol pads. After the skin had dried we applied the electrodes and connected the probes. The backpack unit was attached to a Velcro belt around the subject's waist, and all probes were connected to the assigned ports. Subsequently we wrapped both forearms and arms with elastic Velcro bands, which held the underlying electrodes in place and acted as support for some markers. All probe cables were arranged so that they would not interfere with any movement and were fixed with tape when necessary. We then applied pieces of

Velcro tape to all remaining marker locations, except for the head markers which were positioned on a custom headband. Markers were applied to their predefined locations and connected to the two driver units. We made sure that all wires did not interfere with movements and did not get pulled in any circumstance. In the last phase we tested all connections and markers, adjusted the EMG gains and acquired the static trial.

The final step was to configure OBSIS to acquire all data at the desired sampling frequencies. Kinematic data was collected at 240 frames per second, i.e. the position of each marker was received at 240 Hz. EMG signals were collected and recorded at 2000 Hz.

4.3 Data processing

After the completion of all trials the recorded data was partially processed in OBSIS, while all remaining steps were performed by a custom MATLAB code. OBSIS was mainly used for filtering and interpolating marker positions, calculating joint angles and angular velocities, and for defining the time instants of movement onset and end. The MATLAB code loaded the data obtained with OBSIS and performed some further steps, such as the calculation of the linear EMG envelopes, the extraction of motor modules and of the corresponding activation coefficients, all further calculations related to the extracted motor modules, and the generation of all plots and figures.

4.3.1 Interpolation and smoothing of kinematic data

During the execution of a trial not always all markers can be detected by the PhaseSpace system. For example, a marker could be temporarily covered by an object or a body part, could be visible only to very few cameras or could be in an area of the room that was not calibrated with sufficient accuracy. In all these cases, PhaseSpace will label the marker as not visible and will assign it an arbitrary position. The system is set to place all non visible markers at the origin of the laboratory reference frame.

To obtain a better estimation of the missing marker coordinates, OBSIS reprocesses all the positions and interpolates over small gaps. Bigger gaps are ignored (the coordinate values are set to NaN), as in this case an interpolation could introduce considerable errors in the estimation of the marker position. Figure 4.14 shows an example of the

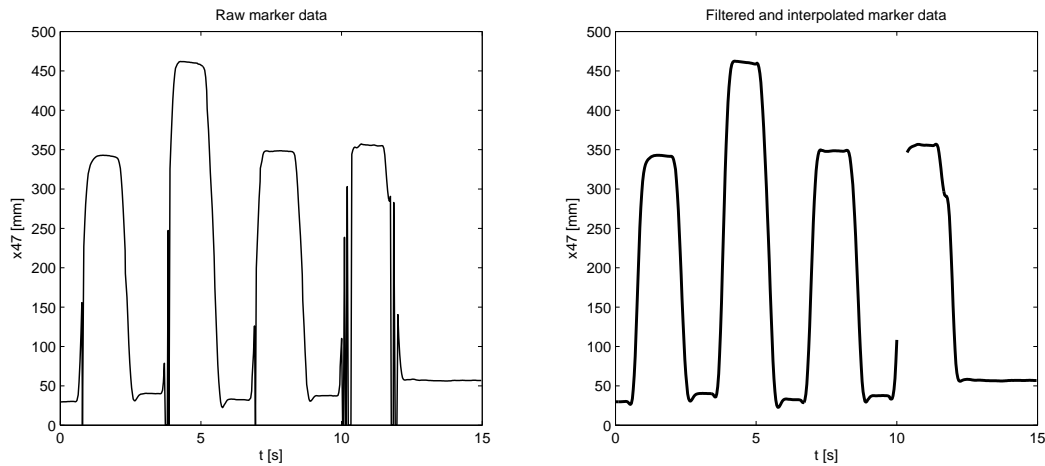


Figure 4.14: Raw and interpolated x-coordinate of marker 47 during a reaching task. When PhaseSpace cannot detect the position of a marker, it sets its position to 0. In the interpolation stage the unknown coordinates can be guessed by using adjacent values. OBSIS does not interpolate over big gaps, as this could lead to errors in the estimated position.

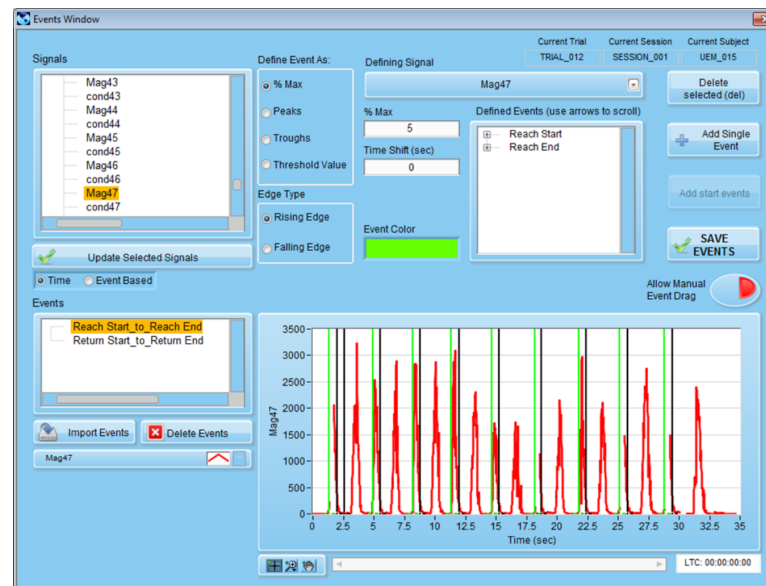
x-coordinate of marker 47 before and after interpolation.

The positional data is further processed in OBSIS by applying a smoothing filter. The software is set to use a 3rd order Savitzky-Golay filter [123] with six side points and a 240 Hz resampling frequency. Besides its documented smoothing properties, the polynomial nature of this filter allows also for a straightforward numerical differentiation. This property is used by OBSIS to obtain velocities and accelerations of each marker. Furthermore, the software also calculates the magnitudes of the velocity and acceleration vectors and provides them in a separate data structure.

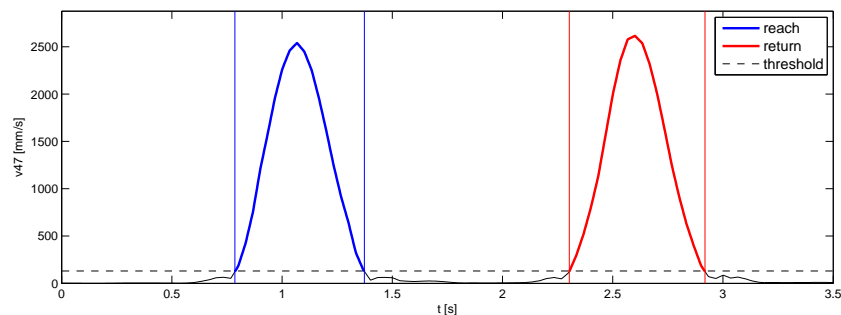
4.3.2 Definition of events

Even though kinematic and EMG data was collected continuously throughout each trial, we were interested only in the EMG activity and kinematic variables during movement execution. For this reason it was necessary to define the onset and end times of each movement, which was done with a tool provided by OBSIS (figure 4.15a).

Movement onset and end times were defined by looking at the profile of the velocity



(a)



(b)

Figure 4.15: (a) Interface of the OBSIS environment used to define events. (b) Movement onset and end times were defined by looking at the velocity magnitude of a wrist marker of the tested side. The subject's hand was considered to be moving when the velocity was higher than 5% of its peak value. Events were defined separately for the reach and for the return movements.

magnitude of a marker on the wrist of the tested side. For tasks involving the left arm we used marker 39, while for tasks performed with the right arm we used marker 47. Both markers were positioned at the base of the third metacarpus. The subject's hand was considered to be moving when the wrist velocity was higher than 5% of the peak value observed during the whole trial. Furthermore, events were defined separately for

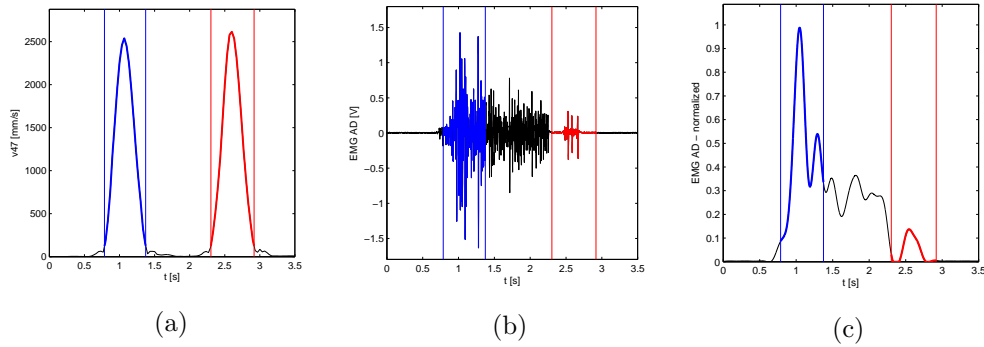


Figure 4.16: (a) Events defined by looking at wrist velocity (blue for reach, red for return). (b) Raw EMG signal as recorded by OBSIS (right anterior deltoid). (c) Linear EMG envelope of the normalized signal; in this case the low-pass filter frequency is of 5.1 Hz.

the reach and for the return movements (figure 4.15b).

4.3.3 EMG processing

The processing of the recorded electromyographic data, so as all following steps, were performed using a custom MATLAB code. EMG data was high-pass filtered with a 30 Hz 4th order Butterworth filter to remove motion artifacts and heartbeat noise [104], demeaned, full-wave rectified and low-pass filtered with a 4th order Butterworth filter (see figures 2.10a, 2.10b and 2.10c). The low-pass cutoff frequency was adapted to the velocity of each movement to obtain a similar smoothing effect across different conditions [102]. This was done by taking the average execution time T of each movement, as obtained from the definition of movement onset and end times, and calculating the cutoff frequency as $f = 3/T$ (figure 4.16). This method yielded frequencies in the range of 3 to 8 Hz, which are common values found in literature (see chapter 1). Each channel was normalized by the maximum average EMG activity in all movements over a 90 ms window and subsequently subsampled to obtain 100 equally spaced samples for each movement repetition. The filtered and subsampled EMG signals of each tested side were stacked in a 7500×8 matrix V , in which each row represents a sample (15 movements \times 5 repetitions \times 100 samples) and each column represents a muscle (figure 3.1) The indices of the block of EMG data in V relative to each movement were saved in a

separate structure, used for example to verify how well the decomposition in modules can describe a single movement (see next section).

4.3.4 Extraction of motor modules

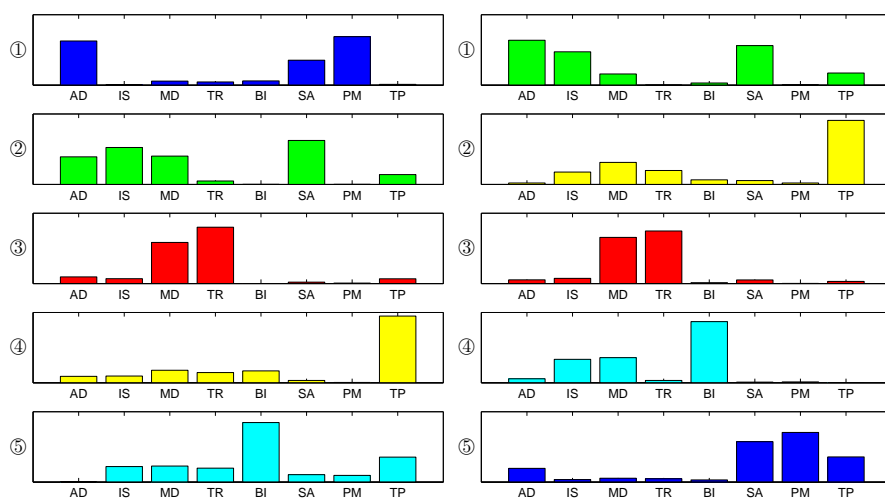
Motor modules were extracted independently from the left and from the right-hand side. We extracted them directly from the pooled EMG data of all movements, i.e. from the matrix V described in the previous paragraph.

The factorization into modules and activation coefficients (equation 3.1) was performed with a non-negative matrix factorization algorithm (NMF) using the multiplicative update rule based on the Euclidean distance cost function. To avoid capturing local minima, we repeated the factorization with 500 random initial guesses of W and H and selected the solution giving the best reconstruction of the original EMG envelopes (measured by the sum of squared errors). Each factorization was stopped after 100 updates. Since the number of modules is needed as an input to the NMF algorithm, we repeated the extraction for values of n ranging from 1 to 8. For each number of modules we calculated the variability accounted for (VAF), as defined in equation 3.4. Additionally, we calculated how well a factorization could reconstruct the muscle activation patterns of each single movement. This was accomplished by rewriting equation 3.4, using only the data blocks of the two matrices V and H relative to the analyzed movement.

We chose the number of modules that explained at least 95% of the pooled EMG signals of all movements and at least 80% of the EMG data of each single movement, similarly as in [59]. This guaranteed a good reconstruction of the original EMG signals, and helped us capturing the overall muscle coordination strategy without losing finer movement-specific details.

4.3.5 Shared and specific modules for each side

In order to determine the number of shared modules between dominant and non-dominant side, or impaired and unimpaired side of the same subject, we paired the modules by looking at their similarity. The similarity was assessed by means of Pearson's correlation coefficient between the normalized modules. We paired first those modules with the highest correlation, and continued in descending order until hitting a threshold



(a) Dominant

(b) Non-dominant

		Dominant				
		1	2	3	4	5
Non-dominant	1	0.276	0.860	-0.372	-0.187	-0.486
	2	-0.533	-0.138	0.090	0.965	0.156
	3	-0.403	-0.068	0.991	-0.105	-0.136
	4	-0.430	-0.184	-0.121	-0.146	0.847
	5	0.672	-0.010	-0.485	-0.022	-0.414

(c) Correlation between modules

Figure 4.17: Comparison between modules of the dominant and non-dominant side. Modules with the highest correlation are shared first. In this case, all five modules can be paired and show a correlation higher than the threshold value.

(figure 4.17). The similarity threshold was determined by calculating the correlation between 4000 random normalized modules and by taking the 95th percentile of this distribution (figure 4.18). Modules with a correlation higher than this threshold are unlikely to be similar by chance. All remaining modules were considered as specific for a side.

4.3.6 Healthy control subjects

Modules extracted from EMG data of healthy control subjects were used to generate a neuromusculoskeletal model that could give us insight in what coordination patterns can be found in different subjects and what biomechanical functions they represent, and

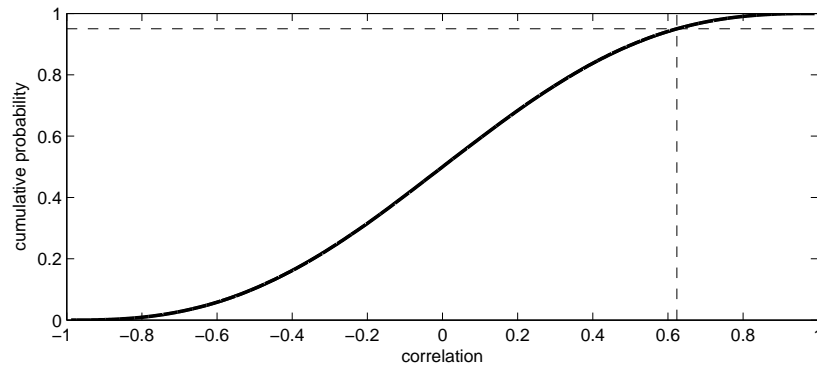


Figure 4.18: Probability distribution of the Pearson's correlation coefficient between random modules with eight muscles. Modules with a correlation higher than 0.62 have less than a 5% probability to be similar by chance.

that could be adopted as a reference to which we could compare stroke patients.

Finding similar coordination strategies between different subjects

We evaluated whether there were shared muscle coordination strategies between subjects by comparing the modules of all subjects. This analysis was performed separately for dominant and non-dominant side. Motor modules were compared through a k means cluster analysis, similarly as in [19, 57], with a cost function based on the Euclidean distance between cluster centroids and the associated data points. The number of clusters was determined iteratively, starting by one and increasing it until all modules in each cluster were sufficiently well correlated with the corresponding cluster centroids. For each number of clusters the analysis was repeated 100 times, and we selected the solution with the lowest cost. The threshold value of the Pearson correlation between cluster centroids and motor modules was determined as in the comparison between dominant and non-dominant side, i.e. by taking the 95th percentile of the correlation distribution of 4000 random modules (figure 4.18).

Biomechanical functions associated with motor modules

The clustering of motor modules of different subjects, as described in the previous paragraph, gave us a general idea of the most commonly used coordination strategies. We looked at how many subjects shared a certain module and sorted all module clusters in order of descending frequency. We then picked the five modules of the dominant and non-dominant side that were shared by most subjects, and analyzed their possible biomechanical function. The analysis was performed qualitatively but in collaboration with trained personnel having multiple years of experience in the field of upper extremity biomechanics.

We analyzed each cluster centroid separately and considered only those muscles that participated significantly to the represented module. To determine if the muscle was participating or not, we chose a value of 0.3 as the threshold for the muscle weights. We then looked at the individual actions of each participating muscle, and estimated what function they would achieve when working synergistically. After determining the possible biomechanical function, we looked at the activation coefficients associated to the module and observed if their timing and use for different tasks were consistent with the hypothesized function.

Most relevant movements

The average time needed for the collection of all 15 movements was of three hours on average. Although the collected data provided us with a lot of information and allowed us to generate a quite detailed model, we wanted to investigate if for the purpose of extracting motor modules some movements were redundant. In essence, the question was if we could determine a subset of movements that could give us similar results with less effort and in less time.

We tried to answer this question by looking at all possible subsets of movements and by extracting motor modules only from the EMG data of each subset. However, from a computational point of view this would be exceptionally challenging. In fact, if considering all possible subsets of movements, one would have to calculate 32767 factorizations per subject (see table 4.11), which, depending on the computer hardware, could take up to multiple weeks. For this reason we limited the maximum number

of movements to five and calculated all possible combinations using from one to five movements. This reduced the total number of calculated factorizations to 4943 per subject.

Number of movements	Possible combinations	Total factorizations
1	15	15
2	105	120
3	455	575
4	1365	1940
5	3003	4943
6	5005	9948
7	6435	16383
8	6435	22818
9	5005	27823
10	3003	30826
11	1365	32191
12	455	32646
13	105	32751
14	15	32766
15	1	32767

Table 4.11: Number of factorizations per subject to calculate as the size of the subset of movements increases. The second column shows the number of possible combinations when picking a certain number of movements out of the initial 15. The second column shows how many factorizations have to be calculated when considering all possible combinations, starting from a subset of one movement.

The modules obtained from each subset of movements were compared to those extracted from the whole set by calculating the scalar product between the best-matching pairs. We then looked at how well a certain subset of movements could replicate the results obtained with all movements, and identified the movement combinations that would give the best matching.

4.3.7 Stroke patients

Modules of stroke patients were processed in a slightly different manner, as many of the techniques used for healthy controls would not be applicable in this case. Furthermore,

the goal was to compare the muscle coordination strategies of stroke patients to the model developed with healthy control data, and not to develop a new model valid only for stroke patients.

The comparison was done on various levels. In a first step we looked at how the number of modules changed in stroke patients when compared to healthy controls, and also when comparing the impaired with the unimpaired side. Secondly, we observed how the severity of motor impairment, as measured by the Fugl-Meyer score, was related to the number of modules. In a third step, we compared the motor modules of stroke patients to those most commonly used by healthy controls.

Number of modules: comparison between impaired and unimpaired side

From the extraction of motor modules we obtained the number of modules needed to explain the muscle activation patterns of both healthy controls and stroke patients. These numbers were calculated independently for the dominant and non-dominant side (control subjects), and for the impaired and unimpaired side (stroke patients).

In order to understand how the number of modules of stroke patients differed between impaired and unimpaired side, we first had to see if there were significant differences between the dominant and non-dominant side in healthy controls. This first comparison was performed with a paired two-tailed t-test. We then used a paired one-tailed t-test to look for differences in the number of modules between impaired and unimpaired side, applying it first to all stroke patients, and then separately to the mildly and moderately impaired groups. The test was one-tailed and not two-tailed because we wanted to understand if the number of modules on the impaired side was smaller than the number of modules on the unimpaired side.

Number of modules: comparison with healthy controls

We wanted to analyze if the number of modules on the impaired side and the number of modules of the unimpaired side were statistically different than the number of modules expected in healthy control subjects. After making sure that there was no significant difference between the number of modules of the dominant and non-dominant side of control subjects, we grouped these two sets of numbers and compared them first with the impaired side and then with the unimpaired side of stroke patients.

Before we performed the comparisons we assessed the similarity of variances through an F-test. The two comparisons were based on a t-test for unequal sample size and equal variance, and were only single-tailed as we wanted to see if the number of modules decreased post-stroke.

Relationship between motor impairment and number of modules

A simple regression analysis between number of modules and Fugl-Meyer score was used to observe if the level of motor impairment was related to the number of modules. The analysis was repeated for both impaired and unimpaired sides, and we assessed the strength of the tested relationship by means of Pearson's correlation coefficient between the two variables and by its p-value.

How do modules change after stroke

In this last step we we wanted to explain the difference between modules of stroke patients and those of healthy controls. We used the five most commonly used modules of healthy subjects as a reference, and compared them with all modules found in each stroke patient. As mentioned in chapter 1, some authors have hypothesized that the changes in muscle weights and timing coefficients could be explained by merging and/or splitting of motor modules found in healthy subjects. In this study we described the modules of stroke patients in three possible ways:

- As coincident with one of the modules found in healthy subjects. In this case it is likely that the module was preserved after the stroke.
- As a result from the merging of two or more modules found in healthy subjects. This could represent the inability of some stroke patients to control each module independently.
- As a completely new module developed after the stroke, if neither of the two previous solutions was applicable. This could represent compensatory strategies developed post stroke.

To accomplish this, we first selected the five modules that were most commonly used by all healthy control subjects on both dominant and non-dominant side, and used

them as a reference. We limited the number to five because we just wanted to use the most significant modules for our comparison.

We then tried to find a combination of one or more reference modules to describe the modules of each stroke patient. To do this, we generated all possible combinations of n reference modules, where n varied from one to five. Each of these combinations was then used to approximate all modules of a stroke patient in form of a linear combination of reference modules:

$$h_{s,i} \approx c H_{r,j} \quad (4.1)$$

$h_{s,i}$ is the i -th module of the analyzed stroke patient, c is a row vector of coefficients, and $H_{r,j}$ is a matrix containing the j -th combination of reference modules. Equation 4.1 was solved for c by using a non-negative least squares algorithm (MATLAB function *lsqnonneg*). The quality of the reconstruction was assessed by looking at the correlation between $h_{s,i}$ and its approximated value $c H_{r,j}$.

We then took only those solutions that gave good matching between reconstruction and original module (as explained in the paragraph on module clustering, and as shown in figure 4.18), and sorted them in descending order of their associated quality of reconstruction. Starting from the best solution, we removed all other solutions that used the same reference module or reconstructed the same module of the analyzed patient, and passed on to the next best solution. This process was iterated until no more solutions were available.

Those modules that could be described with only one reference module were considered as preserved, those described as a linear combination of two or more reference modules were seen as a result from merging, and all remaining modules were regarded as newly developed after the stroke.

Chapter 5

Results

This chapter presents the main findings of this research project, and is structured into three parts. The first part describes the results relative to the number of extracted modules of both healthy subjects and stroke patients, and analyzes how many of these modules are shared between the two tested sides. The second part focuses only on healthy control subjects, showing the coordination strategies shared by most participants and the associated biomechanical functions. Furthermore, this part presents the identified most relevant movements, i.e. the subset of movements that could yield similar results to those obtained with all movements. The third and last part analyzes in more detail the motor modules found in stroke patients. Modules are first compared between impaired and unimpaired side, and then with those of our healthy participants. Subsequently we analyze the relationship between the level of motor impairment and the number of extracted modules, and give a possible explanation for the differences between modules of healthy subjects and those of stroke patients.

5.1 Extracted motor modules

After finding the best factorization of the EMG matrix V in the product WH for each subject, each tested side and each number of modules from one to eight, we assessed the quality of the approximation by calculating the VAF index. The variability accounted for was calculated for the pooled EMG data of all movements and for the data of each single movement. The 15 tested movements were numbered in the following way:

1. Multidirectional reaching, highest row, contralateral column
2. Multidirectional reaching, highest row, central column
3. Multidirectional reaching, highest row, ipsilateral column
4. Multidirectional reaching, central row, contralateral column
5. Multidirectional reaching, central row, central column
6. Multidirectional reaching, central row, ipsilateral column
7. Multidirectional reaching, lowest row, contralateral column
8. Multidirectional reaching, lowest row, central column
9. Multidirectional reaching, lowest row, ipsilateral column
10. Reaching to forehead
11. Reaching to the side
12. Moving objects on transverse plane, reach
13. Moving objects on transverse plane, return
14. Moving objects parallel to sagittal plane, reach
15. Moving objects parallel to sagittal plane, return

5.1.1 Healthy control subjects

The number of modules was chosen by accepting the solution with the lowest dimensionality that would explain at least 95% of all combined movements, and at least 80% of each single movement. Figure 5.1 shows an example of how the number of modules on the dominant side of subject 14 was determined. This example allows us to note one interesting fact found in all analyzed cases. When looking at figure 5.1b one can see that not all movements are reconstructed with the same accuracy. As a consequence, even if the reconstruction of all combined movements reaches the 95% accuracy mark, some movements might not be represented very well. This was the main reason why

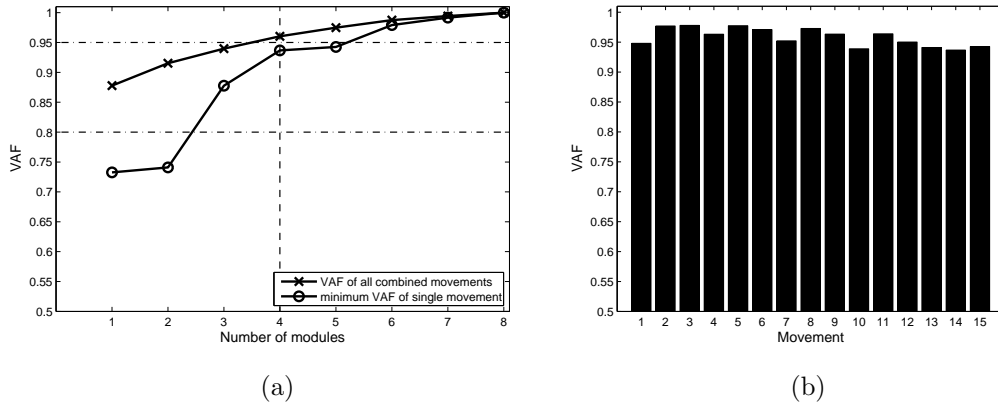


Figure 5.1: (a) Determination of the number of modules needed to meet the desired reconstruction accuracy. In this example (subject 14, dominant side), four modules are sufficient to explain more than 95% of the pooled EMG signals of all movements and more than 80% of the EMG data of each single movement. (b) VAF of each single movement when using four motor modules.

we introduced an additional control on the reconstruction accuracy of all individual movements.

For each subject and for each tested side we stored the factorization results for further processing. Figure 5.2 shows the motor modules and activation coefficients extracted from the dominant side of subject 14. The figure shows also how every module has a very distinct activation pattern specific to each movement. In fact, the time-varying activation coefficients are very consistent from repetition to repetition, showing that the factorization detected the biomechanically significant features of the EMG signal without capturing much noise. Furthermore, by looking at the activation coefficients it is easy to identify the movements and movement phases in which a module is particularly active, and movements where the same module is not significantly participating.

Another way to observe the participation of a module to a certain movement is to analyze its contribution to the activity of each muscle, as shown in figure 5.3. The EMG signal of a muscle results from the sum of the contributions of all modules, each of which may be predominantly active in different phases of the movement. For example, figure 5.3 shows that during movement 5 and for the dominant side of subject 14, the activity of the infraspinatus is mainly determined by module 2 in the first phase of the

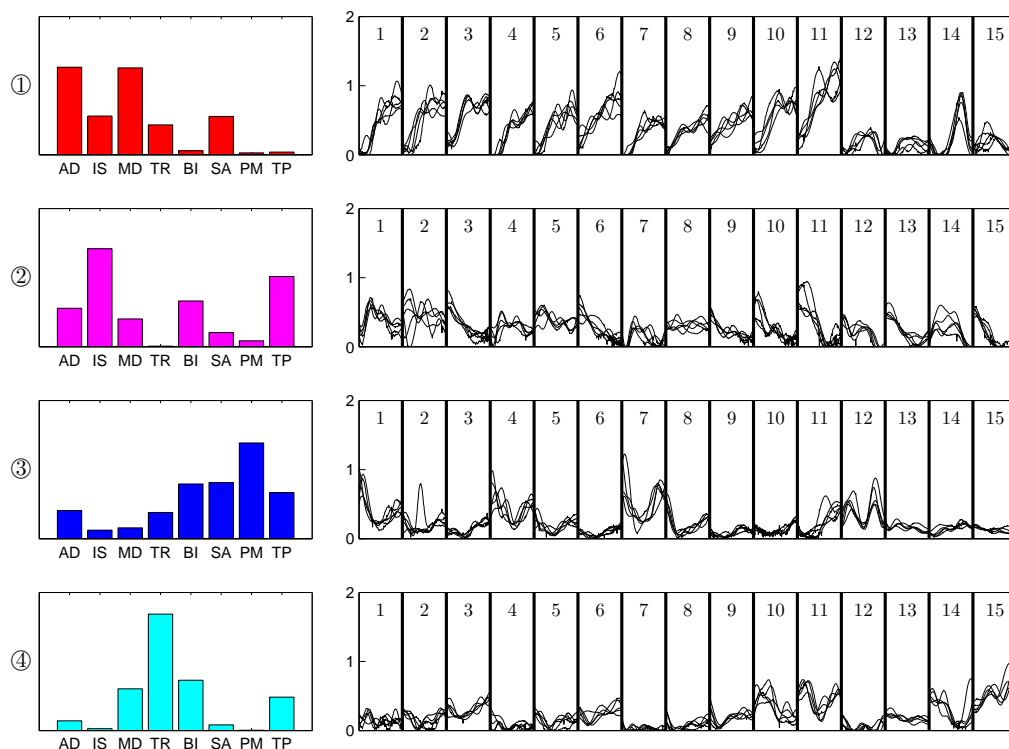


Figure 5.2: Motor modules and associated activation coefficients of the dominant side of subject 14. All four modules are plotted on the left of the figure, and the corresponding time-varying activation coefficients are on the right. The figure shows the activation coefficients associated with each movement (numbered 1 to 15), where each line stands for one of the five movement repetitions. Inside each box, the abscissa axis represents the percentage of movement execution, ranging from 0% to 100%.

movement, while towards the end module 1 starts to give a significant contribution. These observations were used as an additional tool to determine the biomechanical function of each module, as will be explained later in this chapter. In this example, the activation of module two is almost constant over time, indicating that the module might have a stabilizing function. On the other hand, the activation of module one changes significantly during movement execution. Considering that the module activates mainly the deltoids and the serratus anterior, and since the movement consists in a forward reach, the module could be helping during shoulder flexion and compensating for the increasing moment arm of the limb's weight.

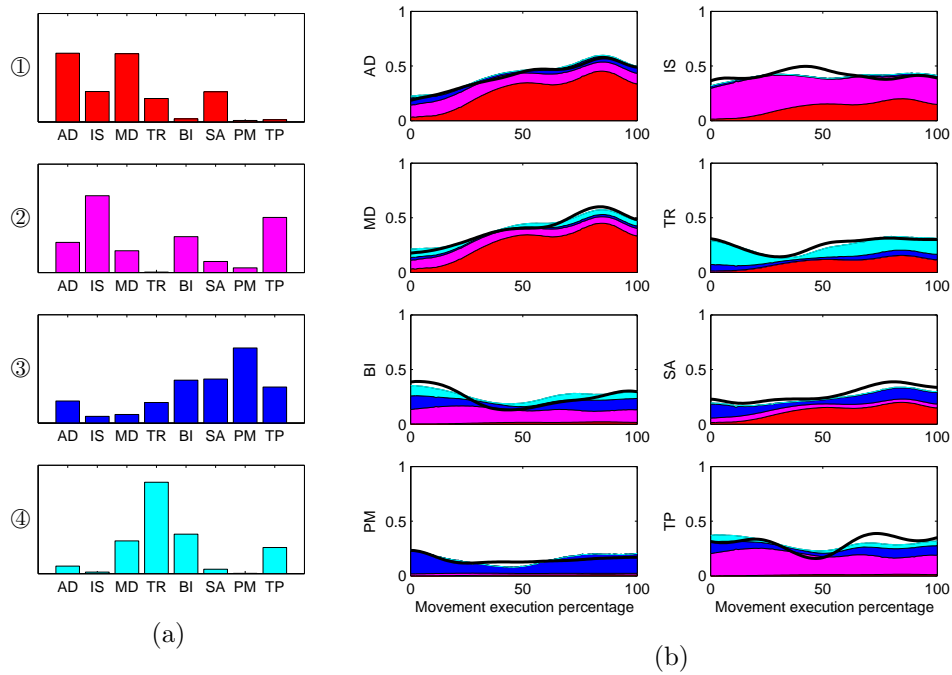


Figure 5.3: (a) Motor modules of the dominant side of subject 14. (b) Contribution of each module to the generated EMG signals. The area under each curve represents the activity of the color-matched module. The figure shows the average EMG signal (black line) and the average activity of each module over all five repetitions of movement 5 (Multidirectional reaching, central row, central column).

Figure 5.4 shows how the extracted motor modules and activation coefficients could reconstruct the measured EMG data. In this figure, which shows data relative to the dominant side of subject 14, we plotted the average EMG activity over all five movement repetitions in black, and the average EMG reconstruction in red. By visual inspection one can see that the 95% and 80% VAF thresholds guaranteed a good reconstruction of the EMG activity of each muscle and for each movement.

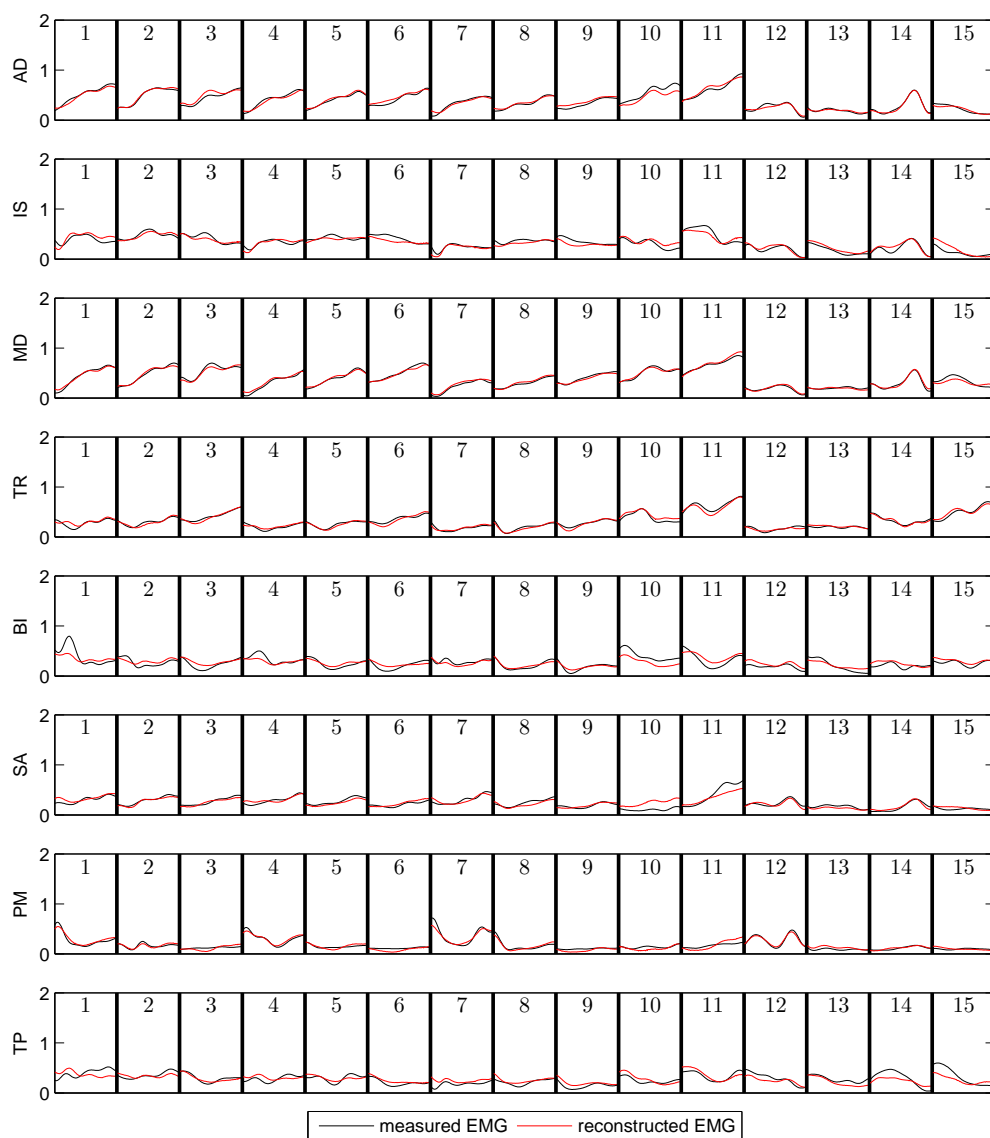


Figure 5.4: Reconstruction of the measured EMG signal by using the extracted motor modules. In this example we show the data of the dominant side of subject 14. The black line represents the average EMG activity over all five repetitions of each movement. The red line is the reconstructed EMG signal, also averaged over all movement repetitions. Each box contains the data of a single movement (numbered 1 to 15) and has the percentage of movement execution on the abscissa axis.

These methods of analysis were applied to the EMG data of both tested sides of all participants. The resulting number of modules for all healthy subjects is shown in table 5.1.

Subject	Left	Right	Dominant	Non-dominant
1	5	5	5	5
2	5	5	5	5
3	5	5	5	5
4	5	4	5	4
5	5	5	5	5
6	5	5	5	5
7	3	4	3	4
8	4	4	4	4
9	5	5	5	5
10	4	4	4	4
11	4	4	4	4
12	4	4	4	4
13	4	4	4	4
14	4	4	4	4
15	5	5	5	5

Table 5.1: Number of motor modules found for each healthy control subject.

On average, all healthy control subjects had 4.4 modules on their dominant side (range 3-5) and 4.5 modules on their non-dominant side (range 4-5). Interestingly, these numbers were very consistent throughout all subjects, and were in agreement with the data reported in literature (see chapter 1).

	Left	Right	Dominant	Non-dominant
mean	4.47	4.47	4.4	4.53
min	3	4	3	4
max	5	5	5	5
σ	0.62	0.5	0.61	0.5

Table 5.2: Average number of modules, range and standard deviation of all healthy subjects.

5.1.2 Stroke patients

Modules of stroke patients were extracted with the same techniques applied to healthy control subjects, and the results are showed in table 5.3.

Subject	Left	Right	Impaired	Unimpaired
1	1	2	2	1
2	2	4	2	4
3	3	3	3	3
4	2	2	2	2
5	3	2	2	3
6	1	3	1	3
7	4	2	2	4
8	3	3	3	3
9	3	3	3	3
10	4	3	3	4
11	3	2	3	2
12	1	4	1	4
13	3	2	2	3
14	3	3	3	3

Table 5.3: Number of motor modules found for each stroke patient.

The only methodological difference to the processing of healthy control data is that we did not assign the modules to dominant and non-dominant side, but instead to impaired and unimpaired side.

	All		Mild		Moderate	
	Impaired	Unimpaired	Impaired	Unimpaired	Impaired	Unimpaired
mean	2.29	3	2.38	3	2.17	3
min	1	1	1	1	1	2
max	3	4	3	4	3	4
σ	0.7	0.85	0.7	0.87	0.43	0.82

Table 5.4: Average number of modules, range and standard deviation of all stroke patients, mildly impaired patients and moderately impaired patients.

As expected, and as found in literature, the number of modules of stroke patients is

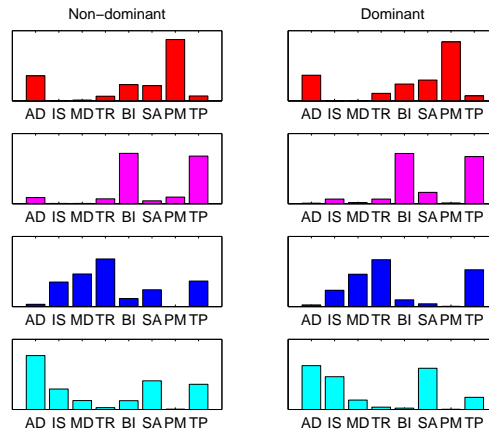


Figure 5.5: Modules of healthy subject 11. Matching modules of dominant and dominant side are represented with the same color. In this case, all modules could be matched between the two tested sides, meaning that all coordination strategies were shared.

lower than that of healthy controls. As shown in table 5.4, on average all stroke patients had 2.3 modules on their impaired side and 3 modules on their unimpaired side. This statistic doesn't change by much when separating the subjects in a mildly impaired group and a moderately impaired group. Interestingly, also the number of modules on the unimpaired side is lower than what found for healthy subjects, indicating that there is some level of motor impairment even on the ipsilesional side. The difference between the number of modules of impaired and unimpaired side, as well as the differences to the healthy control group will be further analyzed later in this chapter.

5.2 Shared and side-specific modules

After the extraction of motor modules, the next step was to compare those of healthy subjects between dominant and non-dominant side. The purpose of this step was to assess whether some coordination strategies were shared between the two sides. The comparison was done by matching modules that were significantly correlated, starting from the best matching pair and continuing until no more pairs were available. All modules that could not be matched were labeled as specific to one side. Figure 5.5 shows the modules of healthy control subject 11, all of whose modules were shared between dominant and non-dominant arm. In a more general case, such as the one showed in

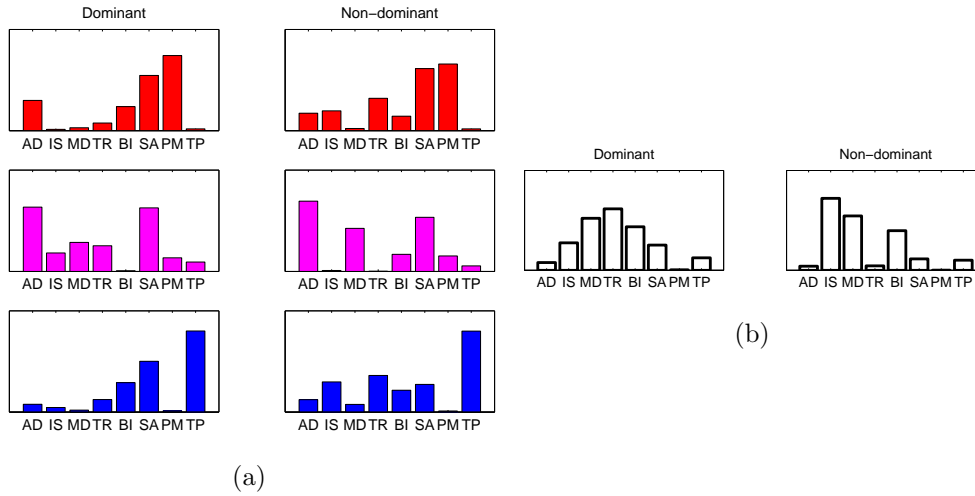


Figure 5.6: Modules of healthy subject 8. (a) In this case, three modules were shared between dominant and non-dominant side. Matching modules are represented in the same row and with the same color. (b) One module per side was specific to only one arm.

figure 5.6, some modules were shared and others were specific to either dominant and non-dominant side.

The number of shared and specific modules for each healthy control subject is shown in table 5.5. On average, participants shared 3.8 modules between dominant and non-dominant side, 0.6 modules were specific to the dominant side and 0.73 to the non-dominant side (table 5.6). Hence we learned that, at least for healthy controls, dominant and non-dominant side use very similar coordination strategies. It also seems that there is no significant difference between the number of specific modules of both sides. This was confirmed with a paired two-tailed Student's t-test, which did not reject the null hypothesis that the two distributions have the same mean ($p = 0.16$).

A similar procedure was applied to the modules of all stroke patients, with the difference that we looked at modules shared between impaired and unimpaired side. The results the stroke patient group are shown in table 5.7. On average, all stroke patients have 1.43 shared modules between impaired and unimpaired arm, 0.86 modules specific to the impaired side and 1.57 specific to the unimpaired side. Stroke patients seem to have less shared modules than the healthy control group, and there seems to be a greater inequality between the two arms. A paired one-tailed t-test confirmed at a 5%

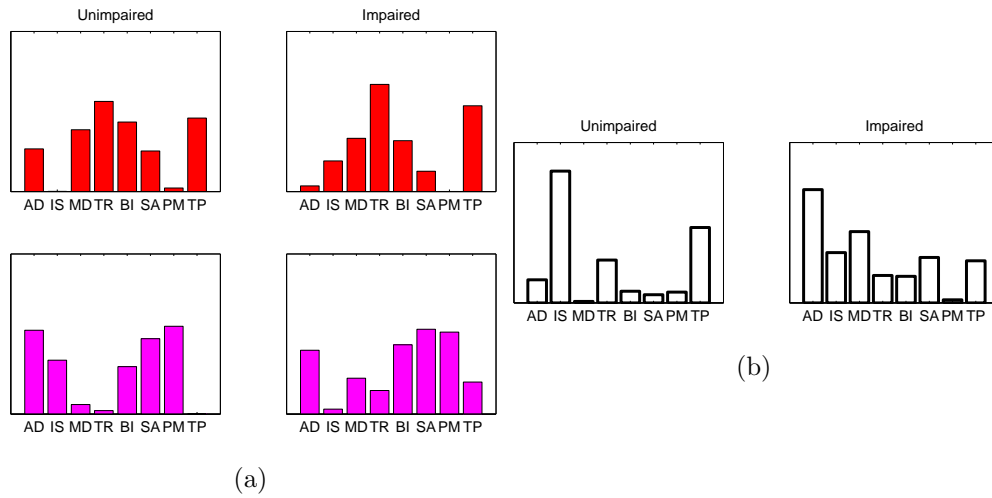


Figure 5.7: Modules of stroke patient 3. (a) Two modules are shared between unimpaired and impaired side. Matching modules are represented in the same row and with the same color. (b) One module per side was specific to only one arm.

confidence level that the number of modules specific to the impaired arm is significantly smaller than the number of modules specific to the unimpaired arm ($p = 0.02$).

The same statistics were calculated independently for the mildly impaired group and the moderately impaired group. We found that, on average, mildly impaired subjects share more modules between the two arms than moderately impaired subjects (1.63 against 1.17), and have less modules that are specific to either side (0.75 against 1 on the impaired side, 1.38 against 1.83 on the unimpaired side). However, these differences were not statistically significant: three one-tailed two-sample t-tests confirmed the null hypotheses that mildly impaired subjects the same number of shared modules ($p = 0.24$), that they as many modules specific to the impaired arm ($p = 0.28$) and that the same number of modules specific to the unimpaired arm ($p = 0.23$) when compared to moderately impaired subjects. However, these results might be due to the limited number of participants, and might change once the sample size is increased.

Subject	Dominant (D)	Non-dominant (ND)	Shared	Specific - D	Specific - ND
1	5	5	5	0	0
2	5	5	5	0	0
3	5	5	4	1	1
4	4	5	4	0	1
5	5	5	3	2	2
6	5	5	5	0	0
7	3	4	3	0	1
8	4	4	3	1	1
9	5	5	5	0	0
10	4	4	2	2	2
11	4	4	4	0	0
12	4	4	2	2	2
13	4	4	3	1	1
14	4	4	4	0	0
15	5	5	5	0	0

Table 5.5: Healthy control subjects: number of modules shared between dominant (D) and non-dominant (ND) side, and number of modules specific to each side.

	Shared	Specific - D	Specific - ND
mean	3.8	0.6	0.73
min	2	0	0
max	5	2	2
σ	1.05	0.8	0.77

Table 5.6: Healthy control subjects: average number, range and standard deviation of shared and specific modules.

Subject	Impaired (I)	Unimpaired (UI)	Shared	Specific - I	Specific - UI
1	2	1	0	2	1
2	2	4	2	0	2
3	3	3	2	1	1
4	2	2	0	2	2
5	2	3	1	1	2
6	1	3	0	1	3
7	2	4	2	0	2
8	3	3	3	0	0
9	3	3	3	0	0
10	3	4	3	0	1
11	3	2	1	2	1
12	1	4	0	1	4
13	2	3	1	1	2
14	3	3	2	1	1

Table 5.7: Stroke patients: number of modules shared between impaired (I) and unimpaired (UI) side, and number of modules specific to each side.

	All			Mild			Moderate		
	Shared	Specific I	Specific UI	Shared	Specific I	Specific UI	Shared	Specific I	Specific UI
mean	1.43	0.86	1.57	1.63	0.75	1.38	1.17	1	1.83
min	0	0	0	0	0	0	0	0	0
max	3	2	4	3	2	3	3	2	4
σ	1.12	0.74	1.05	1.11	0.66	0.86	1.07	0.82	1.21

Table 5.8: Stroke patients: average number, range and standard deviation of shared and specific modules. The values are calculated over all subjects and separately for the mildly impaired and moderately impaired group.

5.3 Healthy control subjects

This section focuses on the results that were obtained only from the healthy control data. We will show what modules are most commonly used by all subjects, how they could be interpreted, and which are the most relevant movements to obtain these results.

5.3.1 Similar coordination strategies between subjects

We searched for coordination strategies shared by multiple subjects by performing a k-means cluster analysis on all modules of the dominant side, and a separate analysis on the modules of the non-dominant side. The number of clusters was increased until all modules in each group were well correlated with the corresponding cluster centroid. We found that, for both sides, seven clusters are sufficient to describe the coordination strategies found in all subjects. Each cluster contains a variable number of module, as not every subject might share that specific coordination strategy. However, some clusters contain modules of up to 14 subjects, and might therefore represent fundamental coordination strategies.

As explained in the previous section, healthy control subjects tend to use similar motor modules on both arms. This could also be seen after we found the module clusters for both sides, as most of the cluster centroids of the dominant side had an equivalent counterpart on the non-dominant side. The same method used in section 5.2 to find shared modules between the two arms of all subjects was applied to the seven cluster centroids. We found that six out of seven clusters were similar between dominant and non-dominant side, while one cluster per side could not be matched. However, these two unmatched clusters are also those containing the least amount of modules, with only five subjects sharing that particular pattern on the dominant side, and as many for the cluster on the non-dominant side.

We then summed the number of modules in each cluster of the dominant side with the number of modules in the matching cluster on the non-dominant side, and sorted all clusters in descending order of the total number of modules. The two unmatched clusters were placed at the bottom of the list. All clusters are shown in figure 5.8, which depicts each cluster centroid and the associated motor modules.

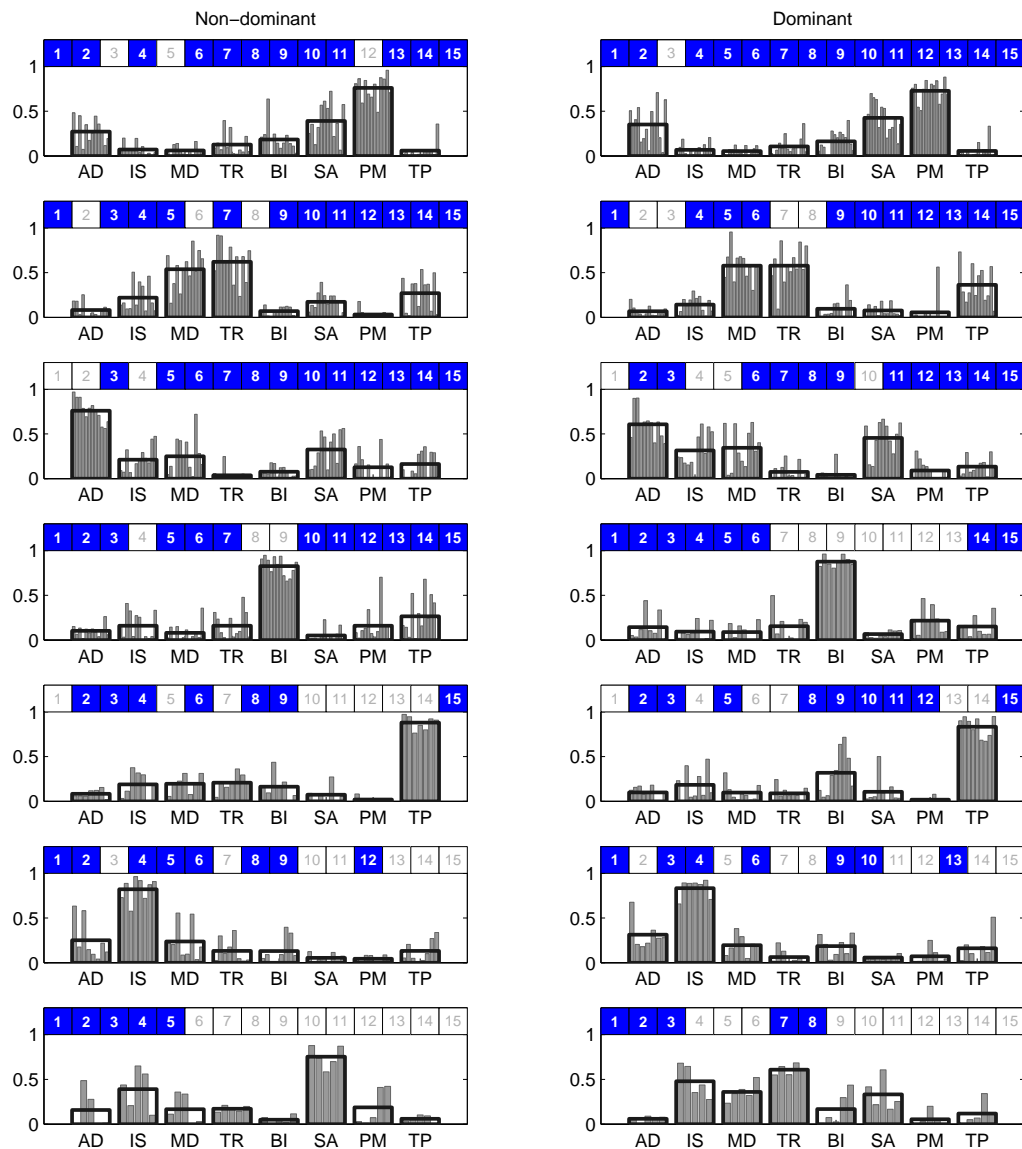


Figure 5.8: Motor modules of all subjects could be clustered into seven groups per side. Each cluster contains a variable number of elements, as not all subjects might have or use that specific module. Cluster centroids are represented as transparent bars with black borders, while all modules in a cluster are shown as grey bars. On the top of each plot, all subjects sharing the module are marked by a blue box. The top six clusters are shared between dominant and non-dominant side, and are placed in descending order of the number of subjects sharing that coordination strategy. Similar clusters are placed on the same row. The two clusters at the bottom could not be matched with any other group, and contain those modules shared by the least amount of subjects.

5.3.2 Biomechanical functions associated with motor modules

Since we found that most healthy subjects use similar motor modules, we hypothesized that these modules could represent specific biomechanical functions that are necessary to execute all measured movements. For this reason we took the first five module clusters of figure 5.8, which represent the coordination strategies shared by most subjects, and associated each one with a biomechanical function.

Each of the five following paragraphs will discuss one module at a time. To determine the function associated with each module, we looked at various factors. First we considered the muscles with the highest weights and their individual actions. We then observed the activation coefficients of the module, the movements where they were highest and the movement phases where they were most active.

The following figures show the analyzed module at the top and its activation coefficients below. The activation coefficients shown separately for each movement (numbered 1 to 15), and the abscissa axis of each plot represents the percentage of movement execution. Each black line represents a single subject's average module activation over all five movement repetitions.

Module 1

The muscles that are mainly participating and have the highest weight are the pectoralis major, the serratus anterior and the anterior deltoid. The main actions of the pectoralis major are flexion, horizontal adduction and medial rotation of the humerus. The serratus anterior protracts the scapula, rotates it upward and holds it close to the thoracic wall. The anterior deltoid acts mainly during flexion and medial rotation of the humerus.

Figure 5.9 shows that the activation coefficients are highest for movements involving reaches to the contralateral side, such as movements 1, 4, 7 and 12. For all heights of the multidirectional reaching task, the activity is highest on the contralateral column, decreases when reaching to the central column and are lowest for reaches to the ipsilateral column. For the task involving the pick and place action of bean bags on the horizontal plane (movements 12 and 13), the activity is highest during movement 12, which is a contralateral reach, and lower during movement 13, which is an ipsilateral reach. Furthermore, there is no significant influence of movement height, as movements 1, 4

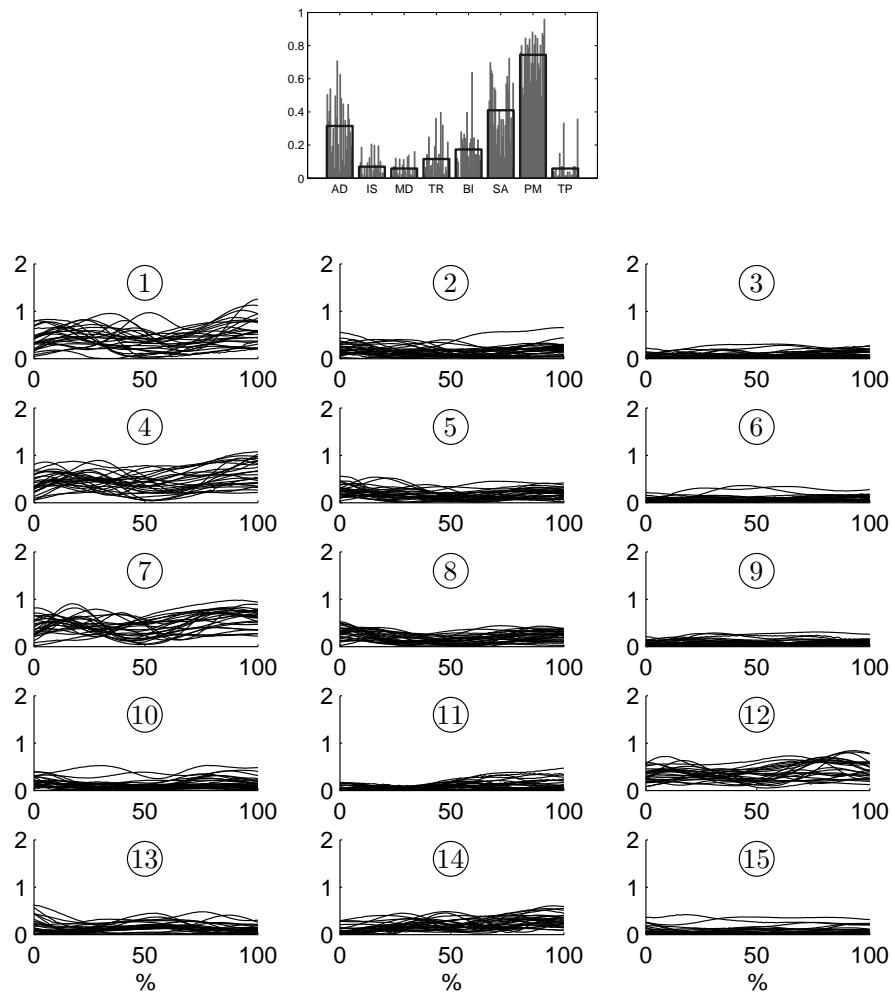


Figure 5.9: Module 1: the main participating muscles are the pectoralis major, the serratus anterior and the anterior deltoid. The module is mainly active in contralateral reaches, such as movements 1, 4, 7 and 12, and is less active in ipsilateral reaches. The function associated with this module could be humeral horizontal adduction, together with scapular protraction.

and 7 have very similar activation amplitudes, and so we excluded shoulder flexion from the possible actions.

We conclude that the function associated with this module is humeral horizontal adduction, combined with scapular protraction to increase the movement range.

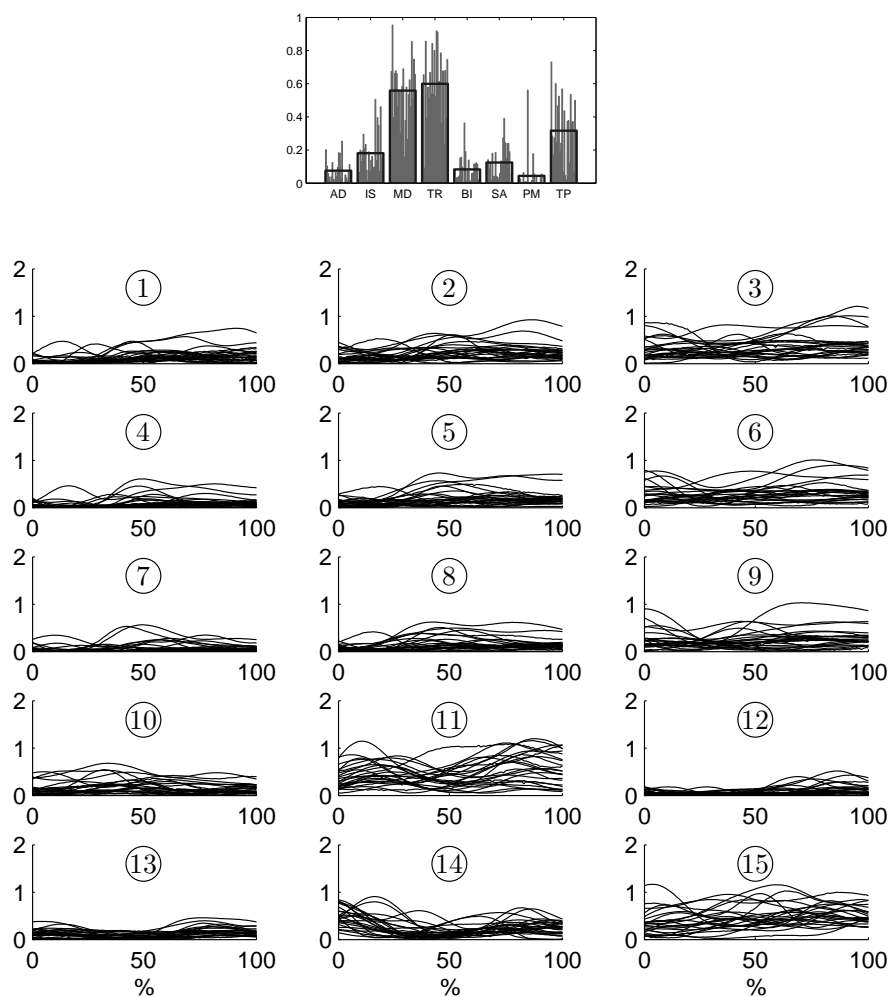


Figure 5.10: Module 2: the main participating muscles are triceps, middle deltoid and trapezius. The module is mainly active during ipsilateral reaches, such as movements 3, 6, 9, 11 and 15. We suggest that the function associated with this module is elbow extension and humeral abduction during outward and backward reaches, combined with scapular upward rotation.

Module 2

Module 2 activates mainly the triceps, the middle deltoid and the trapezius. The triceps acts as an extensor of the elbow joint, the middle deltoid abducts the humerus, and the upper trapezius upwardly rotates the scapula.

The module's activation coefficients shown in figure 5.10 are highest during move-

ments 3, 6, 9, 11 and 15, which are mainly reaches to the ipsilateral side. When looking only at the multidirectional reaching task, the activity increases from the controlateral column to the ipsilateral column. Movement 11, which consists in reaching to the side to grasp a rope shows the highest activity of all. Movement 15 is a reach to the back and has significantly higher activation coefficients than movement 14, which is a reach to the front. All these movements have in common that they require a high degree of elbow extension and of humeral abduction.

These facts suggest that module 2 acts primarily during outward and backward reaches to extend the arm on the ipsilateral side and to abduct the humerus. Furthermore, it combines humeral abduction with scapular upward rotation to avoid shoulder impingement and to maintain the scapulohumeral rhythm.

Module 3

The muscles with the highest weights in module three are the anterior deltoid, serratus anterior, middle deltoid and infraspinatus. The actions of the first three muscles have already been described in the previous paragraphs, while the infraspinatus laterally rotates the arm and stabilizes the glenohumeral joint.

The module is mostly active during all reaches aimed forward, to the side or overhead, including movements 1 to 9, 10, 11 and 14 (figure 5.11). The activation coefficients seem to increase with humeral abduction, as they are low at the beginning of all movements and get higher towards the end when the arm is extended. Furthermore, when looking at the multidirectional reaching task, the magnitude of the activation coefficient is constant across all columns, while it increases from the lowest row to the highest.

The biomechanical function of this module could be to compensate for gravitational effects during arm extension, i.e. for the increasing moment applied by the arm's weight, and to stabilize the shoulder during reaches aimed forward, overhead and to the side.

Module 4

Module 4 primarily controls the biceps, which is the main elbow flexor. In some subjects it also shows a high activity of the trapezius and pectoralis major, but on average their weight is much lower than that of the biceps.

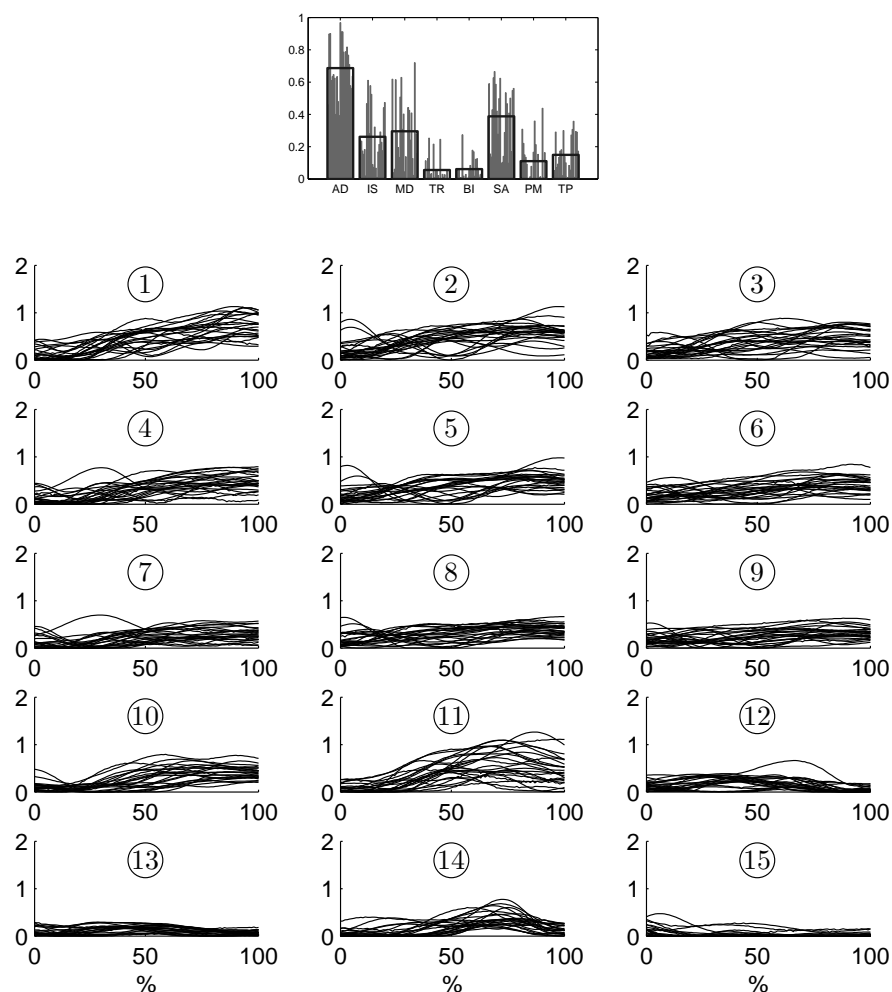


Figure 5.11: Module 3: the main participating muscles are anterior deltoid, serratus anterior, infraspinatus and middle deltoid. The module's activity increases during the execution of most movement, and is highest in reaches aimed forward, to the side and overhead. We suggest that it's function is to compensate for the arm's weight during reach, and to stabilize the shoulder.

Figure 5.12 shows that the module is mainly active during the first phase of all movements. It shows the highest activity during movement 10, which is a reaching motion to the forehead that requires a lot of elbow flexion. Movements 1 to 9 and movement 11 all start with the hand positioned on the side of the subject. In order to initiate the motion, the subjects had to raise the hand by flexing the elbow, which might cause the activity of this module during the initial part of these movements. A

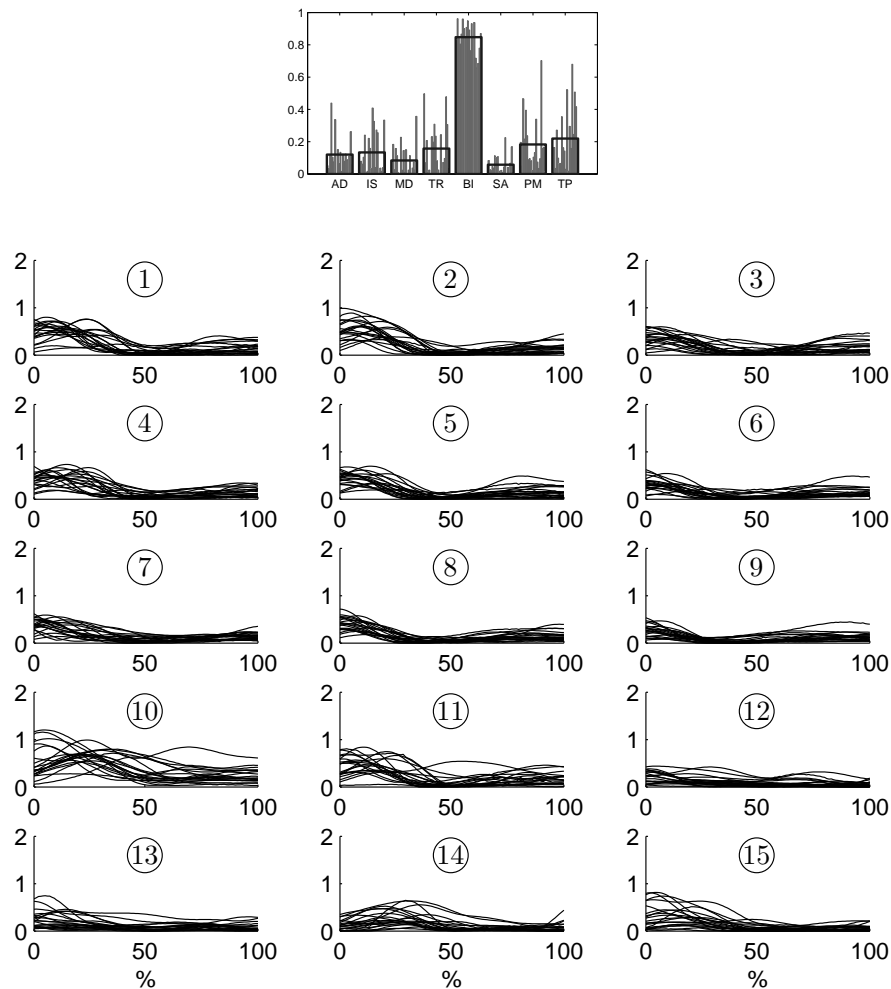


Figure 5.12: Module 4: this module controls primarily the biceps, and is active during the initial phase of all reaches. The highest activity is caused by movement 10, during which the subjects brought the hand to their forehead. The function associated with this module is elbow flexion.

similar reasoning applies to movements 14 and 15, which are reaches from the back to front and from the front to the back respectively. During these movements, the hand had to be brought from over the basket in the back to the table in the front, and then from the table back over the basket. On this trajectory, the subjects had to flex the elbow to avoid the bench and the edge of the table.

We conclude that the function associated with module 4 is mainly elbow flexion.

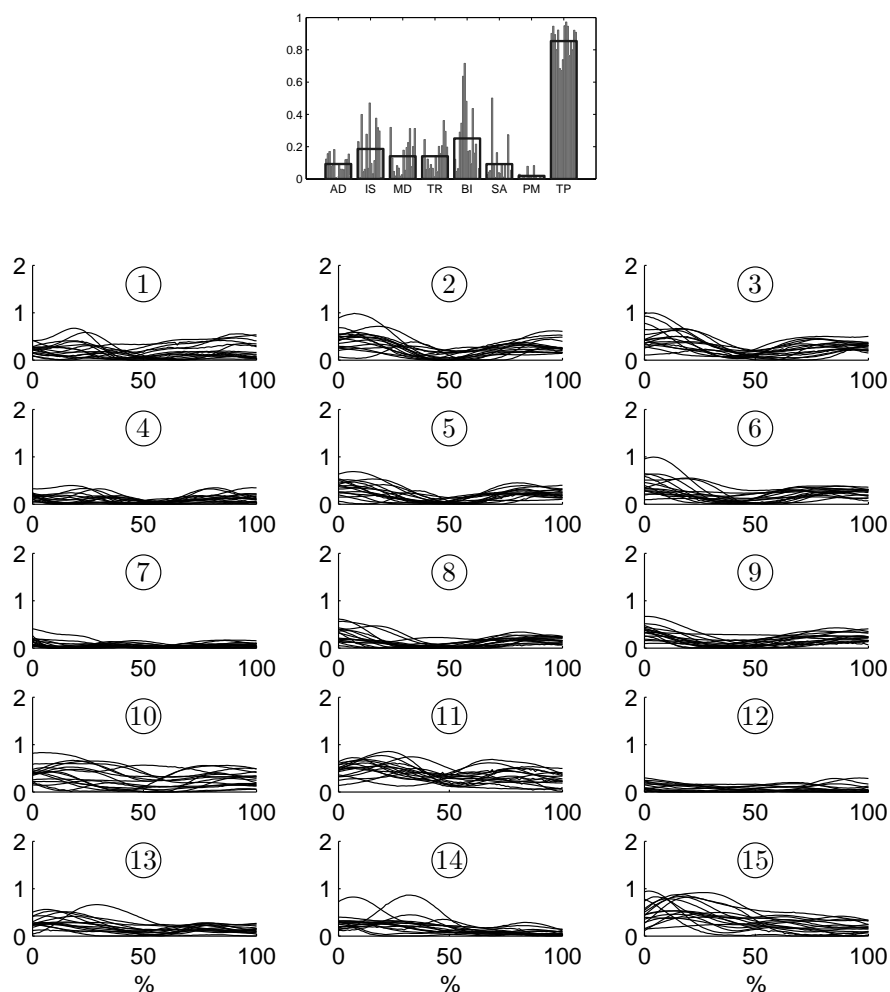


Figure 5.13: Module 5: the trapezius is the main participating muscle, and is mostly active during those movements requiring high humeral abduction angles and in those movements where the subject needs to elevate the shoulder. The suggested biomechanical function is upward rotation and elevation of the scapula.

Module 5

Module 5 is chiefly responsible for the activation of the trapezius. Even though some subjects show also a high activity of the biceps, on average it's weight is much lower than that of the trapezius.

The module's activation coefficients, shown in figure 5.13, are highest during all movements requiring much humeral abduction or when the subject needs to elevate the

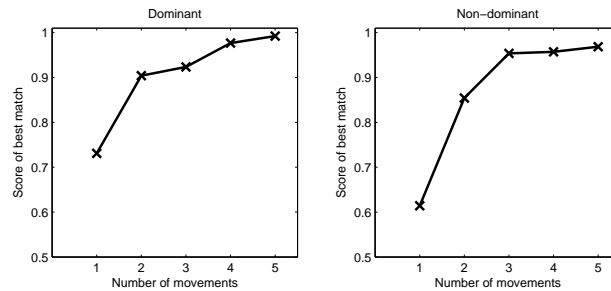


Figure 5.14: Scores of the combinations using either 1, 2, 3, 4 or 5 movements and give modules that are most similar to those extracted from all 15 movements. In this example, which shows the data of subject 1, three movements were already sufficient to get modules that had at least a scalar product of 0.9 with those extracted from all 15 movements.

shoulder. Looking at the multidirectional reaching task, one can see that the activity increases both from the contralateral column to the ipsilateral column and from the lowest row to the highest row. Similarly, the module is very active during movement 11, where the humerus is abducted by 120 degrees and the scapula needs to upwardly rotate in order to avoid impingement. During movement 10 the subject has to elevate the shoulder to bring the arm closer to the forehead, which causes the trapezius to be active during most of the movement. Movements 13 and 15 show another interesting case. During both movements the subject needs to elevate the shoulder in order to lift the picked bean bag from the table. Movement 15 requires a higher activation since the picked object has to be lifted over the edge of the table and brought towards the basket in the back.

These facts suggest that module 5 is associated with the biomechanical function of elevating the shoulder and, in some cases, collaborating with module 2 to upwardly rotate the scapula.

5.3.3 Most relevant tasks

In the first section of this chapter we showed how motor modules were extracted from the pooled EMG data of all 15 movements. In order to find the subset of movements that would give us similar results, we generated all possible combinations using one to

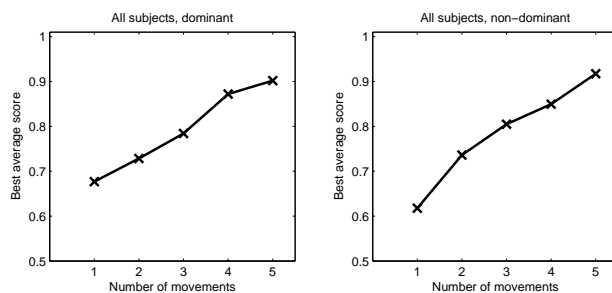


Figure 5.15: Average scores over all subjects of the combinations using either 1, 2, 3, 4 or 5 movements. The graphs show the scores of the movement combinations with the highest average.

five movements and repeated the module extraction on the EMG data relative to each of these combinations. For each subset of movements, we compared the newly found modules with those obtained from all 15 movements, paired the best-matching, and calculated the scalar product between each pair. The lowest value of all scalar products was used as an index to score the movement combination. Figure 5.14 shows the highest scores of the combinations using either 1, 2, 3, 4 or 5 movements and relative to the data of subject 1. Interestingly, in this case three movements were already sufficient to get modules that had at least a scalar product of 0.9 with those extracted from all 15 movements. This process was repeated for all subjects and independently for dominant and non-dominant side.

After calculating the score of each movement combination for all subjects, we wanted to see how well each combination was performing on average. We calculated the average score over all subject for each movement subset, treating dominant and non-dominants side independently. For each side, we identified the combinations of 1, 2, 3, 4 or 5 movements that gave the best average result. Their scores are shown in figure 5.15, while tables 5.9 and 5.10 list the best scoring combinations for dominant and non-dominant side respectively.

Interestingly, for both sides movement 13 is the single movement with the highest score, indicating that this almost horizontal reach to the ipsilateral side represents all 15 tested movements best. Other noteworthy movements are number 7, a reach to the lowest row of the contralateral column, and number 15, a reaching motion to the back.

These two movements appear in most combinations of three or more movements on both arms.

n	Score	Movements
1	0.6768	13. Moving objects on transverse plane, return
2	0.7285	8. Multidirectional reaching, lowest row, central column 14. Moving objects parallel to sagittal plane, reach
3	0.784	2. Multidirectional reaching, highest row, central column 7. Multidirectional reaching, lowest row, contralateral column 15. Moving objects parallel to sagittal plane, return
4	0.8718	6. Multidirectional reaching, central row, ipsilateral column 7. Multidirectional reaching, lowest row, contralateral column 10. Reaching to forehead 15. Moving objects parallel to sagittal plane, return
5	0.902	3. Multidirectional reaching, highest row, ipsilateral column 7. Multidirectional reaching, lowest row, contralateral column 8. Multidirectional reaching, lowest row, central column 10. Reaching to forehead 15. Moving objects parallel to sagittal plane, return

Table 5.9: Movement combinations that, on average, score best on the dominant side of all subjects. The table shows the best combinations using either 1, 2, 3, 4 or 5 movements.

When using a subset of two movements, forward reaches seem to be preferable on both sides. On the dominant side, movement 8 is a central reach at shoulder level, while movement 14 brings the hand from the back to a central location on the table. On the non-dominant side, movement 5 is a central reach at eye level and movement 13 brings the hand from a contralateral location on the table to the ipsilateral side.

With combinations of three movements, the movements become very diversified. On the dominant side, two movements of the multidirectional reaching task, directed to very different targets, are combined with a reach to the back. On the non-dominant side, three movements of the multidirectional reaching task are combined, but each one is aimed at a different column. The diversification of movements increases with the size of the subset, and with it the matching of the extracted modules with those obtained from the whole set of movements.

The last step consisted in the identification of the movement subset that would give best results for all subjects and for both dominant and non-dominant side. We calculated the minimum score between dominant and non-dominant side for all combinations, and sorted them in descending order. Figure 5.16 shows the scores of the combinations of 1 to 5 movements that perform best on both sides. The same movement combinations are listed in table 5.11.

n	Score	Movements
1	0.6176	13. Moving objects on transverse plane, return
2	0.7362	5. Multidirectional reaching, central row, central column 13. Moving objects on transverse plane, return
3	0.8049	5. Multidirectional reaching, central row, central column 6. Multidirectional reaching, central row, ipsilateral column 7. Multidirectional reaching, lowest row, contralateral column
4	0.8493	1. Multidirectional reaching, highest row, contralateral column 11. Reaching to the side 12. Moving objects on transverse plane, reach 15. Moving objects parallel to sagittal plane, return
5	0.9173	1. Multidirectional reaching, highest row, contralateral column 5. Multidirectional reaching, central row, central column 7. Multidirectional reaching, lowest row, contralateral column 11. Reaching to the side 15. Moving objects parallel to sagittal plane, return

Table 5.10: Movement combinations that, on average, score best on the non-dominant side of all subjects. The table shows the best combinations using either 1, 2, 3, 4 or 5 movements.

The results in table 5.11 are compatible with what found specifically for each side. In fact, many movements that were representative for the coordination patterns of either side, such as movements 13 and 15, are present in almost all combinations shown in table 5.11. Furthermore, also in this case combinations of very different movements tend to give the best results, which is in accordance with what found by Muceli et al. [80]. However, the assigned scores are significantly lower than those reported in tables 5.9 and 5.10, which is probably a consequence of the fact that these movements need to be representative for the coordination patterns of all subjects and of both

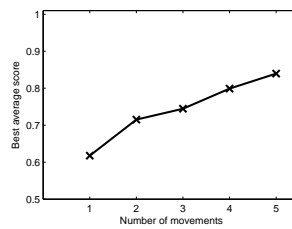


Figure 5.16: Scores of the combinations of 1 to 5 movements that perform best on both sides.

dominant and non-dominant side.

n	Score	Movements
1	0.6176	13. Moving objects on transverse plane, return
2	0.7151	5. Multidirectional reaching, central row, central column 13. Moving objects on transverse plane, return
3	0.7446	2. Multidirectional reaching, highest row, central column 4. Multidirectional reaching, central row, contralateral column 15. Moving objects parallel to sagittal plane, return
4	0.7989	4. Multidirectional reaching, central row, contralateral column 5. Multidirectional reaching, central row, central column 13. Moving objects on transverse plane, return 15. Moving objects parallel to sagittal plane, return
5	0.8395	2. Multidirectional reaching, highest row, central column 4. Multidirectional reaching, central row, contralateral column 6. Multidirectional reaching, central row, ipsilateral column 13. Moving objects on transverse plane, return 15. Moving objects parallel to sagittal plane, return

Table 5.11: Movement combinations that score best on both sides of all subjects. The table shows the best combinations using either 1, 2, 3, 4 or 5 movements.

5.4 Stroke patients

The results presented in the previous two sections allowed us to create a model representing the coordination strategies adopted by most healthy control subjects. In this section we want to further analyze the findings relative to stroke patients, and to identify the main differences between this group and the healthy control group.

5.4.1 Comparison between impaired and unimpaired side

The first question we wanted to find an answer to was whether the number of modules on the impaired side of stroke patients was statistically smaller than that on the unimpaired side, as suggested by table 5.4. However, before we could perform this test, we had to look at the differences between dominant and non-dominant side of healthy controls.

We used a paired two-tailed t-test to see if there was a statistical difference between the number modules on the dominant side and the number on the non-dominant side of healthy control subjects. We found that there was no significant difference, as the test confirmed the null hypothesis with $p = 0.16$. This result is important for two reasons. First, it tells us that we should not expect big differences in the number of modules of both arms of healthy control subjects. Second, we can now assume that if we find a statistical difference between the number of modules of the impaired and unimpaired arm, then this is not caused by pre-existing dissimilarities.

The differences between impaired and unimpaired side of stroke patients were analyzed with a paired one-tailed t-test. We found that, when looking at all stroke subjects, the number of modules on the impaired side is significantly smaller than the number on the unimpaired side ($p = 0.02$). However, when separating mildly impaired from moderately impaired patients, the differences inside either group were not as significant anymore. For the mildly impaired group, we found a p-value of 0.07, while for the moderately impaired group the p-value was of 0.11. However, the number of subjects in these two groups, and especially in the moderately impaired group, were quite low, and probably the sample size was too small to get significant results.

5.4.2 Comparison with healthy controls

The number of modules found on the impaired and unimpaired side of stroke patients was compared to the number of modules extracted from healthy controls. Since we found no significant difference between dominant and non-dominant side of the healthy control group, we grouped the results of both sides and compared this sample to the results found in stroke patients.

We used two-sample one-tailed t-tests to assess whether the number of modules on the impaired or unimpaired side of stroke patients was significantly smaller than the number of modules of healthy controls. These tests were performed on three different groups: all patients, all mildly impaired and all moderately impaired patients. First we had to verify that the compared samples did not have different variances. This was done by performing F-tests comparing the distribution of all healthy control modules to that of the six stroke samples (three groups, two sides each). We found that the variances did not differ significantly, as all F-tests confirmed the null hypothesis with p-values greater than 0.10.

From the performed t-tests we learned that the number of modules on the impaired side of all stroke patients is significantly smaller than the number of modules of healthy controls, with a p-value of 6.2×10^{-13} . This result was confirmed for both the mildly impaired and the moderately impaired group, with p-values of 1.2×10^{-9} and 2.4×10^{-9} respectively.

Interestingly, we also found that the number of modules on the unimpaired side of all patients was statistically smaller than the number of modules of healthy controls, as the t-test gave us a p-value of 1.5×10^{-7} . As with the impaired side, this result was confirmed for the two subgroups of stroke patients, with a p-value of 5.7×10^{-6} for the mildly impaired group and of 2.2×10^{-5} for the moderately impaired group. While the lower number of modules on the impaired side was expected, as it is widely reported in literature, this result indicates that even the unimpaired side suffers from some level of motor impairment.

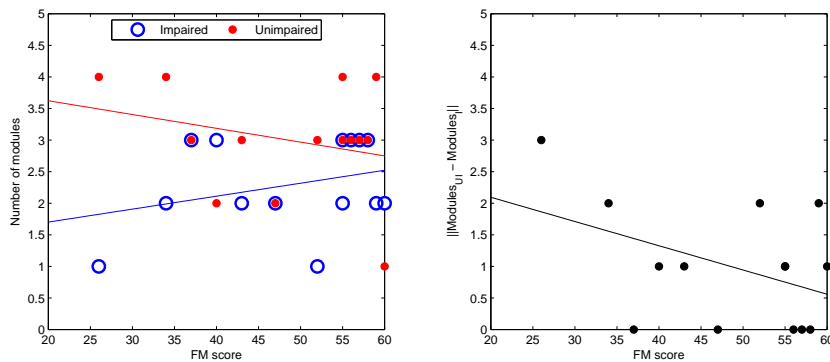


Figure 5.17: Relationship between the level of motor impairment and the number of extracted modules. The plot to the left shows the number of modules of each subject on the ordinate axis and the Fugl-Meyer score on the abscissa axis. Blue circles represent data of the impaired arm, red dots data of the unimpaired arm. The blue line is the result of a linear regression on the data of the impaired arm, while the red line is the regression line relative to the unimpaired arm. The plot to the right shows the absolute value of the difference between the number of modules on either side of each subject, and the associated regression line.

5.4.3 Relationship between level of motor impairment and number of modules

We examined the relationship between the level of motor impairment, as measured by the Fugl-Meyer assessment, and the number of modules on impaired and unimpaired side by performing a correlation analysis. The plot on the left side of figure 5.17 shows the data points of the impaired side as blue circles and those of the unimpaired side as red dots. We found that Fugl-Meyer score and number modules were weakly correlated, the correlation with the number of modules of the impaired side being of 0.3045 and the correlation with the number of modules on the unimpaired side of -0.2684. This can be graphically seen through the two regression lines in the left plot of figure 5.17, where the blue line (impaired side) has a positive slope, while the red line (unimpaired side) has a negative slope. Even though both correlation coefficients are quite weak, it is interesting that the number of modules on the impaired side seems to increase with reduced motor impairment, while at the same time the number of modules on the unimpaired side

seems to decrease. Due to the small sample size, the correlation coefficients of impaired and unimpaired side are not statistically significant, as they have p-values of 0.29 and 0.35 respectively.

These observations suggest that there could be a converging trend in the number of modules of both sides with increasing Fugl-Meyer score. To verify this, we calculated the absolute value of the difference between the number of modules of the two sides, and looked at its correlation with the Fugl-Meyer score (right plot of figure 5.17). In this case the correlation was stronger, having a value of -0.4307, and was also more significant ($p = 0.12$).

These results indicate that, when compared with less impaired patients, subjects with a low Fugl-Meyer score might have a bigger discrepancy between the number of modules of the impaired and unimpaired arm. This difference seems to diminish with decreasing motor impairment. However these findings are not sufficiently significant to draw definitive conclusions, and need to be confirmed with a higher sample size.

5.4.4 Changes after stroke

We explained the differences between the modules of stroke patients and healthy subjects by hypothesizing that, after stroke, modules could either not change, some modules could merge together, and other modules could be newly developed.

Figure 5.18 shows an example of how the two modules of the impaired side of subject 7 could be described as either a combination of three healthy control modules, or as a newly developed module. After having identified the healthy modules that were either merged or preserved, we created a new module matrix H in which we substituted the originally extracted modules with the merged healthy control modules. We then repeated the non-negative matrix factorization by updating only the activation coefficients, thereby finding a new matrix W that contained the activations of the merged modules. We found that the activation coefficients of merged modules tend to be highly correlated, as shown in the example in figure 5.18. This almost synchronous activation of merged modules indicates that the patient might not be able anymore control these modules individually, and could be activating them together as a group.

Figure 5.19 shows the data of the unimpaired side of patient 7. In this case we found that three of the four modules were equivalent to those extracted from healthy

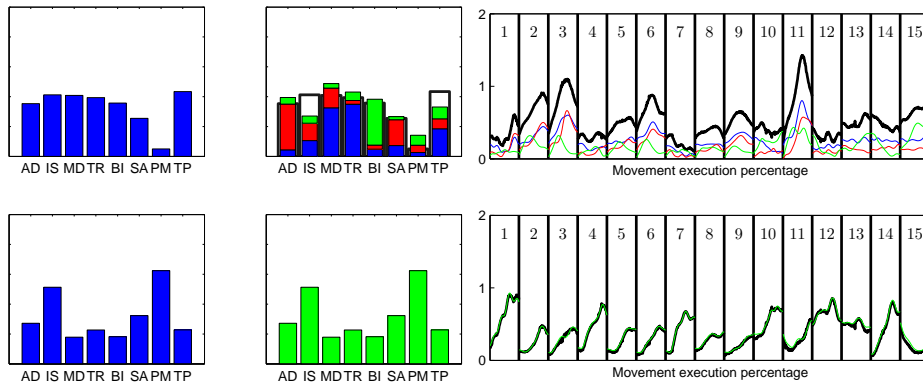


Figure 5.18: Example of how modules of the impaired side can be explained as either the result of merged modules of healthy controls, or as a newly developed module. In this example, showing the data of stroke patient 7, the modules extracted from the subjects EMG data are shown to the far left and are colored blue. The first module could be explained as a combination of three healthy control modules. Each healthy control module is shown in a different color (blue, red and green), while subject's original module is shown by white bars with black borders. The resulting activation coefficients are shown on the right of the same row, and each one is color matched with the respective module. We show the activation coefficients relative to each of the 15 movements, and for each movement we took the average over all five repetitions. The subject's second module was identified as a newly developed coordination strategy and is plotted in green.

individuals (plotted in red), while the fourth module was found to be a combination of two healthy control modules. Also in this example it is possible to see that the activation coefficients of the two merged modules are well correlated and follow the activation of the originally extracted module. The three preserved modules follow the original activation coefficients almost exactly, and are not influenced by the addition of the two merged modules.

Table 5.12 summarizes the results of all 14 stroke patients, listing the number of preserved, merged and new modules found on both impaired and unimpaired side. We found that on the impaired side, on average, 0.29 modules are preserved, 1.29 result from a combination of an average of 2.64 healthy control modules, and 0.71 are newly developed. On the unimpaired side, 0.93 modules are preserved, 1.29 result from a

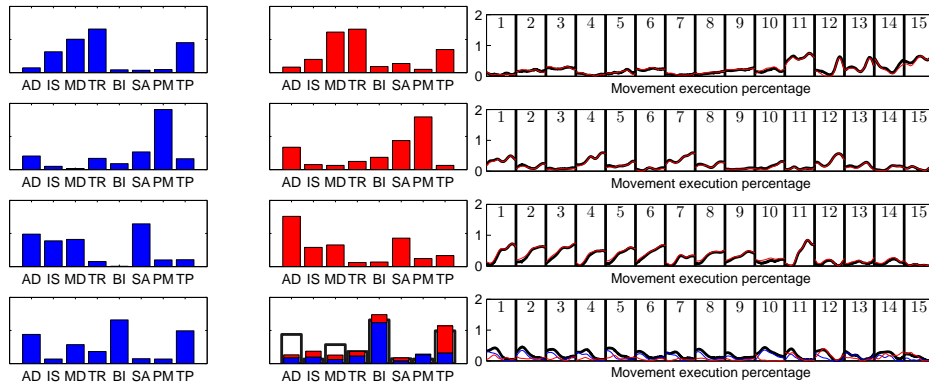


Figure 5.19: Example of how modules of the unimpaired side can be explained either as preserved, i.e. equivalent to those found in healthy controls, or as a result of module merging. In this example, which shows the data of stroke patient 7, the first three modules were found to be very similar to those of healthy controls (plotted in red), and so we marked them as preserved. The module in the last row could be explained as a combination of two healthy control modules (blue and red). On the right side of the figure we show the average activation coefficients over all five repetitions of the 15 movements. The black lines represent the originally extracted activation coefficients, while the colored lines show the activity of the merged or preserved healthy control modules.

combination of an average of 2.64 healthy control modules, and 0.79 are newly developed.

By applying a paired, one-tailed t-test we confirmed that the number of preserved modules on the impaired side is smaller than the number of preserved modules on the unimpaired side ($p = 0.01$). The numbers of merged and newly developed modules did not differ significantly from side to side. This could imply that the differences in the number of modules found between impaired and unimpaired arm could be mainly caused by the different number of preserved modules.

Subject	Impaired					Unimpaired				
	Extracted	Preserved	Merged	Merged in	New	Extracted	Preserved	Merged	Merged in	New
1	2	0	2	1	1	1	1	0	0	0
2	2	0	2	1	1	4	1	2	1	2
3	3	1	4	2	0	3	0	4	2	1
4	2	0	2	1	1	2	0	4	2	0
5	2	0	4	2	0	3	0	4	2	1
6	1	0	0	0	1	3	1	2	1	1
7	2	0	3	1	1	4	3	2	1	0
8	3	1	2	1	1	3	2	3	1	0
9	3	0	4	2	1	3	0	4	2	1
10	3	1	2	1	1	4	2	2	1	1
11	3	1	2	1	1	2	1	2	1	0
12	1	0	2	1	0	4	1	4	2	1
13	2	0	4	2	0	3	1	2	1	1
14	3	0	4	2	1	3	0	2	1	2

Table 5.12: Number of preserved, merged and new modules found on both impaired and unimpaired side of all 14 subjects. The column *Merged* indicates the number of healthy control modules that were found to be merged together. The column *Merged in* indicates the number of modules of a subject that was found to be the result of merged healthy control modules.

Discussion

This research project included 15 healthy control subjects and 14 stroke patients and was aimed at gaining a better understanding of how motor control of the upper limb can be achieved, and how it is influenced by stroke. The goal was to use this information to obtain a model that could represent the muscle coordination strategies of healthy controls, and that could be used to create new rehabilitation protocols tailored to the specific needs of each stroke patient.

We recorded EMG signals of 16 upper limb muscles during the execution of 15 fast reaching movements, and used the recorded data to extract motor modules for each tested side and for all subjects. The motor modules of healthy controls were used to generate a model that could represent the most common muscle coordination strategies, and to which we could compare the modules found in stroke patients.

We found that, on average, four to five modules per side are sufficient to reconstruct the EMG data of all healthy control subjects during the execution of a wide variety of movements with good accuracy. This result is very consistent across all healthy participants and seems to be a distinguished feature of motor control shared by most subjects. We also did not find a significant difference between the number of modules of the dominant and of the non-dominant side. Besides the similarities in their numbers, we discovered that most modules were shared between dominant and non-dominant side. Of the 4-5 extracted modules, an average of 3.8 was shared between the two sides, indicating that healthy subjects adopt similar coordination strategies on both their arms.

By comparing the motor modules of all subjects, we found that the muscle coordination patterns were not only shared between the two sides of each subject, but also that different subjects use very similar modules. In fact, we could group the modules of all

subjects into 7 distinct clusters. Six of these groups were very similar between dominant and non dominant side, further confirming what we had found for each individual subject. The fact that different subjects use similar modules suggests that the extracted motor modules are not just an artifact of an algorithm, but that they represent actual coordination patterns common to most tested individuals. For this reason we picked the five most commonly used modules and associated each with a plausible biomechanical function. We found that module 1 could be responsible for humeral horizontal adduction and scapular protraction during contralateral reaches; module 2 could extend the arm on the ipsilateral side by extending the elbow, abducting the humerus and upwardly rotating the scapula; module 3 could mainly act as a stabilizer of the glenohumeral joint and counteract the effects of gravity during reach; module 4 functions primarily as an elbow flexor; module 5 was associated with shoulder elevation and scapula upward rotation. These results gave us a more detailed understanding of how motor control during reach is achieved by healthy subjects, and provided us with a framework to which we could compare the results found with stroke patients.

When analyzing the muscle activation patterns of all stroke patients, we found that the number of modules of the impaired side is significantly smaller than what seen on the unimpaired side, having an average value of 2.29 against 3 on the unimpaired arm. This trend did not vary when analyzing separately mildly impaired and moderately impaired participants. Furthermore, the number of modules on the impaired arm was significantly smaller than the number of modules of healthy control subjects. Interestingly, we got the same result on the unimpaired side. The fact that stroke patients have less modules on their unimpaired side than healthy control subjects suggests that also the ipsilesional side is somehow affected by the stroke. In fact, it has been reported in literature that the ipsilesional side can be strongly affected by stroke, especially when the stroke occurs in the right hemisphere [124]. The motor deficits on the ipsilesional side could be explained by an over excitation of the contralesional brain hemisphere, and by a disruption in the function of the uncrossed descending neural pathways. Even though the impairment of the ipsilesional side is well known in the stroke literature, to the best of our knowledge it has not yet been reported from the point of view of motor modules. This supports a bilateral rehabilitation approach, and suggest that the therapist should not focus only on the contralesional arm, but work also on the ipsilesional side.

We also found that, while stroke patients still share modules between the impaired and unimpaired arm, they share less modules than our control subjects (1.43 against 3.8 shared modules). Furthermore, while we did not find a significant difference between the number of modules specific to either dominant or non-dominant arm of healthy participants, stroke patients had more modules specific to the unimpaired side than to the impaired side (on average, 1.57 against 0.86).

A correlation analysis between the level of motor impairment, as measured by the Fugl-Meyer assessment, and the number of modules on impaired and unimpaired side revealed that there is no strong relationship between these variables. We found a stronger correlation between the Fugl-Meyer score and the difference in the number of modules on both sides. This suggests that in more severely impaired patients the discrepancy between the number of modules on the impaired and unimpaired side is bigger than in less impaired patients. However, due to the relatively small sample size, these results are not statistically significant and would need to be confirmed.

The motor deficits of stroke patients could be partly explained by the merging of motor modules found in healthy subjects. In fact, on average more than one module of each stroke patient could result from merging two or more healthy control modules. The results suggest that, after stroke, patients are not able anymore to control these modules individually, activating them synchronously as a group. Additionally, we found that some modules on both impaired and unimpaired side were very similar to those found in healthy control subjects, indicating that some modules might be preserved after stroke. More modules were preserved on the unimpaired side than on the impaired side, suggesting that the different number of modules on the two arms could be by the fact that more modules tend to be preserved on the unimpaired arm. On the other side, impaired and unimpaired arm showed no significant difference in the number of modules consisting of merged healthy control modules. Some modules, approximately the same on both sides, could not be explained as preserved or as a result of merging. We suggest that these modules represent newly developed strategies that compensate for the lost or merged motor functions.

Implications for future rehabilitation protocols: The results of this research indicate that new rehabilitation protocols could be based on an analysis of the patient's

muscle activation patterns, and on the information obtained by extracting motor modules. The extracted motor modules could be compared with those of healthy control subjects, which would allow to find preserved, merged and newly developed modules on either sides. Therapy could be aimed at helping the patient to re-learn the individual use of each merged module. In fact, we found that on average 2.64 modules were merged on either side of all stroke patients. By teaching a patient to use these modules again, the number of modules on impaired and unimpaired side would increase significantly, going from an average of 2.28 to 3.64 on the impaired side and from 3 to 4.36 on the unimpaired side. These values are much closer to those of healthy subjects, and the increased number of modules would help stroke patients in the execution of more complex movements that require good muscle coordination. Furthermore, this procedure would provide an objective measure of the patient's disabilities, allowing to tailor the rehabilitation exercises to his/her specific needs, and giving the therapist a quantitative outcome measure.

Such a protocol would be particularly well suited for robotic therapy, as it would lend itself quite well to being automated. In a first phase, the robotic system could guide the patient through a series of movements used to extract motor modules. We showed that this set of movements does not need to be particularly large, as long as it is sufficiently diversified. For example one could use one of the movement subsets proposed in the previous section, which provide the same information as the full set of 15 movements. The system could then perform an on-line processing of the recorded data and find which healthy control modules were merged. Since we associated each module with a biomechanical function, the system could help the patient performing movements that use just one of the merged functions. Motor modules could even be extracted throughout therapy, in order to verify if there were any improvements and to evaluate the efficacy of the treatment.

Implications for the design of rehabilitation robots: With the goal of helping stroke patients to improve their coordination patterns, future robotic rehabilitation systems need to provide the right stimulation and support to re-learn the use of normal motor modules. Traditional approaches involve the use one or multiple feedback sources, such as haptic, visual or auditory feedback. Even though these strategies might be

applicable also in this case, they need to be properly tuned in order to specifically address the training of motor modules. Future studies will need to address this problem and analyze which robotic design and what kind of feedback gives the best results in terms of recovery of motor modules. For example, we need to understand whether isometric force generation exercises can be sufficient, or if the training needs to involve limb movements. In the first case, the patient could be brought into predefined positions and asked to generate a force in the direction of action of one or more modules. This could be done with a variable amount of gravity compensation, and can be transformed into a more dynamic exercise by adding joints with selective and/or adjustable compliance. On the other hand, if movements are included in the therapy, then the robot could provide a variable amount of haptic feedback, either supporting or contrasting the movement execution. Furthermore, the system could track the position of the patient's limb in real time, calculate the direction of action of each motor module, and provide assistance or resistance only along that direction. Another option could be that the robot provides assistance in all directions but the one of the module that needs to be trained, helping the patient focusing on one task at a time. All these could be promising and interesting directions for future research, which will need to provide more evidence supporting the approach based on motor module and muscle coordination.

Motor modules proved to be a powerful tool for studying muscle coordination strategies of both healthy subjects and stroke patients. It has not yet been assessed whether they represent actual neural structures at some cerebral or spinal level, or if they are just preferred patterns used by the motor controller. In either case, they allowed us to find coordination patterns shared by a variety of subjects, and that were used in a very diversified set of movements. More importantly, they can provide us with a quantitative measurement of a patient's motor deficits and could be used to drive new, and hopefully effective, rehabilitation protocols and systems.

References

- [1] N. Hogan, H. Krebs, J. Charnnarong, P. Srikrishna, and A. Sharon, “MIT-MANUS: a workstation for manual therapy and training. I,” in *[1992] Proc IEEE Int Work Robot Hum Commun.* IEEE, 1992, pp. 161–165.
- [2] W. Harwin, J. Patton, and V. Edgerton, “Challenges and Opportunities for Robot-Mediated Neurorehabilitation,” *Proc IEEE*, vol. 94, no. 9, pp. 1717–1726, Sept. 2006.
- [3] V. L. Roger, A. S. Go, and D. M. Lloyd-Jones, “Heart disease and stroke statistics–2012 update: a report from the American Heart Association.” *Circulation*, vol. 125, no. 1, pp. e2–e220, Jan. 2012.
- [4] WHO, *World Health Statistics 2013.* WHO Press, Geneva, Switzerland, 2013.
- [5] T. Truelsen, B. Piechowski-Jóźwiak, R. Bonita, C. Mathers, J. Bogousslavsky, and G. Boysen, “Stroke incidence and prevalence in Europe: a review of available data.” *Eur J Neurol*, vol. 13, no. 6, pp. 581–98, June 2006.
- [6] G. Rosati, “The place of robotics in post-stroke rehabilitation.” *Expert Rev Med Devices*, vol. 7, no. 6, pp. 753–8, Nov. 2010.
- [7] B. T. Volpe, M. Ferraro, H. I. Krebs, and N. Hogan, “Robotics in the rehabilitation treatment of patients with stroke.” *Curr Atheroscler Rep*, vol. 4, no. 4, pp. 270–6, July 2002.
- [8] A. a. a. Timmermans, H. a. M. Seelen, R. D. Willmann, and H. Kingma, “Technology-assisted training of arm-hand skills in stroke: concepts on reacquisition

- of motor control and therapist guidelines for rehabilitation technology design.” *J Neuroeng Rehabil*, vol. 6, no. figure 1, p. 1, Jan. 2009.
- [9] D. J. Reinkensmeyer, J. L. Emken, and S. C. Cramer, “Robotics, motor learning, and neurologic recovery.” *Annu Rev Biomed Eng*, vol. 6, pp. 497–525, Jan. 2004.
- [10] S. Hesse, H. Schmidt, and C. Werner, “Machines to support motor rehabilitation after stroke: 10 years of experience in Berlin.” *J Rehabil Res Dev*, vol. 43, no. 5, pp. 671–8, 2006.
- [11] R. Riener, T. Nef, and G. Colombo, “Robot-aided neurorehabilitation of the upper extremities.” *Med Biol Eng Comput*, vol. 43, no. 1, pp. 2–10, Jan. 2005.
- [12] G. Kwakkel, B. J. Kollen, and H. I. Krebs, “Effects of robot-assisted therapy on upper limb recovery after stroke: a systematic review.” *Neurorehabil Neural Repair*, vol. 22, no. 2, pp. 111–21, 2008.
- [13] H. Krebs, “Robot Mediated Movement Therapy: A Tool for Training and Evaluation,” in *Eur Symp Tech Aids Rehabil - TAR 2007*, Technical University of Berlin, 2007.
- [14] S. Masiero, A. Celia, G. Rosati, and M. Armani, “Robotic-assisted rehabilitation of the upper limb after acute stroke.” *Arch Phys Med Rehabil*, vol. 88, no. 2, pp. 142–9, Feb. 2007.
- [15] S. Masiero, E. Carraro, C. Ferraro, P. Gallina, A. Rossi, and G. Rosati, “Upper limb rehabilitation robotics after stroke: a perspective from the University of Padua, Italy.” *J Rehabil Med*, vol. 41, no. 12, pp. 981–5, Nov. 2009.
- [16] J. Mehrholz, A. Hädrich, T. Platz, J. Kugler, and M. Pohl, “Electromechanical and robot-assisted arm training for improving generic activities of daily living, arm function, and arm muscle strength after stroke.” *Cochrane database Syst Rev*, vol. 6, no. 6, p. CD006876, Jan. 2012.
- [17] N. Kutner, R. Zhang, A. Butler, S. Wolf, and J. Alberts, “Quality-of-life change associated with robotic-assisted therapy to improve hand motor function in patients with subacute stroke: a randomized clinical trial,” *Phys Ther*, vol. 90, no. 4, p. 493, 2010.

- [18] J. L. Allen, S. A. Kautz, and R. R. Neptune, "The influence of merged muscle excitation modules on post-stroke hemiparetic walking performance," *Clin Biomech*, vol. 28, no. 6, pp. 697–704, 2013.
- [19] V. C. K. Cheung, L. Piron, M. Agostini, S. Silvoni, A. Turolla, and E. Bizzi, "Stability of muscle synergies for voluntary actions after cortical stroke in humans." *Proc Natl Acad Sci U S A*, vol. 106, no. 46, pp. 19 563–8, Nov. 2009.
- [20] M. D. Ellis, B. G. Holubar, A. M. Acosta, R. F. Beer, and J. P. a. Dewald, "Modifiability of abnormal isometric elbow and shoulder joint torque coupling after stroke." *Muscle Nerve*, vol. 32, no. 2, pp. 170–8, Aug. 2005.
- [21] A. D'Avella, P. Saltiel, and E. Bizzi, "Combinations of muscle synergies in the construction of a natural motor behavior." *Nat Neurosci*, vol. 6, no. 3, pp. 300–8, Mar. 2003.
- [22] D. J. Clark, L. H. Ting, F. E. Zajac, R. R. Neptune, and S. A. Kautz, "Merging of healthy motor modules predicts reduced locomotor performance and muscle coordination complexity post-stroke." *J Neurophysiol*, vol. 103, no. 2, pp. 844–57, Feb. 2010.
- [23] V. B. Brooks, "Motor control. How posture and movements are governed." *Phys Ther*, vol. 63, no. 5, pp. 664–73, May 1983.
- [24] E. N. Marieb and K. Hoehn, *Human Anatomy and Physiology*, 7th ed. Pearson, 2006.
- [25] N. A. Bernshtein, *The co-ordination and regulation of movements*, 1st ed. Oxford: Pergamon Press, 1967.
- [26] M. C. Tresch, P. Saltiel, A. D'Avella, and E. Bizzi, "Coordination and localization in spinal motor systems." *Brain Res Brain Res Rev*, vol. 40, no. 1-3, pp. 66–79, Oct. 2002.
- [27] P. Saltiel, K. Wyler-Duda, A. D'Avella, M. C. Tresch, and E. Bizzi, "Muscle synergies encoded within the spinal cord: evidence from focal intraspinal NMDA iontophoresis in the frog." *J Neurophysiol*, vol. 85, no. 2, pp. 605–19, Feb. 2001.

- [28] J.-P. Gossard and H. Hultborn, "The organization of spinal rhythm generation in locomotion," in *Plast Motoneuronal Connect*, A. Wernig, Ed. Elsevier, Amsterdam, 1991, pp. 385–404.
- [29] S. Grillner, "Control of Locomotion in Biped, Tetrapods, and Fish," in *Handb Physiol Nerv Syst Mot Control Vol 2*, V. B. Brooks, Ed., 1981, pp. 1179–1236.
- [30] S. Rossignol, "Neural control of stereotypic movements," in *Handb Physiol*, L. B. Rowell and J. T. Sheperd, Eds. American Physiological Society, 1996, pp. 173–216.
- [31] P. S. G. Stein and J. L. Smith, "Neural and biomechanical control strategies for different forms of vertebrate hindlimb motor tasks," in *Neurons, Networks, Mot Behav*, P. S. G. Stein, S. Grillner, A. I. Selverston, and D. G. Stuart, Eds. MIT Press, Cambridge, 1997, pp. 61–73.
- [32] D. N. Levine, "Sherrington's "The Integrative action of the nervous system": a centennial appraisal." *J Neurol Sci*, vol. 253, no. 1-2, pp. 1–6, Feb. 2007.
- [33] C. Sherrington, "Flexion-reflex of the limb, crossed extension-reflex, and reflex stepping and standing," *J Physiol*, vol. 40, no. 1-2, pp. 28–121, 1910.
- [34] R. E. Burke, "Sir Charles Sherrington's the integrative action of the nervous system: a centenary appreciation." *Brain*, vol. 130, no. Pt 4, pp. 887–94, Apr. 2007.
- [35] T. G. Brown, "The Intrinsic Factors in the Act of Progression in the Mammal," *Proc R Soc B Biol Sci*, vol. 84, no. 572, pp. 308–319, Dec. 1911.
- [36] P. S. G. Stein, D. G. Stuart, S. Grillner, and A. I. Selverston, Eds., *Neurons, Networks, and Motor Behavior*. MIT Press, 1999.
- [37] L. M. Jordan, "Brainstem and Spinal Cord Mechanisms for the Initiation of Locomotion," in *Neurobiol Basis Hum Locomot*, M. Shimamura, S. Grillner, and V. R. Edgerton, Eds. Japan Scientific Societies Press, Tokyo, 1991, pp. 3–20.

- [38] P. S. Stein, a. W. Camp, G. a. Robertson, and L. I. Mortin, “Blends of rostral and caudal scratch reflex motor patterns elicited by simultaneous stimulation of two sites in the spinal turtle.” *J Neurosci*, vol. 6, no. 8, pp. 2259–66, Aug. 1986.
- [39] P. S. G. Stein, L. I. Mortin, and G. a. Robertson, “The forms of a task and their blends,” in *Neurobiol Vertebr Locomot*, S. Grillner, P. S. G. Stein, D. G. Stuart, H. Forssberg, and R. M. Herman, Eds. London: Macmillan Press, 1986, pp. 201–216.
- [40] P. S. Stein, J. C. Victor, E. C. Field, and S. N. Currie, “Bilateral control of hindlimb scratching in the spinal turtle: contralateral spinal circuitry contributes to the normal ipsilateral motor pattern of fictive rostral scratching.” *J Neurosci*, vol. 15, no. 6, pp. 4343–55, June 1995.
- [41] P. S. Stein, M. L. McCullough, and S. N. Currie, “Reconstruction of flexor/extensor alternation during fictive rostral scratching by two-site stimulation in the spinal turtle with a transverse spinal hemisection.” *J Neurosci*, vol. 18, no. 1, pp. 467–79, Jan. 1998.
- [42] P. S. G. Stein, M. L. McCullough, and S. N. Currie, “Spinal motor patterns in the turtle,” *Ann N Y Acad Sci*, vol. 860, pp. 142–54, Nov. 1998.
- [43] L. I. Mortin and P. S. Stein, “Spinal cord segments containing key elements of the central pattern generators for three forms of scratch reflex in the turtle.” *J Neurosci*, vol. 9, no. 7, pp. 2285–96, July 1989.
- [44] J. Cheng, R. B. Stein, K. Jovanović, K. Yoshida, D. J. Bennett, and Y. Han, “Identification, localization, and modulation of neural networks for walking in the mudpuppy (*Necturus maculatus*) spinal cord.” *J Neurosci*, vol. 18, no. 11, pp. 4295–304, June 1998.
- [45] M. Wheatley and R. Stein, “An in vitro preparation of the mudpuppy for simultaneous intracellular and electromyographic recording during locomotion,” *J Neurosci Methods*, vol. 42, no. 1, pp. 129–137, 1992.

- [46] E. Bizzi, F. A. Mussa-Ivaldi, and S. Giszter, "Computations underlying the execution of movement: a biological perspective." *Science*, vol. 253, no. 5017, pp. 287–91, July 1991.
- [47] E. Bizzi, M. C. Tresch, P. Saltiel, and a. D'Avella, "New perspectives on spinal motor systems." *Nat Rev Neurosci*, vol. 1, no. 2, pp. 101–8, Nov. 2000.
- [48] S. F. Giszter, F. A. Mussa-Ivaldi, and E. Bizzi, "Convergent force fields organized in the frog's spinal cord." *J Neurosci*, vol. 13, no. 2, pp. 467–91, Feb. 1993.
- [49] F. A. Mussa-Ivaldi, S. F. Giszter, and E. Bizzi, "Linear combinations of primitives in vertebrate motor control." *Proc Natl Acad Sci U S A*, vol. 91, no. 16, pp. 7534–8, Aug. 1994.
- [50] W. J. Kargo and S. F. Giszter, "Rapid correction of aimed movements by summation of force-field primitives." *J Neurosci*, vol. 20, no. 1, pp. 409–26, Jan. 2000.
- [51] P. Saltiel, M. C. Tresch, and E. Bizzi, "Spinal cord modular organization and rhythm generation: an NMDA iontophoretic study in the frog." *J Neurophysiol*, vol. 80, no. 5, pp. 2323–39, Nov. 1998.
- [52] S. Grillner and P. Zangger, "On the central generation of locomotion in the low spinal cat," *Exp Brain Res*, vol. 34, no. 2, pp. 241–261, Jan. 1979.
- [53] Y. Ichikawa, Y. Terakado, and T. Yamaguchi, "Last-order interneurons controlling activity of elbow extensor motoneurons during forelimb fictive locomotion in the cat." *Neurosci Lett*, vol. 121, no. 1-2, pp. 37–9, Jan. 1991.
- [54] D. A. McCrea, "Neuronal Basis of Afferent-evoked Enhancement of Locomotor Activity," *Ann N Y Acad Sci*, vol. 860, no. 1 NEURONAL MECH, pp. 216–225, Nov. 1998.
- [55] M. C. Tresch and O. Kiehn, "Coding of locomotor phase in populations of neurons in rostral and caudal segments of the neonatal rat lumbar spinal cord." *J Neurophysiol*, vol. 82, no. 6, pp. 3563–74, Dec. 1999.

- [56] M. C. Tresch, P. Saltiel, and E. Bizzi, “The construction of movement by the spinal cord.” *Nat Neurosci*, vol. 2, no. 2, pp. 162–7, Feb. 1999.
- [57] V. C. K. Cheung, A. D’Avella, M. C. Tresch, and E. Bizzi, “Central and sensory contributions to the activation and organization of muscle synergies during natural motor behaviors.” *J Neurosci*, vol. 25, no. 27, pp. 6419–34, July 2005.
- [58] A. D’Avella and E. Bizzi, “Shared and specific muscle synergies in natural motor behaviors.” *Proc Natl Acad Sci U S A*, vol. 102, no. 8, pp. 3076–81, Feb. 2005.
- [59] L. H. Ting and J. M. Macpherson, “A limited set of muscle synergies for force control during a postural task.” *J Neurophysiol*, vol. 93, no. 1, pp. 609–13, Jan. 2005.
- [60] G. Torres-Oviedo, J. M. Macpherson, and L. H. Ting, “Muscle synergy organization is robust across a variety of postural perturbations.” *J Neurophysiol*, vol. 96, no. 3, pp. 1530–46, Sept. 2006.
- [61] J. L. McKay and L. H. Ting, “Functional muscle synergies constrain force production during postural tasks.” *J Biomech*, vol. 41, no. 2, pp. 299–306, Jan. 2008.
- [62] S. a. Overduin, A. D’Avella, J. Roh, and E. Bizzi, “Modulation of muscle synergy recruitment in primate grasping.” *J Neurosci*, vol. 28, no. 4, pp. 880–92, Jan. 2008.
- [63] V. C. K. Cheung, A. D’Avella, and E. Bizzi, “Adjustments of motor pattern for load compensation via modulated activations of muscle synergies during natural behaviors.” *J Neurophysiol*, vol. 101, no. 3, pp. 1235–57, Mar. 2009.
- [64] J. Roh, V. C. K. Cheung, and E. Bizzi, “Modules in the brain stem and spinal cord underlying motor behaviors.” *J Neurophysiol*, vol. 106, no. 3, pp. 1363–78, Sept. 2011.
- [65] S. a. Overduin, A. D’Avella, J. M. Carmena, and E. Bizzi, “Microstimulation activates a handful of muscle synergies.” *Neuron*, vol. 76, no. 6, pp. 1071–7, Dec. 2012.

- [66] Y. P. Ivanenko, R. Grasso, M. Zago, M. Molinari, G. Scivoletto, V. Castellano, V. Macellari, and F. Lacquaniti, "Temporal components of the motor patterns expressed by the human spinal cord reflect foot kinematics." *J Neurophysiol*, vol. 90, no. 5, pp. 3555–65, Nov. 2003.
- [67] Y. P. Ivanenko, R. E. Poppele, and F. Lacquaniti, "Five basic muscle activation patterns account for muscle activity during human locomotion." *J Physiol*, vol. 556, no. Pt 1, pp. 267–82, Apr. 2004.
- [68] G. Cappellini, Y. P. Ivanenko, R. E. Poppele, and F. Lacquaniti, "Motor patterns in human walking and running." *J Neurophysiol*, vol. 95, no. 6, pp. 3426–37, June 2006.
- [69] Y. P. Ivanenko, G. Cappellini, N. Dominici, R. E. Poppele, and F. Lacquaniti, "Coordination of locomotion with voluntary movements in humans." *J Neurosci*, vol. 25, no. 31, pp. 7238–53, Aug. 2005.
- [70] E. Morin, "Lower limb muscle synergies during gait in humans." *Conf Proc IEEE Eng Med Biol Soc*, vol. Suppl, pp. 6667–9, Jan. 2006.
- [71] G. Torres-Oviedo and L. H. Ting, "Muscle synergies characterizing human postural responses." *J Neurophysiol*, vol. 98, pp. 2144–2156, 2007.
- [72] R. R. Neptune, D. J. Clark, and S. A. Kautz, "Modular control of human walking: a simulation study." *J Biomech*, vol. 42, no. 9, pp. 1282–7, June 2009.
- [73] C. P. McGowan, R. R. Neptune, D. J. Clark, and S. a. Kautz, "Modular control of human walking: Adaptations to altered mechanical demands." *J Biomech*, vol. 43, no. 3, pp. 412–9, Feb. 2010.
- [74] F. Hug, N. A. Turpin, A. Couturier, and S. Dorel, "Consistency of muscle synergies during pedaling across different mechanical constraints." *J Neurophysiol*, vol. 106, no. 1, pp. 91–103, July 2011.
- [75] S. a. Chvatal and L. H. Ting, "Voluntary and reactive recruitment of locomotor muscle synergies during perturbed walking." *J Neurosci*, vol. 32, no. 35, pp. 12 237–50, Aug. 2012.

- [76] S. A. Chvatal and L. H. Ting, “Common muscle synergies for balance and walking.” *Front Comput Neurosci*, vol. 7, no. May, p. 48, Jan. 2013.
- [77] A. D’Avella, A. Portone, L. Fernandez, and F. Lacquaniti, “Control of fast-reaching movements by muscle synergy combinations.” *J Neurosci*, vol. 26, no. 30, pp. 7791–810, July 2006.
- [78] A. D’Avella, L. Fernandez, A. Portone, and F. Lacquaniti, “Modulation of phasic and tonic muscle synergies with reaching direction and speed.” *J Neurophysiol*, vol. 100, no. 3, pp. 1433–54, Sept. 2008.
- [79] A. B. Ajiboye and R. F. Weir, “Muscle synergies as a predictive framework for the EMG patterns of new hand postures.” *J Neural Eng*, vol. 6, no. 3, p. 036004, June 2009.
- [80] S. Muceli, A. T. l. Boye, A. D’Avella, and D. Farina, “Identifying representative synergy matrices for describing muscular activation patterns during multidirectional reaching in the horizontal plane.” *J Neurophysiol*, vol. 103, no. 3, pp. 1532–42, Mar. 2010.
- [81] J. Roh, W. Z. Rymer, and R. F. Beer, “Robustness of muscle synergies underlying three-dimensional force generation at the hand in healthy humans.” *J Neurophysiol*, vol. 107, no. 8, pp. 2123–42, Apr. 2012.
- [82] “Stroke — World Heart Federation.”
- [83] A. Di Carlo, “Human and economic burden of stroke.” *Age Ageing*, vol. 38, no. 1, pp. 4–5, Jan. 2009.
- [84] “American Stroke Association.”
- [85] J. P. Dewald and R. F. Beer, “Abnormal joint torque patterns in the paretic upper limb of subjects with hemiparesis.” *Muscle Nerve*, vol. 24, no. 2, pp. 273–83, Feb. 2001.
- [86] J. P. Dewald, R. F. Beer, J. D. Given, J. R. McGuire, and W. Z. Rymer, “Reorganization of flexion reflexes in the upper extremity of hemiparetic subjects.” *Muscle Nerve*, vol. 22, no. 9, pp. 1209–21, Sept. 1999.

- [87] J. Li, Z. J. Wang, J. J. Eng, and M. J. McKeown, "Bayesian network modeling for discovering "dependent synergies" among muscles in reaching movements." *IEEE Trans Biomed Eng*, vol. 55, no. 1, pp. 298–310, Jan. 2008.
- [88] L. Gizzi, J. r. F. k. Nielsen, F. Felici, Y. P. Ivanenko, and D. Farina, "Impulses of activation but not motor modules are preserved in the locomotion of subacute stroke patients." *J Neurophysiol*, vol. 106, no. 1, pp. 202–10, July 2011.
- [89] V. C. K. Cheung, A. Turolla, M. Agostini, S. Silvoni, C. Bennis, P. Kasi, S. Paganoni, P. Bonato, and E. Bizzi, "Muscle synergy patterns as physiological markers of motor cortical damage." *Proc Natl Acad Sci U S A*, vol. 109, no. 36, pp. 14 652–6, Sept. 2012.
- [90] J. J. Kutch, A. D. Kuo, A. M. Bloch, and W. Z. Rymer, "Endpoint force fluctuations reveal flexible rather than synergistic patterns of muscle cooperation." *J Neurophysiol*, vol. 100, no. 5, pp. 2455–71, Nov. 2008.
- [91] M. C. Tresch and A. Jarc, "The case for and against muscle synergies." *Curr Opin Neurobiol*, vol. 19, no. 6, pp. 601–7, Dec. 2009.
- [92] F. J. Valero-Cuevas, M. Venkadesan, and E. Todorov, "Structured variability of muscle activations supports the minimal intervention principle of motor control." *J Neurophysiol*, vol. 102, no. 1, pp. 59–68, July 2009.
- [93] F. Hug, N. a. Turpin, S. Dorel, and A. Guével, "Smoothing of electromyographic signals can influence the number of extracted muscle synergies." *Clin Neurophysiol*, vol. 123, no. 9, pp. 1895–6, Sept. 2012.
- [94] A. de Rugy, G. E. Loeb, and T. J. Carroll, "Are muscle synergies useful for neural control?" *Front Comput Neurosci*, vol. 7, no. March, p. 19, Jan. 2013.
- [95] U. Windhorst and H. k. Johansson, Eds., *Modern Techniques in Neuroscience Research*, 1st ed. Berlin, Heidelberg: Springer Berlin Heidelberg, 1999.
- [96] "SENIAM (Surface ElectroMyoGraphy for the Non-Invasive Assessment of Muscles)."

- [97] H. J. Hermens, B. Freriks, C. Disselhorst-Klug, and G. Rau, "Development of recommendations for SEMG sensors and sensor placement procedures." *J Electromyogr Kinesiol*, vol. 10, no. 5, pp. 361–74, Oct. 2000.
- [98] C. D. Luca, "The use of surface electromyography in biomechanics," *J Appl Biomech*, vol. 13, no. 2, pp. 135–163, 1997.
- [99] J. H. T. Viitasalo and P. V. Komi, "Signal characteristics of EMG during fatigue," *Eur J Appl Physiol Occup Physiol*, vol. 37, no. 2, pp. 111–121, 1977.
- [100] a. Georgakis, L. K. Stergioulas, and G. Giakas, "Fatigue analysis of the surface EMG signal in isometric constant force contractions using the averaged instantaneous frequency." *IEEE Trans Biomed Eng*, vol. 50, no. 2, pp. 262–5, Feb. 2003.
- [101] A. Burden, "How should we normalize electromyograms obtained from healthy participants? What we have learned from over 25 years of research." *J Electromyogr Kinesiol*, vol. 20, no. 6, pp. 1023–35, Dec. 2010.
- [102] F. Hug, "Can muscle coordination be precisely studied by surface electromyography?" *J Electromyogr Kinesiol*, vol. 21, no. 1, pp. 1–12, Feb. 2011.
- [103] K. G. Keenan, D. Farina, R. Merletti, and R. M. Enoka, "Amplitude cancellation reduces the size of motor unit potentials averaged from the surface EMG." *J Appl Physiol*, vol. 100, no. 6, pp. 1928–37, June 2006.
- [104] J. D. M. Drake and J. P. Callaghan, "Elimination of electrocardiogram contamination from electromyogram signals: An evaluation of currently used removal techniques." *J Electromyogr Kinesiol*, vol. 16, no. 2, pp. 175–87, Apr. 2006.
- [105] M. Bilodeau, S. Schindler-Ivens, D. M. Williams, R. Chandran, and S. S. Sharma, "EMG frequency content changes with increasing force and during fatigue in the quadriceps femoris muscle of men and women." *J Electromyogr Kinesiol*, vol. 13, no. 1, pp. 83–92, Feb. 2003.

- [106] B. I. Prilutsky, "Coordination of two- and one-joint muscles: functional consequences and implications for motor control." *Motor Control*, vol. 4, no. 1, pp. 1–44, Jan. 2000.
- [107] C. Angeloni, P. Riley, and D. Krebs, "Frequency content of whole body gait kinematic data," *IEEE Trans Rehabil Eng*, vol. 2, no. 1, pp. 40–46, Mar. 1994.
- [108] D. A. Winter, *The Biomechanics and Motor Control of Human Gait: Normal, Elderly and Pathological*. Waterloo Biomechanics, 1991.
- [109] M. C. Tresch, V. C. K. Cheung, and A. D'Avella, "Matrix factorization algorithms for the identification of muscle synergies: evaluation on simulated and experimental data sets." *J Neurophysiol*, vol. 95, no. 4, pp. 2199–212, Apr. 2006.
- [110] D. D. Lee and H. S. Seung, "Learning the parts of objects by non-negative matrix factorization." *Nature*, vol. 401, no. 6755, pp. 788–91, Oct. 1999.
- [111] P. Paatero and U. Tapper, "Positive matrix factorization: A non-negative factor model with optimal utilization of error estimates of data values," *Environmetrics*, vol. 5, no. 2, pp. 111–126, June 1994.
- [112] D. D. Lee and H. S. Seung, "Algorithms for non-negative matrix factorization," *Adv Neural Inf Process Syst*, no. 1, 2001.
- [113] C.-J. Lin, "Projected gradient methods for nonnegative matrix factorization." *Neural Comput*, vol. 19, no. 10, pp. 2756–79, Oct. 2007.
- [114] J. Piper, P. V. Pauca, R. J. Plemmons, and M. Giffin, "Object Characterization from Spectral Data Using Nonnegative Factorization and Information Theory," *Proc Amos Tech Conf, Maui, HI*, 2004.
- [115] C. Lin, "On the Convergence of Multiplicative Update Algorithms for Nonnegative Matrix Factorization," *IEEE Trans Neural Networks*, vol. 18, no. 6, pp. 1589–1596, Nov. 2007.
- [116] P. Paatero, "The Multilinear Engine: A Table-Driven, Least Squares Program for Solving Multilinear Problems, Including the n -Way Parallel Factor Analysis Model," *J Comput Graph Stat*, vol. 8, no. 4, pp. 854–888, Dec. 1999.

-
- [117] M. Chu, F. Diele, R. Plemmons, and S. Ragni, “Optimality, computation, and interpretation of nonnegative matrix factorizations,” *SIAM J Matrix Anal*, 2004.
- [118] W. J. Kargo and S. F. Giszter, “Individual premotor drive pulses, not time-varying synergies, are the units of adjustment for limb trajectories constructed in spinal cord.” *J Neurosci*, vol. 28, no. 10, pp. 2409–25, Mar. 2008.
- [119] A. D’Avella and M. C. Tresch, “Modularity in the motor system : decomposition of muscle patterns as combinations of time-varying synergies,” *Adv Neural Inf Process Syst*, vol. 14, pp. 141–148, 2002.
- [120] R. Shiavi, S. Champion, F. Freeman, and P. Griffin, “Variability of electromyographic patterns for level-surface walking through a range of self-selected speeds.” *Bull Prosthet Res*, vol. 10-35, pp. 5–14, Jan. 1981.
- [121] J. A. Magarik, E. C. Jauch, S. J. Patel, R. J. Adams, R. D. Turner, M. I. Chaudry, J. A. Chalela, A. Hays, M. I. Chimowitz, T. N. Turan, C. A. Holmstedt, E. Debenham, D. T. Lackland, and A. S. Turk, “MUSC’s comprehensive stroke program: changing what’s possible in stroke care across South Carolina.” *J S C Med Assoc*, vol. 108, no. 5, pp. 128–31, 2012.
- [122] M. L. Woodbury, C. a. Velozo, L. G. Richards, and P. W. Duncan, “Rasch analysis staging methodology to classify upper extremity movement impairment after stroke.” *Arch Phys Med Rehabil*, vol. 94, no. 8, pp. 1527–33, Aug. 2013.
- [123] A. Savitzky and M. J. E. Golay, “Smoothing and Differentiation of Data by Simplified Least Squares Procedures.” *Anal Chem*, vol. 36, no. 8, pp. 1627–1639, July 1964.
- [124] J. J. Baskett, H. J. Marshall, J. B. Broad, P. H. Owen, and G. Green, “The good side after stroke: ipsilateral sensory-motor function needs careful assessment.” *Age Ageing*, vol. 25, no. 3, pp. 239–44, May 1996.